

POLITECNICO DI TORINO

Collegio di Ingegneria Chimica e dei Materiali

Corso di Laurea Magistrale in Ingegneria Chimica e dei Processi Sostenibili

Tesi di Laurea Magistrale

Improving the sustainability of the synthesis of MOFs used for the production of catalysts for dry reforming of methane



Relatori

prof. Stefania Specchia

firma del relatore

Stefania Specchia

Candidato

Arianna Miglio

firma del candidato

Arianna Miglio

Ottobre 2019

*“Ai miei zii Mimmo e Giuseppina
esempio di vita, amore e famiglia.”*

The project has been carried out at ‘Laboratoire de Réactivité de Surface’
during an Erasmus project at Sorbonne Université of Paris.



Table of contents

1.Riassunto in italiano.....	I
1.1 Introduzione.....	I
1.1.1 Metal-organic frameworks (MOFs): definizione, proprietà e struttura.....	II
1.1.2 Metodi di sintesi dei metal-organic frameworks.....	III
1.1.3 Applicazione dei MOFs in catalisi.....	IV
1.1.4 MIL-53(Al)	V
1.1.5 Dry reforming del metano	VI
1.2 Materiali e metodi.....	VIII
1.2.1 Sintesi in un solo step del MIL-53(Al).....	VIII
1.2.2 Sintesi in due step del MIL-53(Al).....	VIII
1.2.3 Preparazione del catalizzatore.....	IX
1.2.4 Diffrazione raggi X.....	X
1.2.5 Analisi termogravimetrica.....	X
1.2.6 Fisisorbimento dell'azoto.....	X
1.2.7 Microscopia elettronica a trasmissione e a scansione.....	X
1.2.8 Risonanza magnetica nucleare.....	X
1.2.9 Riduzione a temperatura programmata.....	XI
1.2.10 Misurazioni catalitiche.....	XI
1.3 Risultati e discussione.....	XI
1.3.1 Sintesi in un solo step del MIL-53(Al) e preparazione del catalizzatore.....	XII
1.3.2 Sintesi in due step del MIL-53(Al) e preparazione del catalizzatore.....	XVII
1.4 Conclusioni.....	XX
2. Introduction.....	1
2.1 Metal-organic frameworks (MOFs): definition, properties and structures	2
2.1.1 Metal Ions and organic ligands as Building Units of MOFs.....	3
2.1.2 Open Metal Sites in MOFs.....	4
2.2 Methods of synthesis of metal-organic frameworks.....	5
2.3 Applications of MOFs in catalysis.....	6
2.4 MIL-53 (Al).....	7
2.5 Dry reforming of methane.....	9

2.5.1 Thermodynamics.....	10
2.5.2 Coke formation	11
2.5.3 Catalysts and catalytic property.....	12
2.6 Poly (ethylene terephthalate)	13
3. Methods and material.....	14
3.1 MIL-53(Al) synthesis.....	14
3.1.1 One step synthesis of MIL-53(Al)	15
3.1.2 Two steps synthesis of MIL-53(Al)	15
3.2 Catalyst preparation.....	16
3.3 Physicochemical characterization techniques.....	17
3.3.1 X-ray diffraction.....	17
3.3.2 Thermo Gravimetric Analysis.....	18
3.3.3 N ₂ physisorption.....	19
3.3.4 Transmission electron microscopy (TEM)	21
3.3.5 Nuclear magnetic resonance (NMR)	22
3.3.6 Temperature-programmed reduction (TPR)	23
3.3.7 Scanning electron microscopy (SEM)	25
3.4 Catalytic measurements.....	25
3.4.1 Description of the equipment.....	25
3.4.2 Catalytic test conditions.....	27
4. Results and discussion.....	28
4.1 One step synthesis.....	28
4.1.1 As-synthesized MIL-53(Al)	28
4.1.2 Activated MIL-53(Al)	30
4.1.3 Impregnated MIL-53(Al)	33
4.1.4 Calcined MIL-53(Al)	35
4.1.5 Reduced MIL-53(Al)	38
4.2 Two steps synthesis.....	41
4.2.1 Alcoholysis of PET.....	41
4.2.2 Synthesis and activation of MIL-53(Al)	41
4.2.3 Nickel impregnation of MIL-53(Al)	43
4.2.4 Calcination of MIL-53(Al)	46

5. Conclusion.....	48
6. Abbreviations.....	50
7. References.....	52
8.Acknowledgements.....	55

1.Riassunto in italiano

1.1 Introduzione

Il lavoro è parte di un progetto più ampio che coinvolge una ricerca sulla sintesi di nuove strutture porose che possano fungere da supporti nella reazione di dry reforming del metano.

Negli ultimi venti anni, c'è stato un aumento del consumo di energia, principalmente a causa di una rapida crescita della popolazione umana.¹ Per soddisfare la crescente domanda di energia, vengono utilizzati combustibili fossili come petrolio, gas naturale e carbone. La dipendenza dai combustibili fossili per soddisfare la domanda di energia ha creato problemi ambientali attraverso la produzione di gas a effetto serra (GHG). Il metano e il biossido di carbonio costituiscono una parte importante dei gas a effetto serra, e hanno contribuito in modo determinante al cambiamento climatico, che incide sulla produttività, sugli ecosistemi naturali, sull'agricoltura e sulla società.² Sebbene la concentrazione di metano nell'atmosfera sia inferiore a quella di CO₂, ha causato sorprendentemente circa il 20% del riscaldamento globale.³⁻⁴ Tradizionalmente il metano è prodotto da due fonti; in primo luogo proviene da fonti naturali come termiti, praterie, incendi, laghi e zone umide, e in secondo luogo da attività umane come l'estrazione del carbone, le discariche, la lavorazione di petrolio e gas e le attività agricole.⁵ È quindi necessario ridurre la quantità di metano e anidride carbonica nell'atmosfera; per fare questo sono state condotte ricerche approfondite per trovare modi efficaci per convertire questi gas serra in altri prodotti di valore. Il metodo industriale più comune e più comunemente usato è il reforming, che converte gli idrocarburi in gas di sintesi (CO e H₂). Il reforming può avvenire attraverso tre processi: steam reforming del metano (SRM), ossidazione parziale del metano (POM) e dry reforming del metano (DRM).⁶ Tra i tre processi sopra menzionati il DRM è il più promettente, poiché utilizza due abbondanti gas a effetto serra (CO₂ e CH₄) per produrre gas di sintesi utili a livello industriale, e allo stesso tempo riduce le emissioni nette di gas a effetto serra.⁷

Il dry reforming del metano offre preziosi benefici ambientali: l'utilizzo del biogas⁸, la rimozione di GHG (metano e anidride carbonica), e la conversione del gas naturale con un alto contenuto di anidride carbonica in syngas.⁹ Il dry reforming del metano ha prodotto un rapporto di syngas inferiore (H₂ / CO = 1), che è adatto per la sintesi di sostanze chimiche ossigenate¹⁰ e idrocarburi per la sintesi di Fischer-Tropsch. Inoltre, il processo DRM è anche più economico rispetto ad altri metodi poiché elimina la complicata separazione dei gas dai prodotti finali.¹¹ La reazione di dry reforming del metano è endotermica e per il suo raggiungimento richiede temperature elevate. Pertanto, sono necessari catalizzatori che riducono significativamente la temperatura di reazione e massimizzano la produzione di syngas per far sì che questa reazione avvenga.¹²

Al momento, i catalizzatori più comunemente usati nel DRM sono basati su metalli nobili che hanno lo svantaggio di essere rari e costosi. Pertanto, si stanno compiendo sforzi per sviluppare catalizzatori basati su fasi attive più economiche ed abbondanti. Tra la famiglia di metalli di transizione che rappresenta la migliore alternativa, il nichel è il più promettente.¹⁴⁻¹⁵ Tuttavia, i catalizzatori esistenti presentano due importanti inconvenienti: la sinterizzazione dei metalli dovuta all'alta temperatura e la formazione di depositi di carbonio che portano alla perdita di attività del catalizzatore.¹⁶⁻¹⁷ Per risolvere questi problemi e progettare catalizzatori resistenti, sono stati utilizzati supporti mesoporosi con un'area specifica elevata in cui possono essere occluse le nanoparticelle di nichel.¹⁸⁻¹⁹ In

questa prospettiva, le strutture metallo-organiche (MOF) hanno attirato l'attenzione a causa della loro elevata area superficiale, basse densità e alta porosità, stabilità termica e funzionalità chimiche regolabili.²⁰ I MOF sono solidi cristallini composti da ioni metallici (normalmente chiamati nodi) collegati da ligandi organici (come linker). Questi materiali spesso formano strutture tridimensionali estese con strutture porose. I linker sono spesso molecole organiche con specifici gruppi funzionali come il carbossilato, che possono coordinarsi a nodi metallici come Zn, Al, Fe. Inoltre, le dimensioni dei pori e la chimica superficiale dei MOF possono essere modulate sistematicamente modificando i ligandi organici o cambiando gli ioni metallici usati nella sintesi di questi materiali.²¹ In questo lavoro, ($\text{Al(OH)}[\text{O}_2\text{C-C}_6\text{H}_4-\text{CO}_2]$) uno dei MOF più studiati e spesso indicato come MIL-53 (Al) è stato sintetizzato con il metodo idrotermale, poi è stato aggiunto il nichel alla struttura originale MIL-53 (Al) per investigare il suo effetto come catalizzatore, in particolare nella reazione di dry reforming del metano.²² Per sintetizzare MIL-53(Al) nel modo tradizionale sono necessari due costosi precursori: acido tereftalico e cloruro di alluminio. Inoltre, durante la preparazione del catalizzatore si ha una perdita di circa il 70% del MOF iniziale. Per limitare i costi e sintetizzare MIL-53(Al) in modo più sostenibile e green, in questo lavoro sono state utilizzate le bottiglie di plastica (PET) come fonte diretta dell'acido tereftalico durante la sintesi di MIL-53(Al).

1.1.1 Metal-organic frameworks (MOFs): definizione, proprietà e struttura

I Metal Organic Framework (MOF) sono sistemi ibridi inorganici-organici costruiti dalla combinazione di ioni metallici (generalmente denominati ‘node’) con leganti organici politopici (generalmente denominati ‘linker’), tramite legami di coordinazione per creare strutture cristalline in una, due o tre dimensioni con porosità permanente. I centri metallici, normalmente denominati ‘node’, possono essere costituiti dal solo ione metallico, oppure da ‘cluster’ polinucleari detti Secondary Building Units (SBU). Le SBU presentano una particolare geometria dettata dall’unione di uno specifico numero di centri metallici tramite leganti politropici. Questi cluster polinucleari possono essere uniti tra loro da leganti differenti, portando ad una enorme varietà di framework consentendo la modulazione delle proprietà dei composti, in particolare della porosità. Negli ultimi decenni, questi materiali porosi hanno catturato l’attenzione di molti gruppi di ricerca in tutto il mondo a causa delle loro eccezionali proprietà come l’elevata superficie, bassa densità, alta porosità, stabilità termica e funzionalità chimiche regolabili.²³

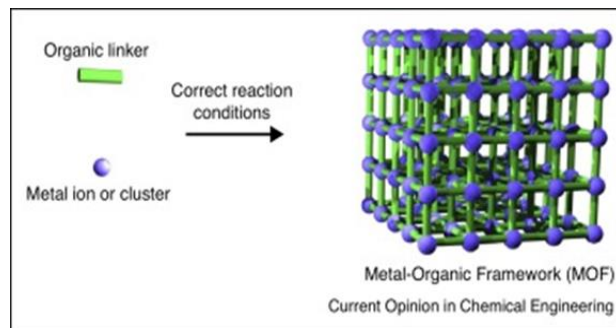


Figura 1.1 Rappresentazione schematica dei metal-organic frameworks

I solidi porosi possono essere classificati in tre categorie in base alle dimensioni dei loro pori: materiali microporosi, mesoporosi e macroporosi. I solidi che hanno una dimensione dei pori di 2 nm o inferiore sono noti come microporosi. I solidi mesoporosi hanno una dimensione compresa nell’intervallo di 2 nm-50 nm, e oltre i 50 nm sono conosciuti come macroporosi. La presenza di cavità (canali monodimensionali 1D, piani 2D e canali

intersecati 3D) consentono l'ingresso e l'uscita di molecole ospiti dette 'guest', utili ad esempio quando i MOF sintetizzati cosituiscono il supporto di un catalizzatore.

I principali termini di confronto per quanto riguarda la porosità di questi materiali sono le zeoliti ed i carboni attivi, già impiegati su scala industriale per svariate applicazioni. I carboni attivi presentano sia un'elevata porosità che la possibilità di interagire con molecole organiche, ma al tempo stesso anche una struttura irregolare dei pori e questo limita il loro utilizzo. A differenza delle zeoliti che hanno dimensioni dei pori fisse e dell'ordine di qualche nanometro, i MOF possono realizzare strutture porose con differente dimensione, forme e proprietà. Questo, come detto in precedenza, è possibile grazie all'utilizzo di leganti politopici con differente lunghezza e rigidità.^{24,26}

Grazie alle loro caratteristiche, all'utilizzo di leganti funzionalizzati ad hoc per il campo di applicazione del prodotto e all'ottimizzazione delle interazioni host-guest, i metal-organic frameworks possono essere usati in svariate applicazioni come la sperazione chimica, la catalisi eterogenea, l'adsorbimento di gas, e nella fotocatalisi.

1.1.2 Metodi di sintesi dei metal-organic frameworks

I MOF possono essere sintetizzati tramite svariati metodi: sintesi idrotermale anche nota come solvotermica, sintesi tramite l'uso di microonde e sintesi elettrochimica. La sintesi idrotermale / solvotermica è un metodo facile e prominente per formare un'ampia varietà di strutture organizzate che sono difficili da ottenere con altre tecniche disponibili. Le condizioni di sintesi del MOF in questi studi sono state condotte al fine di ottenere rese elevate di prodotti solidi, che verranno successivamente sottoposti ad altri trattamenti al fine di ottenere il catalizzatore per la reazione di dry reforming del metano. La sintesi di MOF avviene semplicemente utilizzando sali solubili come fonte per il componente metallico come cloruri, nitrati metallici o acetati; e un solvente organico polare come un'ammina o ammide come fonte di ingredienti inorganici. Tutti i reagenti (precursori dell'ossido di metallo, stabilizzatore del pH e H₂O / solvente) vengono miscelati insieme, introdotti in un'autoclave di acciaio inossidabile rivestita di teflon e riscaldati. La cristallizzazione e la crescita delle particelle possono essere controllate da parametri di processo, come temperatura, pressione e tempo. L'applicazione della temperatura richiesta produce una pressione autogena. Dopo che la reazione è completa, l'autoclave viene raffreddata a temperatura ambiente e il prodotto viene lavato ed essiccato. I MOF possono facilmente trasportare dal 50 al 150% in peso di solvente occluso. Questo è un ordine di grandezza superiore a una preparazione di ossido di zeolite o metallo di base. Pertanto, è consigliabile rimuovere la grande quantità di solvente adsorbito prima di procedere con un'elevata attivazione termica.

I MOF derivano da un processo di cristallizzazione; in queste strutture acqua, solventi organici e residui riempiono i pori. Pertanto, l'incapsulamento delle molecole ospiti nella struttura porosa e la presenza di molecole inorganiche svolgono un ruolo fondamentale nella formazione dei MOF. Quando si lavora con i MOF, occorre prestare attenzione anche ai trattamenti post-sintetici come la purificazione, l'attivazione e la riproducibilità.

La purificazione è molto importante per le applicazioni catalitiche dei MOF, poiché le impurità dei sottoprodoti della reazione possono limitare l'attività catalitica e diminuire la possibilità di assorbimento. La purificazione viene solitamente effettuata con un solvente ad alta temperatura.

Per attivare il materiale, è necessario svuotare i pori, procedere in questo modo non è molto semplice in quanto la rimozione di inclusioni da una struttura porosa può portare al collasso

della struttura stessa. Ciò accade specialmente se le molecole ospiti e la struttura sono tenute insieme da legami piuttosto forti o se la rimozione di inclusioni richiede temperature elevate. Per semplificare l'attivazione dei MOF è possibile sostituire il solvente con uno più volatile, in questo modo si riduce la temperatura di trattamento. Un altro fattore importante è la riproducibilità dei risultati di riepilogo. Ciò è dovuto alla presenza di pori e componenti organici nella struttura, che portano a deviazioni della struttura da quella ideale e alle proprietà dei campioni che variano in ogni esperimento.³³⁻³⁴

1.1.3 Applicazione dei MOFs in catalisi

Negli ultimi anni l'industria chimica ha cercato di sviluppare processi che producono meno rifiuti chimici e allo stesso tempo aumentano la produttività. Ne consegue, che lo studio della catalisi è un fattore chiave per lo sviluppo di processi chimici sostenibili. Catalizzatori omogenei sono stati usati in molti processi industriali ma hanno diversi svantaggi come scarsa stabilità termica e difficoltà nel recuperare il catalizzatore dalla miscela di reazione. Invece, catalizzatori eterogenei hanno una vita più lunga di quelli omogenei, consentono una separazione più semplice e un riciclaggio più efficiente.

Le alte superfici, le modificabili dimensioni dei pori e l'alta densità di siti attivi all'interno delle strutture aperte dei MOF offrono molti vantaggi per il loro uso nella catalisi. Grazie alla struttura aperta, i coefficienti di autodiffusione delle molecole nei pori sono leggermente inferiori a quelli del solvente alla rinfusa. Ciò implica che il trasporto di massa nei pori non è ostacolato. L'elevata area superficiale dei MOF consente di realizzare catalizzatori con una densità molto elevata di siti attivi completamente esposti e ciò porta a una maggiore efficacia e attività del catalizzatore.³⁵

I MOF contengono tre parti ben distinte: i nodi metallici, il legante organico e il sistema poroso. La funzione catalitica si può essere trovare in una delle tre parti; inoltre, i MOF sono noti per contenere contemporaneamente due o più tipi di siti catalitici. Di seguito, verrà mostrato che ci sono tre diversi approcci per preparare i MOF in cui la funzione catalitica si trova in una di queste tre parti.

Il primo approccio è l'uso di siti attivi in metallo che sono collegati tra loro attraverso linkers organici. In questo approccio vengono utilizzati due tipi di MOF, il primo include materiali con un singolo tipo di metallo (M) che agisce contemporaneamente come sito catalitico attivo e come componente strutturale, mentre il secondo tipo comprende materiali con due tipi di metalli. In quest'ultimo caso un metallo (M1 = sito di un singolo metallo) è responsabile dell'attività catalitica, e l'altro (M2 = ione metallico o cluster) non è coinvolto nella catalisi e pertanto svolge un ruolo puramente strutturale. Il secondo approccio prevede l'uso dei gruppi funzionali della componente organica. In questi MOF i siti attivi capaci di catalizzare una reazione si trovano nella molecola organica e non nello ione metallico. I ligandi organici devono avere due tipi di gruppi funzionali: i gruppi coordinativi (L1) che legandosi ai metalli portano alla struttura del MOF e ai gruppi reattivi (L2) responsabili dell'attività catalitica. I metalli tendono ad interagire molto facilmente con i gruppi funzionali delle componenti organiche, questo implica che i gruppi reattivi L2 siano collegati agli ioni metallici e che non possano interagire con i substrati catalitici. Per questo motivo, la quantità di MOF appartenenti a questa categoria è veramente limitata. Nel terzo e ultimo approccio il sistema poroso del materiale fornisce lo spazio fisico (cavità di reazione nanometrica) in cui avviene la catalisi e intrappola i centri catalitici al suo interno (matrici ospite).²⁴

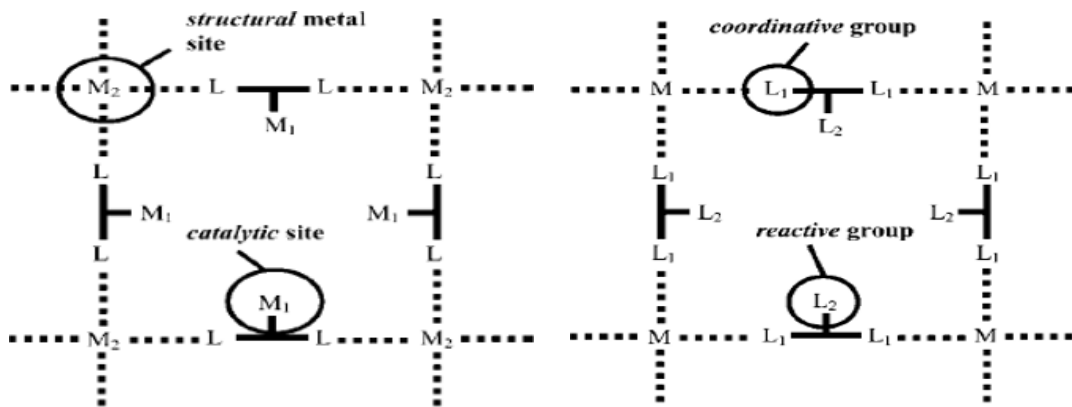


Figura 1.2 Rappresentazione di MOF bimetallico con entrambi i siti *Strutturale* (M₂) e *Catalitico* (M₁) sulla sinistra, e di un MOF con entrambi i gruppi funzionali *Cordinativo* (L₁) e *Reattivo* (L₂) sulla destra

1.1.4 MIL-53(Al)

I metal-organic frameworks designati come serie MIL-n (Materials of the Institute Lavoisier) sono state sintetizzati per la prima volta dal gruppo di Ferey nel 2002. I materiali nanoporosi di tipo MIL-n sono particolarmente interessanti a causa della loro struttura semplice e della loro maggiore stabilità termica rispetto ad altri MOF. Tra i materiali MIL-n, il MIL-53 (Al) ha attirato molta attenzione perché è in grado di assorbire grandi quantità di gas come CH₄ e CO₂. La struttura del MIL-53(Al) è costituita da catene infinite di ottaedri AlO₄(OH)₂ (dove M=Al³⁺) interconnessi da unità di acido 1,4-benzendicarbossilico (BDC). Ciò si traduce in una struttura 3D metallo-organica contenente canali a forma di diamante che si sviluppano in una dimensione (framework 1D) con pori di diametro di circa 8,5 Å. La formula chimica del materiale MIL-53(Al) è Al(OH)(O₂C-C₆H₄-CO₂).³⁶⁻³⁷

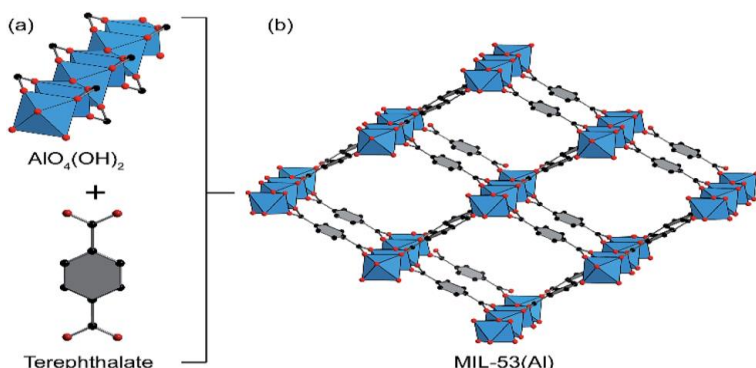


Figura 1.3 La combinazione di infiniti ottaedri AlO₄(OH)₂ con unità di acido tereftalico (a) porta alla formazione di una struttura porosa tridimensionale con canali rombici in una dimensione (b). Colore degli atomi: C, nero; O, rosso; Al, blu; H è omesso per una maggiore chiarezza

La struttura metallo-organica MIL-53 (Al) è stata sintetizzata con un metodo solvotermale usando cloruro di alluminio come fonte di alluminio, acido tereftalico (BDC) come ligando organico e acqua deionizzata. Il MIL-53 (Al) offre numerosi vantaggi rispetto ad altri MOF come elevata stabilità termica, elevata area superficiale, elevata resistenza all'umidità ed è sintetizzato utilizzando sostanze chimiche disponibili anche se non molto economiche.

Il MIL-53 (Al) mostra un ‘comportamento respiratorio’, ovvero è in grado di regolare il volume dei suoi pori in modo reversibile per ottimizzare le interazioni tra le molecole ospiti e la struttura, senza evidente rottura dei legami o collasso della struttura. Nella forma idratata (Figura 2.5, a sinistra) la dimensione dei canali è di $2.6 \times 13.6 \text{ \AA}^2$, e i pori sono leggermente deformati a causa delle interazioni tra gli atomi di idrogeno della molecola d’acqua e gli ossigeni del carbossilato e il gruppo μ_2 -idrossile. L’acqua viene rapidamente rimossa per riscaldamento per dare una struttura con la porosità più aperta (Figura 2.5, a destra), con dimensione dei canali pari a $8.5 \times 8.5 \text{ \AA}^2$. Le interazioni di legame idrogeno tra le molecole d’acqua intrappolate nei canali e i gruppi carbossilati dei linker BDC sono responsabili del comportamento dinamica della struttura.^{22,38}

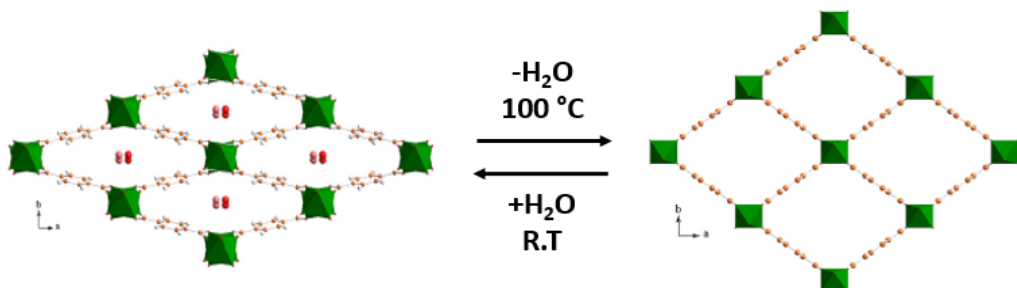


Figura 1.4 Comportamento dinamico del MIL-53(Al). Sinistra: MIL-53_{LT} (idratato); destra: MIL-53_{HT} (disidratato).

Il MIL-53 (Al) può essere utilizzato come materiale di supporto nei catalizzatori grazie alle sue particolari caratteristiche che sono riassunte di seguito:

- Le strutture porose e i siti di coordinamento insaturi dei MOF possono limitare l’aggregazione e la migrazione delle nanoparticelle portando ad un’elevata dispersione di nanoparticelle.
- I siti di coordinazione MOF insaturi aumentano l’attività nelle reazioni catalitiche.
- Enorme superficie, elevata stabilità termica e grazie ai suoi canali monodimensionali le molecole di reazione possono arrivare o lasciare la superficie del catalizzatore senza problemi.³⁹

1.1.5 Dry reforming del metano

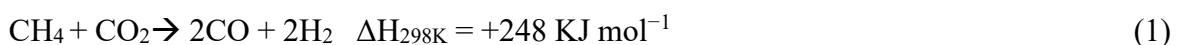
Il reforming a secco del metano (DRM) è un processo chimico che consiste nel convertire metano e anidride carbonica, identificati come i gas serra più abbondanti al mondo (GHG), in syngas (idrogeno e monossido di carbonio), con un rapporto molare H₂/CO uguale ad 1.

Uno degli ostacoli incontrati nell’applicazione di questo processo è la rapida disattivazione del catalizzatore, che è principalmente dovuta all’accumulo di coke, e alla sinterizzazione del supporto e delle particelle metalliche attive. Inoltre, i lunghi tempi di reazione e la necessità di CO₂ pura rendono il DRM un processo sconosciuto che necessita ancora di ulteriore sviluppo. I catalizzatori a base di metalli nobili come Rh, Pt, Pd o Ru mostrano eccellenti prestazioni in termini di stabilità e attività del catalizzatore; questi catalizzatori sono meno sensibili al coking rispetto ai catalizzatori a base di nichel. Considerando l’alto costo e la disponibilità limitata di metalli nobili, tuttavia, è più vantaggioso sviluppare un catalizzatore a base di nichel, che sia resistente all’accumulo di coke e presenti stabilità a lungo termine.⁴⁰ Per evitare la sinterizzazione del nichel e la deposizione di carbonio sono state sviluppate varie strategie:

- 1) aggiunta di una piccola quantità di un secondo metallo solitamente metalli nobili
- 2) variazione del tipo di supporto
- 3) rafforzare l'interazione tra Ni e il suo supporto

Pertanto, si può affermare che le prestazioni dei catalizzatori utilizzati per il reforming a secco del metano dipendono fortemente dalla selezione di metalli attivi, supporti e promotori.⁴¹

La reazione di dry reforming del metano è:



CH_4 and CO_2 sono molecole molto stabili con alta energia di dissociazione: 435 ($\text{CH}_3\text{-H}$) and 526 (CO-O) $\text{kJ}^*\text{mol}^{-1}$, rispettivamente. DRM è una reazione endotermica e richiede elevate temperature, generalmente comprese tra 630-1000 °C, per raggiungere il desiderato livello di conversione. Rispetto al reforming autotermico (ATR) e allo steam reforming (SRM), il dry reforming del metano è la reazione più endotermica. Ciò può essere attribuito al fatto che la CO_2 , l'agente ossidante utilizzato nel DRM, è più stabile rispetto all'ossigeno e al vapore utilizzati rispettivamente in ATR e SRM. Sebbene il DRM sia principalmente governato dalla reazione tra CH_4 e CO_2 (reazione 1), durante il processo possono verificarsi anche altre reazioni come la decomposizione del metano e la reazione di Boudouard, che causano la produzione di quantità elevate di carbonio che portano conseguentemente alla fatale disattivazione del catalizzatore.



Wang et al. hanno riportato che la decomposizione di CH_4 si verifica al di sopra di 557 °C, mentre la reazione di Boudouard si verifica al di sotto di 700 °C. Hanno inoltre scoperto che il carbonio si forma dalla decomposizione di CH_4 o dalla reazione di Boudouard nell'intervallo di temperatura compreso tra 557 a 700 °C, e hanno suggerito che la temperatura ottimale al rapporto di alimentazione di $\text{CO}_2/\text{CH}_4 = 1: 1$ è compresa tra 870 e 1040 °C, considerando la conversione e la formazione di carbonio.^{41,42} Le alte temperature richieste nel reforming a secco del metano portano alla deposizione di carbonio sui catalizzatori. Ciò accade perché, a queste temperature, viene raggiunta abbastanza energia per dividere il legame C-H delle molecole di metano. È quindi desiderabile comprendere le condizioni in cui si forma il carbonio per minimizzarne la formazione. Una formazione significativa di carbonio comporterà un eccessivo accumulo di perdite di carico e successivamente un'interruzione dell'impianto per la sostituzione del catalizzatore.⁴³

Il catalizzatore è costituito da due parti: la specie attiva (Ni) e il supporto. La specie attiva è il componente che determina effettivamente l'attività catalitica, mentre il supporto, che è il composto più presente, ha diverse funzioni, tra cui:

- fornire una superficie elevata per la dispersione di metalli attivi
- migliorare la resistenza meccanica
- aumentare la capacità di scambio termico
- assicurare stabilità, specialmente quando si opera a temperature elevate

Un buon supporto manterrà un'elevata dispersione di nichel (quindi un'elevata resistenza al coke) e sarà resistente alla sinterizzazione durante la reazione di reforming ad alta temperatura.⁴⁶ Oltre allo sviluppo del catalizzatore a base di Ni con alcuni agenti modificanti durante la preparazione del catalizzatore, l'incorporazione delle particelle di Ni

all'interno del supporto mesoporoso potrebbe anche aumentare la conversione dei reagenti e la resa dei prodotti, evitando la sinterizzazione delle particelle di metallo e rafforzando l'interazione metallo-supporto. Ciò è dovuto all'elevata superficie specifica dei materiali mesoporosi che può migliorare la dispersione delle particelle di Ni sul catalizzatore supportato.⁴⁹ Lo scopo di questo lavoro è di sintetizzare MIL-53(Al), che sarà quindi utilizzato come supporto per realizzare un catalizzatore a base di Ni/allumina particolarmente stabile e attivo nella reazione di reforming a secco del metano. Nel mio nuovo approccio ecologico, il polietilene tereftalato (PET) presente nelle bottiglie di plastica è stato effettivamente utilizzato come fonte di acido tereftalico per la sintesi del MIL-53 (Al).

1.2 Materiali e metodi

1.2.1 Sintesi in un solo step del MIL-53(Al)

Per sintetizzare il MIL-53(Al) tramite un solo step le bottiglie di plastica sono state lavate e tagliate in piccoli pezzi. Questi frammenti di PET sono stati inseriti insieme ad acqua deionizzata e $\text{AlCl}_3 \cdot 6\text{H}_2\text{O}$, in un'autoclave d'acciaio rivestita in teflon da 50 ml. Dopo aver chiuso attentamente l'autoclave, la si pone nel forno per 26 ore a 220 °C. In questo tipo di sintesi il PET viene utilizzato direttamente, e ciò che accade è un'idrolisi in situ. Il PET viene depolimerizzato nei monomeri che lo costituiscono grazie alla presenza di acido cloridrico (derivante dall'uso di AlCl_3 come fonte di alluminio).

Dopo il completamento della reazione, l'autoclave è stata raffreddata naturalmente a temperatura ambiente. Il solido è stato recuperato mediante filtrazione sotto vuoto e lavato con DMF, acqua deionizzata e infine con etanolo per garantire la completa rimozione dei residui indesiderati. Successivamente, il solido che si è depositato sulla carta filtro viene posto in forno per ottenere una polvere bianca. Dopo aver rimosso la polvere bianca dalla carta dal filtro, vengono aggiunti circa 50 ml di DMF e la soluzione viene agitata per circa 5 ore. Il solido è stato recuperato nuovamente per filtrazione, lavato come precedentemente riportato ed essiccato. Alla fine, l'eccesso di acido 1,4-benzenedicarbossilico adsorbito nei pori viene rimosso mediante trattamento termico a 330 °C per tre giorni. In questo modo è stato ottenuto il campione MIL attivato. Al fine di confrontare i risultati e per essere certi che sia stato ottenuto il MIL-53(Al) puro, il MIL-53(Al) è stato sintetizzato in condizioni tradizionali. Per far ciò, si utilizza acido tereftalico commerciale al posto dei frammenti di PET, nelle stesse condizioni di temperatura, tempo e pressione.

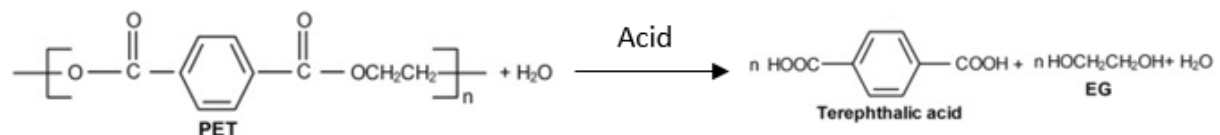


Figura 1.5 Idrolisi in situ del polietilene tereftalato

1.2.2 Sintesi in due step del MIL-53(Al)

Al fine di ridurre ulteriormente l'impatto economico, è stata utilizzata la bohemite come fonte di alluminio anziché AlCl_3 . Per fare ciò, non è stato possibile applicare una sintesi in un'unica fase che richiede la presenza di un ambiente acido per idrolizzare il PET, e quindi l'uso di una fonte di alluminio che sia in grado di creare tali condizioni (AlCl_3). Si è deciso, quindi, di sviluppare una sintesi a due fasi, in cui la prima fase è l'alcolisi del PET che porta ad ottenere BDC puro e la seconda fase è la sintesi di MIL-53(Al) in condizioni idrotermali,

utilizzando l'acido tereftalico sintetizzato nella prima fase. L'alcolizzazione del PET (2g) è stata eseguita in presenza di EG (5 ml), e con rapporti molari del PET: NaOH (1: 2,25); tutti i reagenti sono stati posti in un'autoclave, che successivamente è stata posta in forno per un periodo di 1 ora a 160 °C. I prodotti di reazione sono stati filtrati sottovuoto, e quello che precipita è acido tereftalico. Per neutralizzare la soluzione, è stato aggiunto acido solforico e ciò che è stato ottenuto ottiene è una soluzione contenente acido tereftalico e solfato di sodio. Per separare questi due composti e ottenere acido tereftalico puro, la soluzione è stata centrifugata più volte ed è stata aggiunta acqua distillata per favorire la separazione. Infine, il precipitato è stato essiccato ad 80 °C. Per verificare la purezza dell'acido tereftalico ottenuto è stata utilizzata la risonanza magnetica nucleare (NMR).

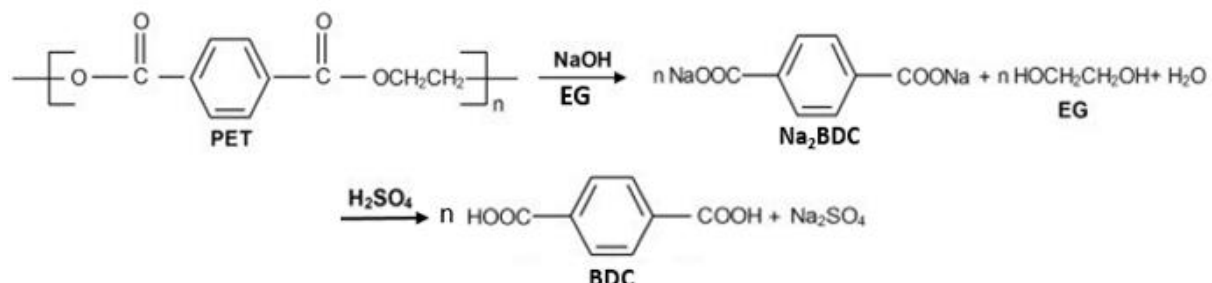


Figura 1.6 Alcolisi del PET

Dopo essere certi di aver ottenuto acido tereftalico puro, questo reagente è stato posto insieme a una fonte di alluminio (AlCl_3 o AlO(OH)) e acqua deionizzata in un'autoclave, il tutto è stato posto in un forno per 26 ore a 220 °C. Da qui in avanti è stata seguita la stessa procedura descritta precedentemente per la sintesi ad uno step, fino ad ottenere il campione MIL attivato.

1.2.3 Preparazione del catalizzatore

La strategia seguita per la preparazione del catalizzatore è illustrata nella Figura 1.8. Dopo la sintesi idrotermica e l'attivazione a 330 °C (rimozione del solvente) del MIL-53 (Al), i pori sono stati impregnati con un precursore di nichel cationico $\text{Ni}(\text{NO}_3)_2 \cdot 6\text{H}_2\text{O}$ mediante ‘incipient wetness impregnation’. Prima del trattamento di impregnazione, il campione è stato disidratato a 80 °C per tutta la notte, e poi trattato termicamente a 200 °C per 15 ore, per essere sicuri di aver rimosso l'acqua contenuta nei pori. Dopo l'impregnazione, il solido (Ni/MIL-53(Al)) è stato calcinato in aria a 500 °C per 5 ore per formare $\text{Ni}^{2+}@\text{Al}_2\text{O}_3$, che infine è stato trattato termicamente sotto idrogeno a 800 °C per formare le nanoparticelle di nichel ridotte che costituiscono la fase attiva per DRM.

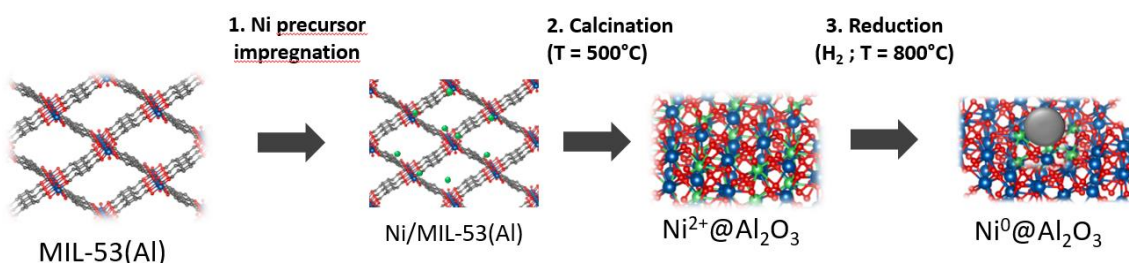


Figura 1.7 Schema di preparazione del catalizzatore a base di nichel-allumina

1.2.4 Diffrazione raggi X

La diffrazione di raggi X è una potente tecnica non distruttiva che rivela informazioni sulla struttura e l'orientamento dei cristalli, le composizioni chimiche e le proprietà fisiche dei materiali. I raggi X sono generati da un tubo a raggi catodici, l'interazione dei raggi incidenti con il campione produce interferenze costruttive quando le condizioni soddisfano la Legge di Bragg. Il dispositivo che sfrutta questo principio è il diffrattometro, che è composto da: una sorgente di raggi X, un monocromatore e collimatore, un rivelatore e un computer dotato di software per interpretare il segnale ricevuto dal rivelatore. Il risultato ottenuto dal programma è un grafico che mostra l'andamento dell'intensità della radiazione diffratta in funzione dell'angolo 2θ su cui è posizionato il rivelatore; questo grafico si chiama ‘pattern’ ed è caratteristico per ciascuna tipologia di materiale cristallino. Questa tecnica è stata usata per analizzare la struttura del MIL-53(Al) prima e dopo i vari trattamenti.⁵³

1.2.5 Analisi termogravimetrica

L'analisi termogravimetrica è una tecnica in cui la massa di una sostanza viene monitorata in funzione della temperatura o del tempo quando il campione viene sottoposto ad un programma a temperatura controllata in atmosfera controllata. Il dispositivo è costituito da un supporto (pan) in cui viene inserito il campione da analizzare, che viene posto su una bilancia di precisione. Il ‘pan’ con all'interno il campione viene posto all'interno di una fornace che riscalderà o raffredderà il campione a seconda delle esigenze.⁵⁴ Questa tecnica è stata usata per determinare la stabilità termica e la decomposizione del materiale.

1.2.6 Fisisorbimento dell'azoto

Il fisisorbimento dell'azoto è un metodo che si basa sull'adsorbimento fisico dell'azoto gassoso alla temperatura dell'azoto liquido (77 K). I materiali porosi sono ben noti per la loro capacità di assorbire specie sia liquide che gassose. Quando un solido viene esposto a un fluido gassoso, le molecole di gas vengono adsorbite dalla superficie per un tempo finito, dopo di che vengono desorbite e sostituite da altre. Il volume adsorbito dipende dalla pressione alla quale si verifica l'adsorbimento e dalla natura del gas e del solido. La quantità di gas assorbito vengono misurate (volumetricamente o gravimetricamente) in funzione della pressione relativa. Dall'isoterma risultante, è possibile caratterizzare il materiale a seconda della sua porosità, e tramite apposite equazioni (BET) calcolare il volume dei pori, l'area superficiale e la dimensioni dei pori.^{55,56}

1.2.7 Microscopia elettronica a trasmissione e a scansione

Un microscopio elettronico produce la sua immagine ultra fine facendo passare un fascio di particelle di elettroni attraverso lenti elettrostatiche o elettromagnetiche. Tuttavia, poiché la lunghezza d'onda di un fascio di elettroni è molto più breve. Una lunghezza d'onda più corta significa una risoluzione più alta. I microscopi elettronici a trasmissione (TEM) formano immagini da elettroni trasmessi attraverso il campione, mentre i microscopi elettronici a scansione (SEM) utilizzano elettroni riemessi dalla superficie del campione. Mentre il TEM è stato impiegato per analizzare la struttura interna del materiale e verificare la presenza di particelle di nichel all'interno dei pori, il SEM ha permesso di esaminare in dettaglio le superfici delle varie forme del MIL-53(Al).^{57,61}

1.2.8 Risonanza magnetica nucleare

La spettroscopia di risonanza magnetica nucleare (NMR) è una tecnica di chimica analitica che è stata utilizzata per determinare il contenuto e la purezza di un campione, nonché la sua struttura molecolare. Uno strumento NMR consente di analizzare la struttura molecolare di un materiale osservando e misurando l'interazione degli spin nucleari quando posizionati

in un potente campo magnetico. Quando un nucleo che possiede un momento magnetico (come un nucleo di idrogeno 1H, o nucleo di carbonio 13C) viene posto in un campo magnetico forte, inizierà a roteare, come una trottola. Se il campione posizionato in questo campo magnetico viene irradiato con onde radio alla stessa frequenza della frequenza di precessione, è possibile ottenere uno spettro NMR.⁵⁸ Da uno spettro NMR si possono ottenere informazioni sulla composizione dei gruppi atomici all'interno della molecola, sugli atomi adiacenti, sulla dinamica molecolare, e informazioni quantitative utili per determinare la struttura molecolare.

1.2.9 Riduzione a temperatura programmata

La riduzione programmata della temperatura viene utilizzata per determinare la riducibilità dei catalizzatori. In questo metodo, i catalizzatori riducibili sono esposti al flusso della miscela gassosa riducente tipicamente H₂ in Ar. Durante l'analisi un ossido di metallo reagisce con l'idrogeno per formare un metallo puro, secondo la reazione chimica mostrata qui: M_xO_y + yH₂ → xM + yH₂O. Nel corso dell'analisi la quantità di idrogeno nella miscela di argon/idrogeno all'interno dell'analizzatore diminuisce e la proporzione tra i due gas si sposta nella direzione dell'argon, così come la conducibilità termica della miscela. Un rilevatore di conducibilità termica (TCD) viene utilizzato per misurare i cambiamenti nella conduttività termica del flusso di gas. La quantità totale di H₂ consumata è determinata dall'area sotto il picco e viene utilizzata per calcolare il grado di riduzione e l'ossidazione media del materiale solido dopo la riduzione.^{59,60}

1.2.10 Misurazioni catalitiche

I test di attività e stabilità catalitica sono stati eseguiti utilizzando un reattore tubolare Hastelloy-X (PID Eng. & Tech). Il reattore Hastelloy X è dotato di una piastra porosa e una termocoppia, ha una lunghezza di 305 mm, un diametro esterno e interno di 14,5 e 9 mm rispettivamente, e un volume interno di 20 ml. I test catalitici sono stati condotti a pressione atmosferica in un reattore a flusso fisso continuo a forma di U in quarzo. Circa 20 mg di polvere sono stati caricati su un tappo di lana di quarzo. Questa massa è stata scelta per fornire informazioni sulla cinetica intrinseca e i limiti di diffusione, poiché con una bassa quantità di massa sono garantiti sia bassi livelli di conversione, sia assenza di effetti di trasporto. Prima della reazione catalitica, si applica il pretrattamento dei catalizzatori laddove ciascun campione è stato ridotto termicamente in situ a 800 °C per circa 2 ore in un flusso di H₂/Ar al 5% (30 ml*min⁻¹). In questo passaggio, l'ossido di nichel NiO viene convertito in Ni⁰ attraverso la seguente equazione: NiO (s) + H₂ (g) → Ni⁰ (s) + H₂O (g). La conversione di NiO in Ni⁰ è un passaggio fondamentale per evitare l'ossidazione di CH₄ e la perdita di reagenti. Dopo aver raffreddato la temperatura a circa 200 °C, sono stati introdotti i reagenti (rapporto molare CH₄/CO₂ = 1:1), la temperatura di reazione è stata aumentata (5 °C*min⁻¹) da 200 °C a 800 °C.

1.3 Risultati e discussione

Dalle approssimazioni termodinamiche è stato rivelato che il legame chimico più debole nella catena del PET è il legame estere, indicato dalla freccia rossa nella Figura 1.9. Pertanto, è necessaria meno energia per rompere questo legame e quindi i meccanismi di attacco degli agenti degradanti si concentrano ampiamente su questo legame. I due diversi tipi di sintesi del MIL-53 (Al) si concentrano entrambi sull'idrolisi di questo legame.

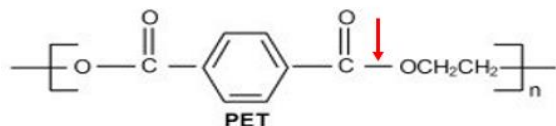


Figura 1.8 Idrolisi del legame estere del PET

1.3.1 Sintesi in un solo step del MIL-53(Al) e preparazione del catalizzatore

Dopo la sintesi in condizioni idrotermali, il MIL-53(Al) è stato caratterizzato da un diffraffogramma a raggi X (Figura 1.9). Il modello di diffrazione indica chiaramente che il materiale è ben cristallino e che i picchi ottenuti corrispondono a quelli MIL-53(Al) riportato in letteratura. Inoltre, dal confronto con il MIL-53(Al) sintetizzato usando acido tereftalico puro si può dire che è possibile usare il PET come fonte di acido tereftalico.

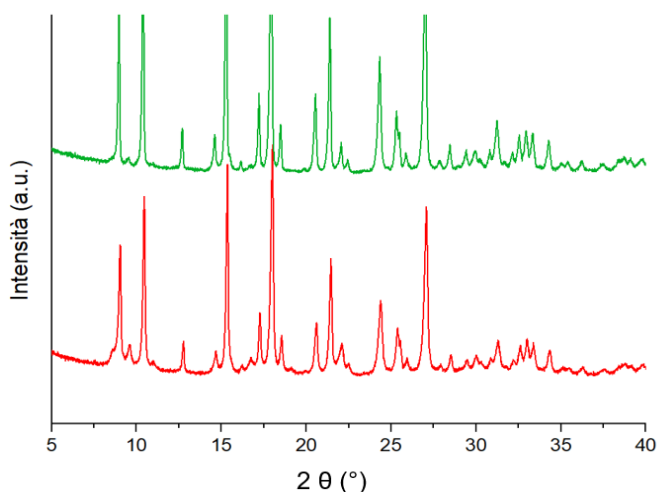


Figura 1.9 Pattern di diffrazione ai raggi X del: MIL-53-PET (linea rossa), MIL-53-BDC (linea verde)

Dalle immagini SEM (figura 1.10) si è potuto notare che in entrambi i casi si ottengono cristalli di grandi dimensioni, ma con una forma più definita quando si usa il BDC commerciale. Inoltre, è stato notato che le dimensioni dei cristalli del MIL-53(Al) sintetizzato utilizzando il PET sono relativamente più grandi di quelle ottenute dal BDC commerciale. Questa osservazione può trovare ulteriore conferma nelle differenze di cristallinità relativa osservata dal pattern in Fig 1.9.

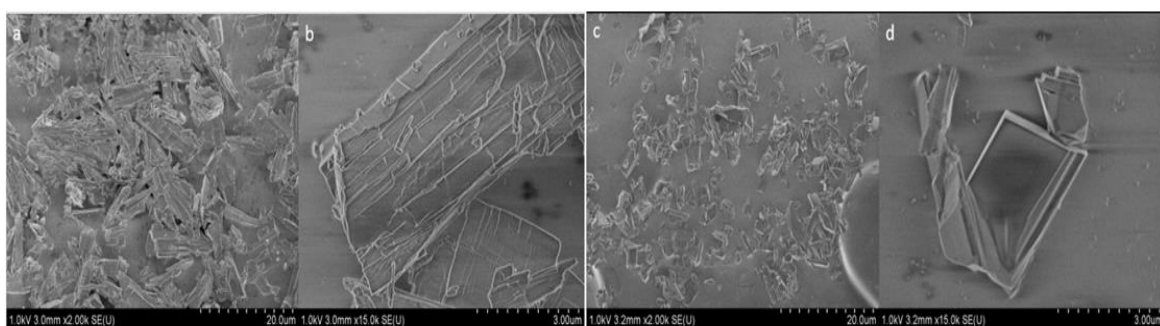


Figura 1.10 Immagini rappresentative di microscopia a scansione del: (a) e (b) MIL-53-PET attivato, (c) e (d) MIL-53-BDC attivato

La curva termogravimetrica del MIL-53(Al) non attivato ha mostrato due perdite di peso tra la temperatura ambiente e 900 °C. La prima si ha tra 330 e 430 °C, ed è dovuta alla presenza di molecole di DMF e di altre impurità all'interno di pori. La seconda perdita di peso è dovuta alla decomposizione dei linker BDC, e si ha quando la temperatura è compresa tra 500 e 600 °C. Al di sopra di 600 °C, i cristalli MIL-53(Al) vengono trasformati in gamma allumina (Al_2O_3). Il comportamento termico del MIL-53 attivato a 330°C per 72 h è caratterizzato da due perdite di peso. La prima, da 25 a 100 °C, corrisponde alla rimozione di un equivalente di molecole d'acqua dai pori del MIL-53(Al). La seconda perdita di peso, da 500 a 560 °C, corrisponde nuovamente alla decomposizione dei linker BDC. A 900 °C, il residuo finale è di nuovo Al_2O_3 . Dalla formula chimica di MIL-53(Al) si evince che in teoria il rapporto tra il numero di mole di Al e BDC deve essere uguale a uno. Dalla curva TG è possibile conoscere la quantità di BDC e Al_2O_3 e quindi calcolare il rapporto, che nel mio caso è intorno a uno, quindi si può concludere che è stato ottenuto MIL-53(Al) puro e che non è presente PET.

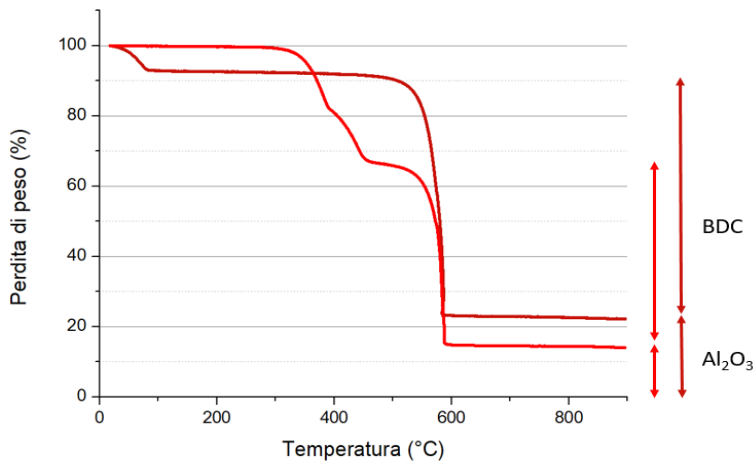


Figura 1.11 Curva termogravimetrica del: MIL-53-PET non attivato (linea rossa), e del MIL-53-PET attivato (linea rosso scuro)

Le isoterme di adsorbimento-desorbimento dell'azoto del MIL-53(Al) prima e dopo l'impregnazione con il nichel hanno mostrato isoterme di tipo I, caratteristiche di un materiale microporoso. Dalla figura 1.12, si è potuto notare che le isoterme di adsorbimento non hanno mostrato alcuna isteresi al desorbimento, e che il maggiore adsorbimento di azoto è stato verificato a pressione relativa relativamente bassa e poi è stato raggiunto un plateau.

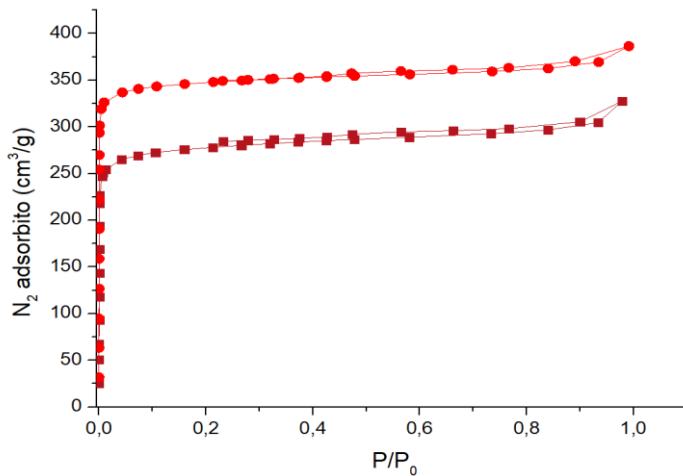


Figura 1.12 Isoterme di adsorbimento-desorbimento dell'azoto del MIL-53-PET attivato (linea rossa) e del MIL-53-PET impregnato

Dopo l'impregnazione con il nichel è stato osservato dal fisisorbimento dell'azoto una perdita del volume dei pori, il che significa che il nichel sta bloccando i pori. Per essere certi che il nichel sia effettivamente all'interno dei pori e non blocchi solo l'ingresso dei pori, è stato controllato il PXDR dopo l'impregnazione (figura 1.13).

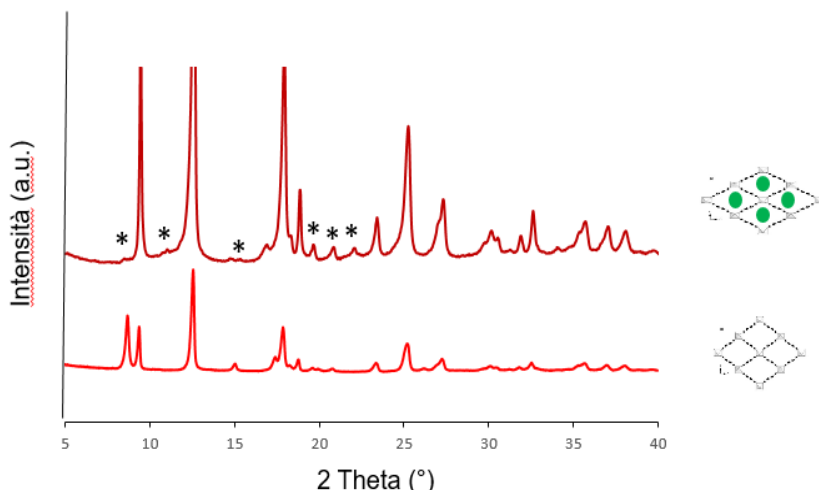


Figura 1.13 Pattern di diffrazione ai raggi X del: MIL-53-PET attivato (linea rossa), e del MIL-53-PET impregnato (linea rosso scuro)

Il MIL-53(Al) mostra flessibilità strutturale, infatti la struttura del MIL-53(Al) che è completamente aperta dopo l'attivazione ad alta temperatura, cambia drasticamente sotto adsorbimento molecolare perché le dimensione dei pori si adattano alle molecole ospiti, e questo fenomeno ha una conseguenza diretta sul XRD pattern. Nuovi picchi (indicati dagli asterischi) sono apparsi dopo l'impregnazione con il nichel e non sono attribuibili alla forma chiusa o aperta, ma ad una forma intermedia, suggerendo che il nichel si trova all'interno dei pori. L'intima miscelazione tra i precursori del nichel e il supporto poroso (MIL-53(Al)) è inoltre evidenziata da analisi termogravimetriche (figura 1.14) che hanno mostrato una perdita di peso di circa il 15% tra 200 °C e 450 °C che corrisponde alla degradazione del sale nitrato negli NOx. Alla luce di questi profili TG, abbiamo deciso di impostare la temperatura di calcinazione del Ni/MIL durante la preparazione del campione a 500 °C, una temperatura abbastanza elevata da degradare i linkers ma sufficiente a garantire lo sviluppo della porosità e un'ampia superficie.

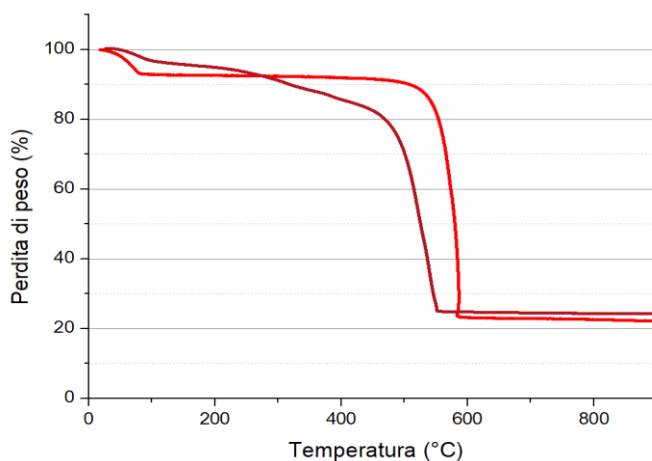


Figura 1.14 Curva termogravimetrica del: MIL-53-PET non attivato (linea rossa), e del MIL-53-PET attivato (linea rosso scuro)

Dopo calcinazione a 500 °C, è stato osservato dal pattern XRD (figura 1.15) la presenza di nuovi picchi dovuti alla formazione di alluminato di nichel. Non sono stati evidenziati picchi attribuibili alla presenza di NiO cristallino, a conferma dell'ipotesi di un'intima miscelazione tra Ni e il supporto.

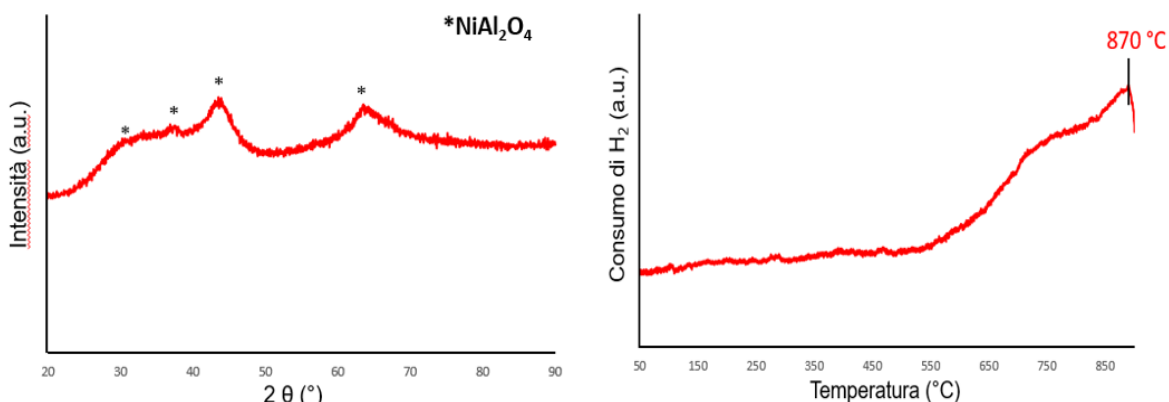


Figura 1.15 Pattern di diffrazione ai raggi X del MIL-53-PET calcinato (sulla sinistra), riduzione a temperatura programmata del MIL-53-PET calcinato (sulla destra)

La dispersione di Ni^{2+} nella forma dello spinello NiAl_2O_4 è stata dimostrata anche dal profilo TPR (riduzione a temperatura programmata) del MIL-53-PET calcinato (figura 1.15), che ha mostrato solo un picco con massimo centrato ad una temperatura di circa 870 °C, il che significa che il nichel è presente in una sola forma, e che è disperso in modo omogeneo nella matrice Al_2O_3 .

Le immagini SEM hanno mostrato che i cristalli MIL-53 sono stati trasformati in strati sovrapposti di Al_2O_3 , pur mantenendo la stessa morfologia.

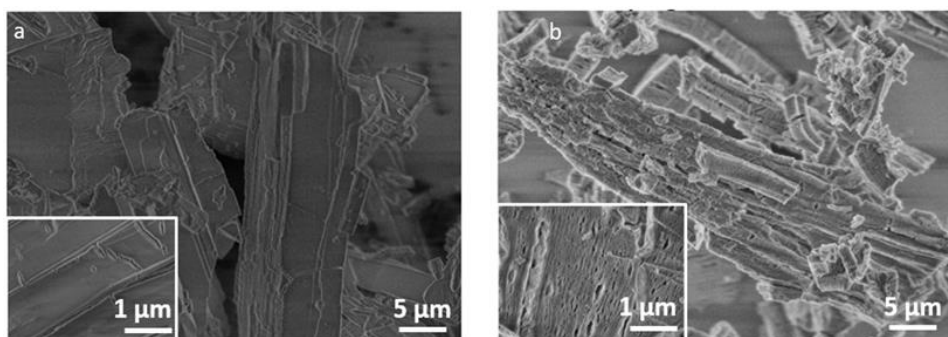


Figura 1.16 Immagini rappresentative di microscopia elettronica a scansione del: (a) MIL-53-PET impregnato, e (b) del MIL-53-PET calcinato

Tale morfologia è in linea con quella dedotta dall'isoterma di adsorimento-desorbimento dell'azoto (figura 1.17) che ha mostrato le caratteristiche tipiche dei materiali mesoporosi stratificati (isoterma di tipo IV), vale a dire un aumento progressivo del volume di N_2 adsorbito, e un'isteresi estesa da 0,7 a 1. È stato possibile concludere che il nichel è ben disperso nella matrice Al_2O_3 e che è stato ottenuto un materiale mesoporoso di alluminato di Ni.

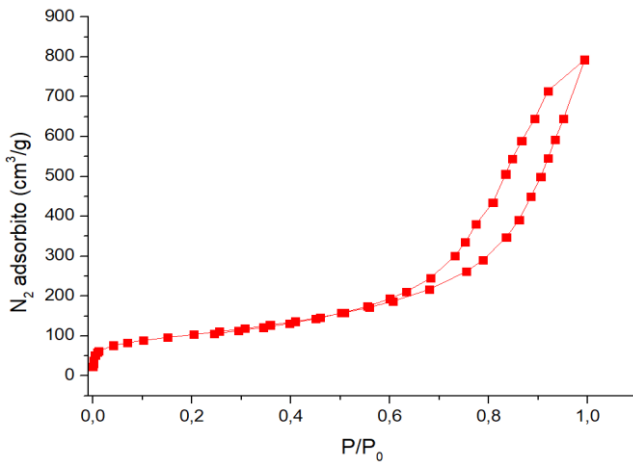


Figura 1.17 Isoterma di adsorbimento-desorbimento dell'azoto del MIL-53-PET calcinato

Prima dei test catalitici, il materiale calcinato ($\text{Ni}^{2+}@\text{Al}_2\text{O}_3$) è stato ridotto tramite un flusso di idrogeno per ottenere Ni^0 , che costituisce la fase attiva per la reazione di reforming secco del metano. Il consumo di H_2 durante il TPR è stato utilizzato per stimare la quantità di Ni^{2+} riducibile presente nel campione contenente nichel. Il contenuto di nichel previsto è prossimo al 5% in peso. Il pattern XRD del campione ridotto a 800 °C è mostrato nella Figura 1.18, insieme a quello precedente la riduzione. La riduzione di $\text{Ni}^{2+}@\text{Al}_2\text{O}_3$ a $\text{Ni}^0@\text{Al}_2\text{O}_3$, porta alla formazione di nuovi picchi di diffrazione a $2\theta = 44,7^\circ$, $51,56^\circ$, $67,15^\circ$ e $76,37^\circ$. Sono ancora presenti bande attribuibili a una fase a base di allumina ma sono leggermente spostate (rispetto a quelle precedenti la riduzione) verso posizioni caratteristiche della γ -allumina, questo attesta l'estrazione della specie Ni dalla matrice di ossido verso la superficie dei pori.

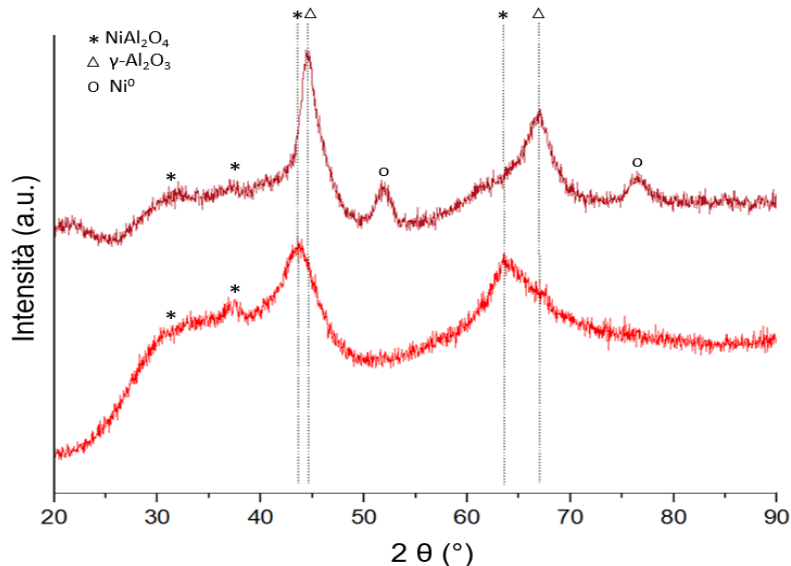


Figura 1.18 Pattern di diffrazione ai raggi X del MIL-53-PET calcinato (linea rossa), e del MIL-53-PET ridotto (linea rosso scuro)

La Figura 1.19 mostra la distribuzione della dimensione dei pori e l'isoterma di adsorbimento-desorbimento del campione ridotto. L'isoterma del MIL-53(Al) ridotto mostra ancora un'isteresi simile a quella riportata dal materiale calcinato, quindi si ha ancora

un materiale mesoporoso stratificato. La quantità di N_2 adsorbita a $P/P_0 > 0,8$ è superiore a quella precedente la riduzione, e questo indica la formazione di ulteriori mesopori di grandi dimensioni all'interno del materiale.

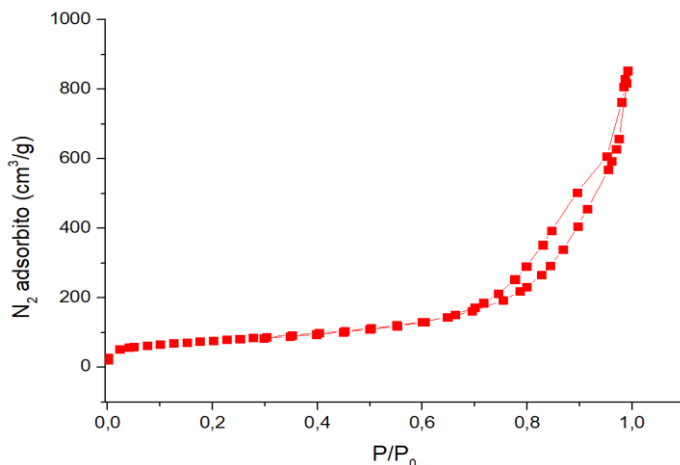


Figura 1.19 Isoterma di adsorbimento-desorbimento dell'azoto del MIL-53-PET ridotto

1.3.2 Sintesi in due step del MIL-53(Al) e preparazione del catalizzatore

Al fine di ridurre ulteriormente l'impatto economico, è stata utilizzata la boehmite come fonte di alluminio anziché AlCl_3 . Per fare ciò, non è stato possibile applicare una sintesi in un'unica fase in quanto necessita della presenza di condizioni acide per idrolizzare il PET, condizioni garantite dall'uso di AlCl_3 ma non dall'uso della boehmite. Quindi è stata sviluppata una sintesi in due fasi. L'alcolisi del PET è il primo step e viene generalmente eseguita con l'uso di idrossido di sodio e glicole etilenico. Una polvere bianca di Na_2BDC , che si è formata nel corso della reazione in EG, è stata separata, sciolta in acqua e acidificata con una quantità in eccesso di acido solforico per ottenere acido tereftalico e sulfato di sodio. La figura 1.20 mostra dettagliatamente la procedura che è stata seguita per ottenere acido tereftalico.

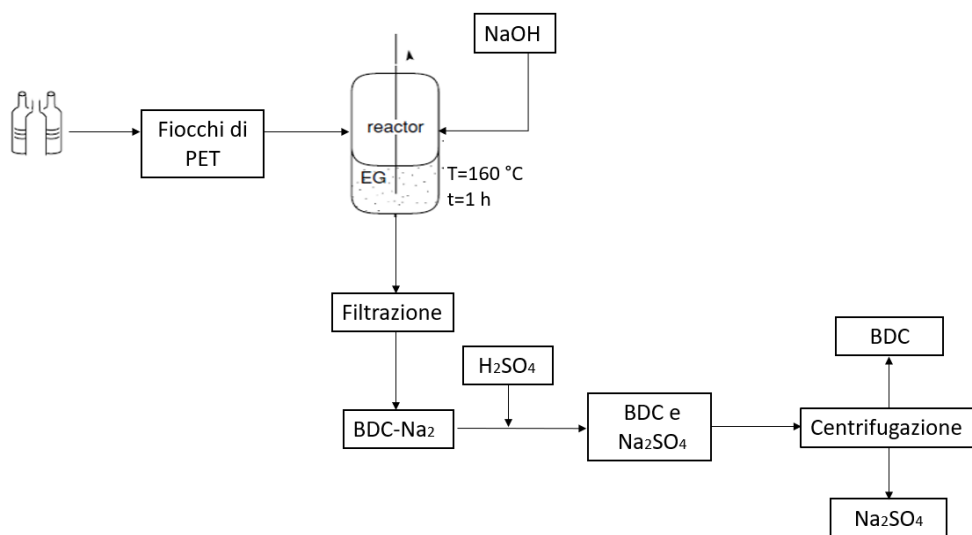


Figura 1.20 Schema dettagliato della produzione di acido tereftalico partendo da bottiglie di plastica

Il BDC separato è stato sciolto in dimetilsolfossido (DMSO) e la sua purezza è stata esaminata dall'analisi FT-1H NMR. Dallo spettro NMR mostrato nella figura 1.21 si può vedere che è stato ottenuto il BDC puro, in effetti ci sono solo due picchi. Il primo $\delta = 2,52$ ppm è dovuto all'uso di DMSO come solvente, il secondo $\delta = 8,06$ ppm è dovuto alla presenza di BDC.

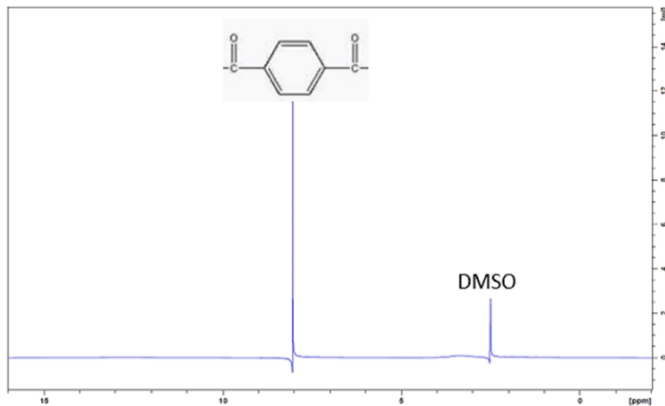


Figura 1.21 Spettro 1H-NMR di BDC ottenuto dall'alcolisi del PET riscaldato a 160 °C per 1 ora.

Nella seconda fase, l'acido tereftalico ottenuto nella prima fase è stato utilizzato come reagente insieme a una fonte di alluminio (boehmite o cloruro di alluminio esaidsrato) per sintetizzare MIL-53 (Al). Dopo la sintesi in condizioni idrotermali, il campione MIL-53(Al) è stato caratterizzato da un diffratogramma a raggi X. I modelli di diffrazione dei campioni sintetizzati mostrano un'elevata cristallinità con riflessi nell'intervallo 29 di 4°-40° che sono caratteristici del MIL-53(Al). I pattern XRD dei framework MIL-53(Al) preparati con cloruro di alluminio e boehmite (MIL-53-AlCl₃ e MIL-53-AlO(OH), rispettivamente) sono per lo più identici e in buon accordo con quelli ottenuti dalla sintesi in un solo step.

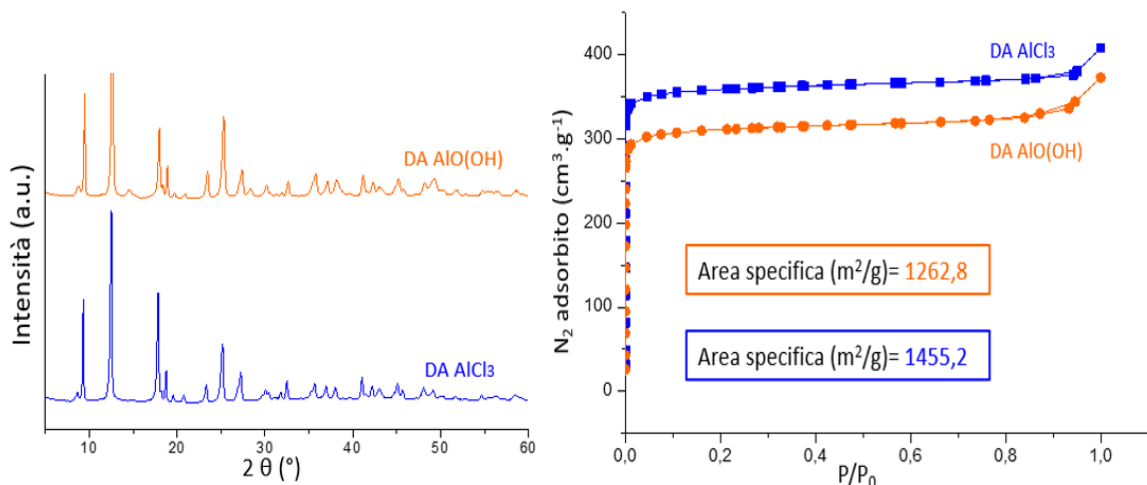


Figura 1.22 Pattern di diffrazione ai raggi X del MIL-53(Al) sintetizzato usando AlCl₃ (linea blu) e AlO(OH) (linea arancione) sulla sinistra, e isoterma di adsorbimento-desorbimento dell'azoto del MIL-53-AlCl₃ (linea blu), e del MIL-53-AlO(OH) (linea arancione) sulla destra.

Le misure isometriche di adsorbimento-desorbimento dell'azoto su campioni MIL-53(Al) hanno mostrato isoterme di tipo I, caratteristiche di un materiale microporoso. Si può inoltre notare che il volume adsorbito dal campione sintetizzato usando il boehmite è più piccolo di quello sintetizzato usando AlCl₃.

Focalizzando l'attenzione sul campione sintetizzato usando la boehmite come fonte di alluminio, dall'assorbimento dell'azoto si può vedere che dopo l'impregnazione del nichel si è verificata una perdita molto piccola del volume dei pori. Ciò è dovuto al fatto che le particelle di nichel non sono presenti all'interno dei pori ma solo sulla superficie della matrice.

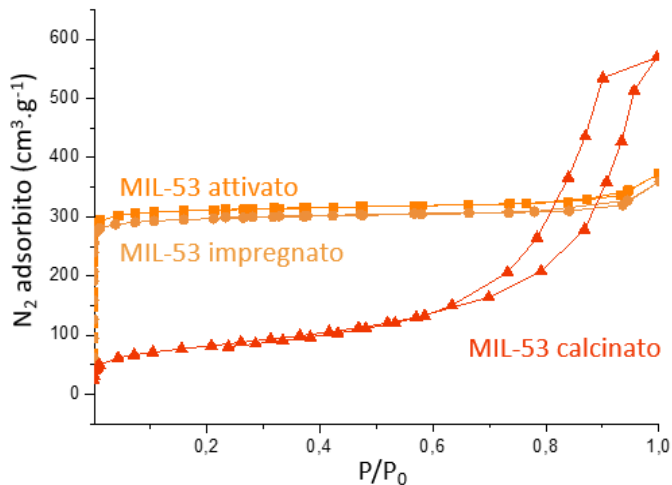


Figura 1.23 Isoterma di adsorbimento-desorbimento dell'azoto del MIL-53-AlO(OH) dopo l'attivazione, dopo l'impregnazione con il nichel e dopo la calcinazione a 500°C.

Questo può essere ulteriormente confermato dal modello XRD, rilevando che i picchi dopo la calcinazione non sono dovuti alla presenza di alluminato di Ni ma alla presenza di gamma allumina.

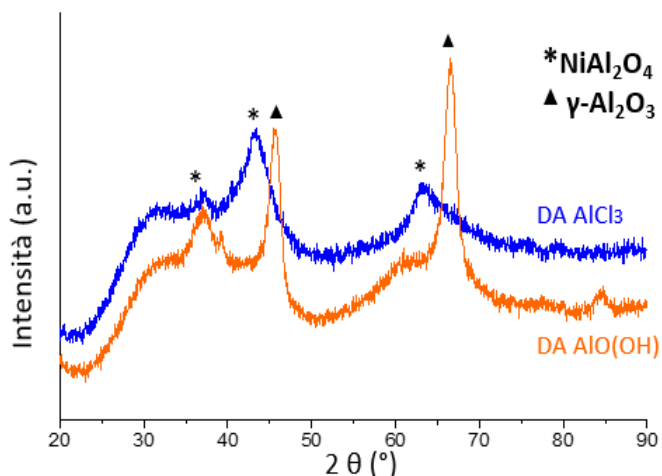


Figura 1.24 Pattern di diffrazione ai raggi X del MIL-53-AlCl₃ (linea blu) e del MIL-53-AlO(OH) (linea arancione)

2. Introduction

In the last twenty years, there has been an increase in energy consumption, mainly due to a rapid growth of human population.¹ To satisfy the growing demand for energy, fossil fuels such as oil, natural gas and coal are used. The dependence on fossil fuels to meet energy demand has created environmental issues by the production of greenhouse gases (GHG). Methane and carbon dioxide constitute a major part of GHG and have the key contributions in climate-change, affecting productivity, natural ecosystems, agriculture, and society.² Although the concentration of methane in the atmosphere is lower than CO₂, surprisingly caused about 20% of global warming.³⁻⁴ Traditionally, methane is produced from two sources; firstly, it comes from natural sources such as termites, grasslands, fires, lakes and wetlands and, secondly, from human activities such as coal mining, landfills, oil and gas processing, and agricultural activities.⁵ It is therefore necessary to reduce the amount of methane and carbon dioxide in the atmosphere; to do this, extensive research has been carried out to find effective ways of converting these greenhouse gases into other valuable products. The most common and most commonly used industrial method is reforming, which converts hydrocarbons into syngas (CO and H₂). Reforming can take place through three process: steam reforming of methane (SRM), partial oxidation of methane (POM) and dry reforming of methane (DRM).⁶ Among the three processes mentioned above, DRM is the most promising, as it utilizes two abundant greenhouse gases (CO₂ and methane) to produce syngas that is important for industries, and at the same time can reduce the net emissions of greenhouse gases to the environment.⁷

Dry reforming of methane offers valuable environmental benefits: biogas utilization⁸, removal of GHG (methane and carbon dioxide) and conversion of natural gas with a high carbon dioxide content to valuable syngas.⁹ Dry reforming of methane yielded a lower syngas ratio (H₂/CO=1), which is suitable for the synthesis of oxygenated chemicals¹⁰ and hydrocarbons from Fischer-Tropsch synthesis. In addition, the DRM process is also cheaper than other methods since it eliminates the complicated gas separation of end products.¹¹ The reaction of dry reforming of methane is endothermic, and to take place requires high temperatures. Therefore, catalysts that significantly reduce the reaction temperature, and maximize the production of syngas, are needed to make this reaction happen.¹²

At the present, the most commonly used catalysts in DRM are based on noble metals which have the disadvantage of being rare and expensive.¹³ Hence, efforts are being made to develop catalysts based on more economical and abundant active phases. Among the family of transition metals that represents the best alternative, nickel is the most promising one.¹⁴¹⁵ However, existing catalysts have two important drawbacks: the sintering of metals due to the high temperature, and the formation of carbon deposits which leads to the loss of catalyst activity.¹⁶⁻¹⁷ To resolve these problems and design resistant catalysts, mesoporous supports were used with a high specific area where nickel nanoparticles can be occluded¹⁸⁻¹⁹ In this view, metal-organic frameworks (MOFs) have attracted attention owing to their high surface area, low densities, and high porosity, thermal stability and adjustable chemical functionalities.²⁰ MOFs are crystalline solids composed of metal ions (normally called nodes) linked by organic ligands (as linkers). These materials often form three-dimensional extended frameworks with porous structures. The linkers are often organic molecules with specific functional groups such as carboxylate, that can coordinate to metal nodes such as Zn, Al, Fe. Moreover, the pore dimensions and surface chemistry of MOFs can be

systematically modulated by modifying the organic ligands or changing metal ions used in the synthesis of these materials.²¹

In this work, ($\text{Al(OH)}[\text{O}_2\text{C}-\text{C}_6\text{H}_4-\text{CO}_2]$), one of the most studied MOFs and often denoted as MIL-53(Al) was synthesized by the hydro(solvo)thermal method, then nickel was added to the original MIL-53(Al) structure to investigate its effect as a catalyst, in particular in the reaction of dry reforming of methane.²² To synthesize MIL-53 in the traditional way two expensive precursors are needed: terephthalic acid and aluminum chloride. Moreover, during the preparation of the catalyst there is a loss of about 70% of the starting MOF. To limit costs and synthesize MIL-53(Al) in a more sustainable and green way, in this work the waste of PET bottles it will be use as direct source of BDC acid linker during the synthesis of MIL-53(Al). The PET-derived MIL-53 materials showed even better textural properties than that of commercial BDC (Sigma-Aldrich).

2.1 Metal-organic frameworks (MOFs): definition, properties and structures

Metal-organic frameworks (MOFs) have attracted foremost attention in recent past because of their potential applications in chemical separations, heterogeneous catalysis, gas adsorption applications, proton conduction, sensing and drug delivery. These inorganic-organic hybrid materials are a class of hybrid microporous materials built up from the combination of metal ions [secondary building units (SBUs)] with organic linkers, using strong bonds (reticular synthesis) to create open crystalline frameworks with permanent porosity.²³

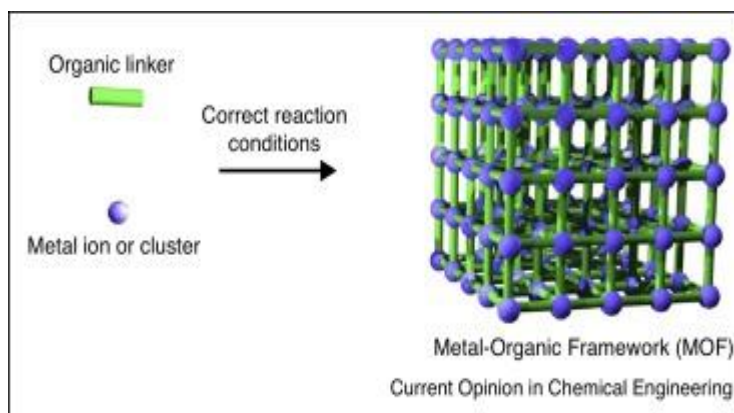


Figure 2.1 Schematic representation of metal-organic frameworks

MOFs are characterized by large surface areas, tunable chemical properties, very low density and narrow pore size distributions compared to the zeolite and carbon materials makes them suitable for gas adsorption and storage applications.

The choice of the initial building units makes it possible to vary some parameters, such as the pore size (to increase pore diameter from 0 to 98 Å), density, as well as the specific surface area, which opens up new ways to produce materials with tailored physicochemical properties. MOFs have been proven to be outstanding candidates for bridging the gap between zeolites and mesoporous silica.²⁴ There are two ways to tune the pore size and provide desired surface chemistries: direct assembly of new MOFs from particular metal nodes and organic linkers, and the pre-constructed robust precursor MOFs are modified by the post-synthesis.²⁵

Porous solids can be classified into three categories based on sizes of their pores: microporous, mesoporous and macroporous materials. Solids which have a pore size of 2

nm or below are known as microporous. The mesoporous solids are in the range of 2 nm–50 nm and above 50 nm are known as macroporous. Like zeolites and aluminophosphates, metal–organic frameworks, also known as porous coordination polymers (PCPs), are crystalline porous materials, but unlike zeolites they are not purely inorganic compounds and belong to organic–inorganic hybrid compounds. The major disadvantage of the MOF is the low thermal stability compared to zeolites and carbon based adsorbents which restricts their large scale industrial applications. In contrast to zeolites, for which a relatively limited number of structures exists, MOFs provide diverse combinations of coordination chemistry, organic linkers and terminated ligands (F-, OH- and H₂O, among others), which make it possible to design an almost infinite variety of MOF structures.²⁶ To date, there are more than 20,000 different structures of MOFs being reported and studied.²⁷

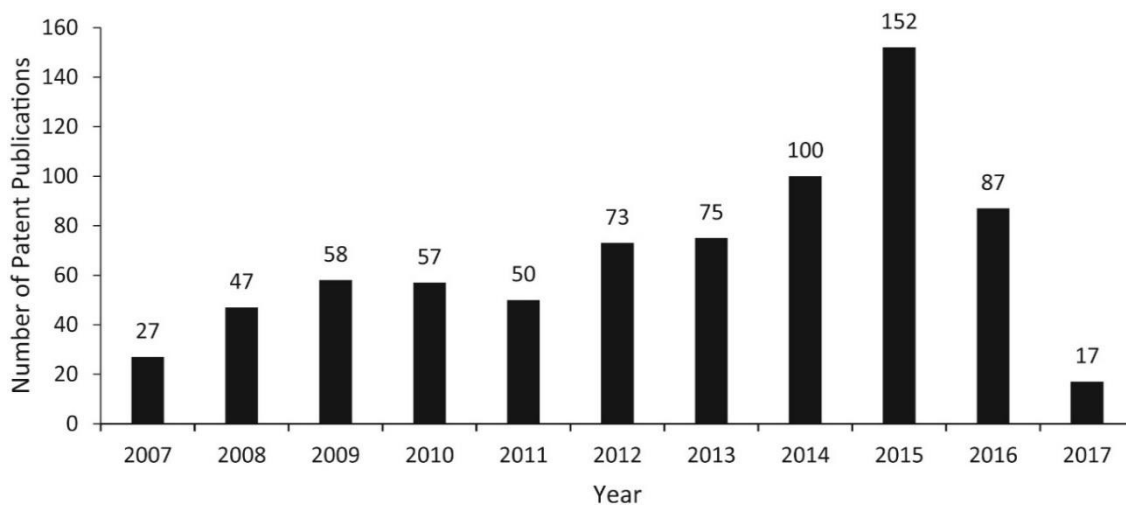


Figure 2.2 Number of patent publications from 2007 to 2017, according to the World Intellectual Property Organization database.

The structural stability of MOFs is a very important factor. The structure of the materials should be stable upon exposure to high temperatures. If the structure of the material is affected, it leads to changes in the surface area, pore size and pore volume. The adsorption of the gases decreases depending on the pore size. Zeolites have high thermal stability compared to MOFs but these materials require high temperatures for regeneration of adsorbents and they can be used only in shape selective separation of gases. Because their pores are like molecular sieves which can absorb only certain specific gases, understanding the multicomponent adsorption equilibrium is essential for designing adsorption-based separation processes. The MOFs have an additional advantage as they can be regenerated under milder conditions than most zeolites which require considerable heating and high costs.²⁸

2.1.1 Metal Ions and organic ligands as Building Units of MOFs

Metal ions, with a preferred coordination number and geometry, in combination with divergent linker molecules can create extended networks in one, two, or three dimensions. Metal center in MOF structure are usually metal clusters, like metal–carboxylate clusters, metal–azolate clusters. First row transition metals are well known to be able to coordinate with carboxylate groups under hydro(solvothermal) conditions and these metal centers are often chosen because of the coordination properties of these transition metals. The organic linkers are multidentate organic ligands, such as 1,4 benzenedicarboxylate (BDC) and 1,3,5-benzenetricarboxylate (BTC) which offers advantages due to their rigidity and consequent

tendency to form rigid metal carboxylate clusters. The choice of ligand is particularly important because the structure and length of the ligand will directly affect the size and architecture of the framework. Ligands with this linear orientation are known to generate square planar or cubic MOFs in the presence of transition metal ions. Many MOFs reported in the literature have a cubic architecture composed of orthogonal intersecting channels exposed at the faces of the cube through which guest solvents can pass.²⁷

MOF materials can be classified into different families according to the dimensionality of the inorganic framework (Figure 2.3)²⁹:

- 1D inorganic chains such as MIL-53
- 2D inorganic layers that are separated by organic pillars such as MIL-71
- 3D structures such as MIL-73 with 3D porous channels

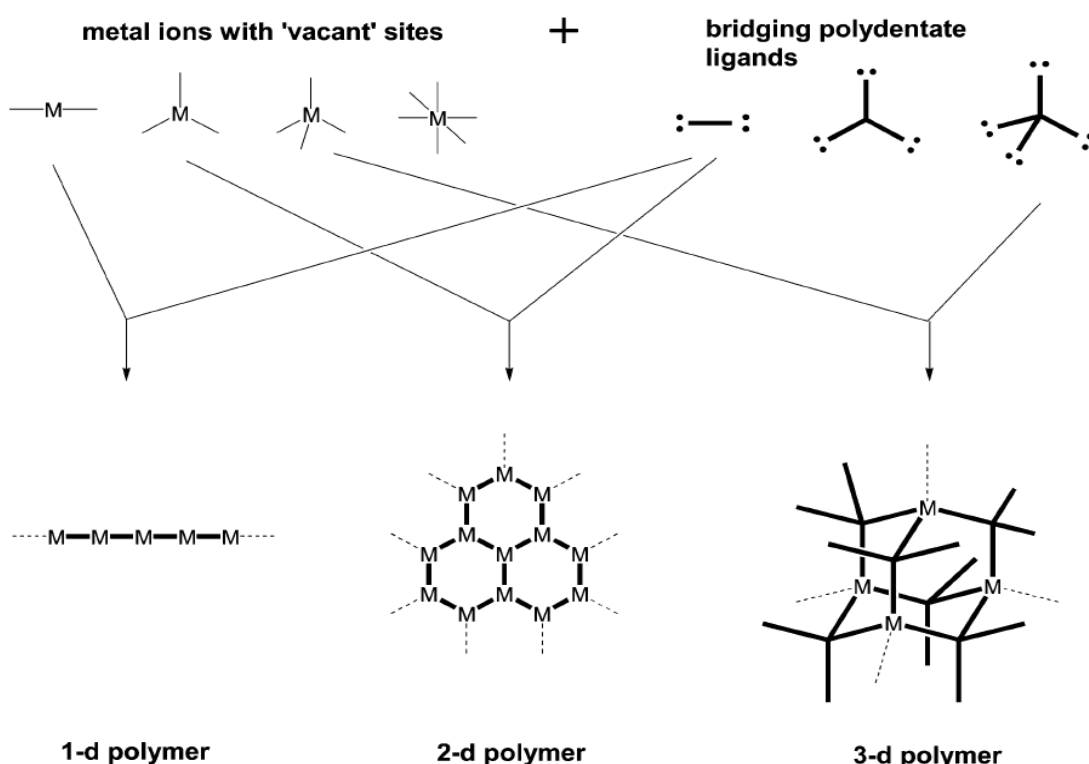


Figure 2.3 The building block, or ‘modular’, principle behind forming coordination polymers.

2.1.2 Open Metal Sites in MOFs

In some MOFs, metal atoms are partially coordinated by solvent molecules from the synthesis. It is important to activate MOFs at elevated temperature to remove the solvent and open the void space for desired guest molecules. Removing these coordinated solvent molecules leaves coordinatively unsaturated open-metal sites that have been shown to promote high gas uptake, especially for H₂ adsorption. The open space created after removal of coordinated solvent molecules is called open metal site.³⁰⁻³¹ Bae et al showed that in a carborane-based MOF, removal of coordinated dimethylformamide (DMF) increased CO₂ and CH₄ adsorption and led to high selectivity for CO₂ over CH₄.³² From this concept it can be expected that adsorption selectivity can be enhanced.

2.2 Methods of synthesis of metal-organic frameworks

Different types of synthesis methods have been applied in the literature for MOF materials. Among them, classical hydro(solvo)thermal synthesis, microwave and electrochemical synthesis, mechanochemical and sonochemical techniques. Hydrothermal/solvothermal synthesis is a facile and prominent method to form a wide variety of organized structures that are difficult to obtain with other available techniques. MOF synthesis conditions in these studies were carried out in order to obtain high yields of solid products for industrial applications. MOF synthesis occurs simply by using soluble salts as a source for the metal component such as chlorides, metal nitrates or acetates; and a polar organic solvent such as an amine or amide as a source of inorganic ingredients. All reagents (metal oxide precursors, pH stabilizer, and H₂O/solvent) are mixed together, introduced into a Teflon-lined stainless steel autoclave, and heated. The crystallization and growth of particles may be controlled by process parameters, such as temperature, pressure, and time. Applying the required temperature produces an autogenous pressure. After the reaction is complete, the autoclave is cooled to room temperature and the product is washed and dried. MOFs may easily carry 50 to 150 wt% of occluded solvent. This is an order of magnitude higher than a preparation of zeolite oxide or base metal. Therefore, it is advisable to remove the large quantity of adsorbed solvent before proceeding with a high thermal activation.

MOFs derive from a crystallization process; in these structures water, organic solvents and residues fill the pores. Therefore, encapsulation of guest molecules in the porous structure and the presence of inorganic molecules play a fundamental role in the formation of MOFs. When working with MOFs, attention must also be paid to postsynthetic treatments, such as purification, activation, and reproducibility.

Purification is very important for the catalytic applications of MOFs, since the impurities of the reaction by-products can limit the catalytic activity and decrease the possibility of absorption. Purification is usually carried out with a high temperature solvent.

To activate the material, it is necessary to empty the pores, proceeding in this way is not very simple because the removal of inclusions from a porous structure can lead to the collapse of the structure itself. This happens especially if the guest molecules and the structure is held together by rather strong bonds or if inclusions removal requires high temperatures. To simplify the activation of the MOFs the solvent could be replaced with a more volatile one, in this way the treatment temperature is reduced. Another important factor is the reproducibility of the summary results. This is due to the presence of pores and organic components in the structure, which lead to deviations of the structure from the ideal one, and to the properties of the samples that vary in each experiment.³³⁻³⁴

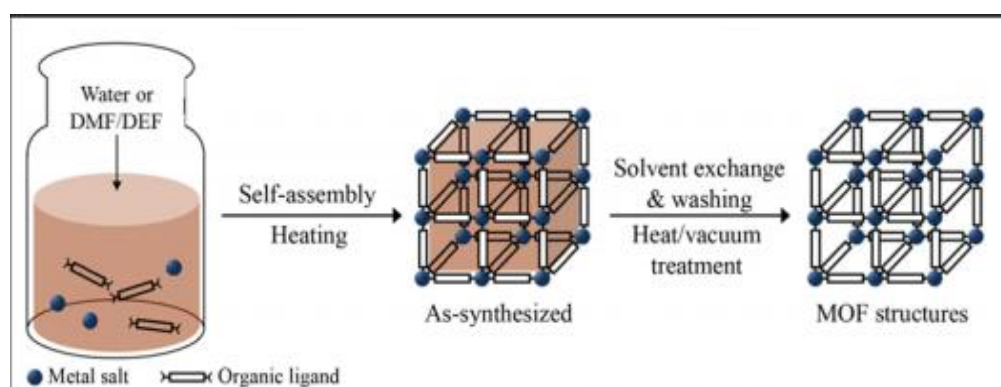


Figure 2.4 Conventional hydro(solvo)thermal synthesis of MOF structures

2.3 Applications of MOFs in catalysis

In recent years the chemical industry has been trying to develop processes that produce less chemical waste and at the same time increase productivity. It follows that the study of catalysis is a key factor for the development of sustainable chemical processes. Homogeneous catalysts have been used in many industrial processes but have several disadvantages such as poor thermal stability and difficulty in recovering the catalyst from the reaction mixture. Instead, heterogeneous catalysts have a longer life than homogeneous ones, they allow for easier separation and more efficient recycling.

The high surface areas, tunable pore metrics, and high density of active sites within the very open structures of MOFs offer many advantages to their use in catalysis. Thanks to the open structure, the self-diffusion coefficients of the molecules in the pores are slightly smaller than those in the bulk solvent. This implies that mass transport in the pores is not hindered. The high surface area of the MOFs allows catalysts to be made with a very high density of fully exposed active sites, and this leads to greater efficacy and activity of the catalyst.³⁵

MOFs contain three well distinguishable parts: the metallic nodes, the organic linker and the porous system. The catalytic function can be found in one of the three parts; furthermore, the MOFs are known to simultaneously contain two or more types of catalytic sites. In the following, it will be shown that there are three different approaches to prepare MOFs in which the catalytic function is found in one of these three parts.

The first approach is the use of metal active sites that are linked together through organic links. In this approach two types of MOF are used, the first includes materials with a single type of metal (M) that acts simultaneously as an active catalytic site and as a structural component, while the second type includes materials with two types of metals. In the latter case a metal (M₁=single metal site) is responsible for the catalytic activity, and the other (M₂=single metal ion or cluster) is not involved in the catalysis and therefore plays a purely structural role.

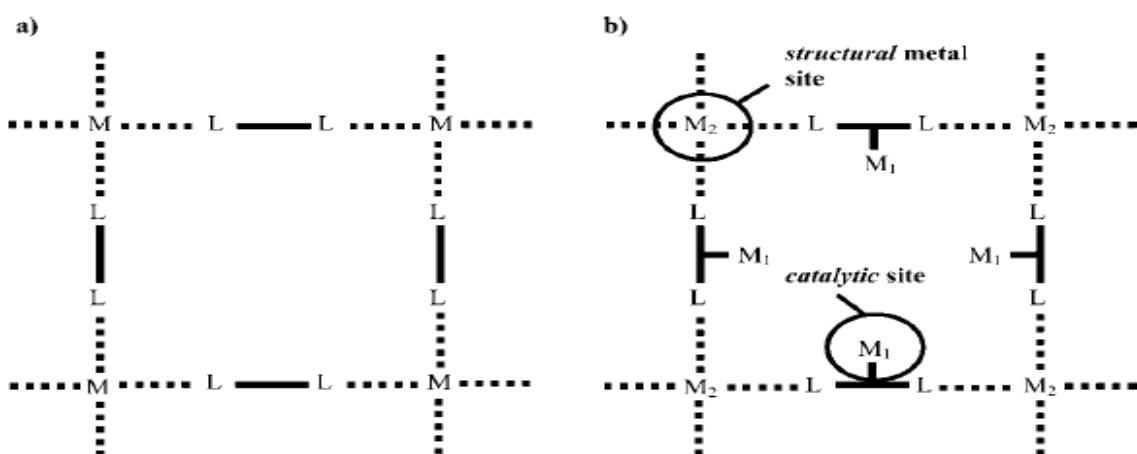


Figure 2.5 Representation of (a) a Monometallic MOF with Only One Type of Metal Center (M) and (b) a Bimetallic MOF with Both *Structural* (M₂) and *Catalytic* (M₁) Sites

The second approach is the use of the functional groups of the organic component. In these MOFs the active sites capable of catalyzing a reaction are found in the organic molecule and not in the metal ion. The organic ligands must have two types of functional

groups: the coordinative groups (L1) that by binding to metals lead to the structure of the MOF, and the reactive groups (L2) that are responsible for the catalytic activity.

Metals tend to interact very easily with the functional groups of the organic components, this implies that the L2 reactive groups are unlikely to be free and can interact with the catalytic substrates, but that they are linked to metal ions. Because of this, the quantity of MOFs belonging to this category is really limited. In the third and last approach the porous system of the material provides the physical space (nanometric reaction cavity) in which the catalysis takes place and traps the catalytic centers inside it (host matrices). ²⁴

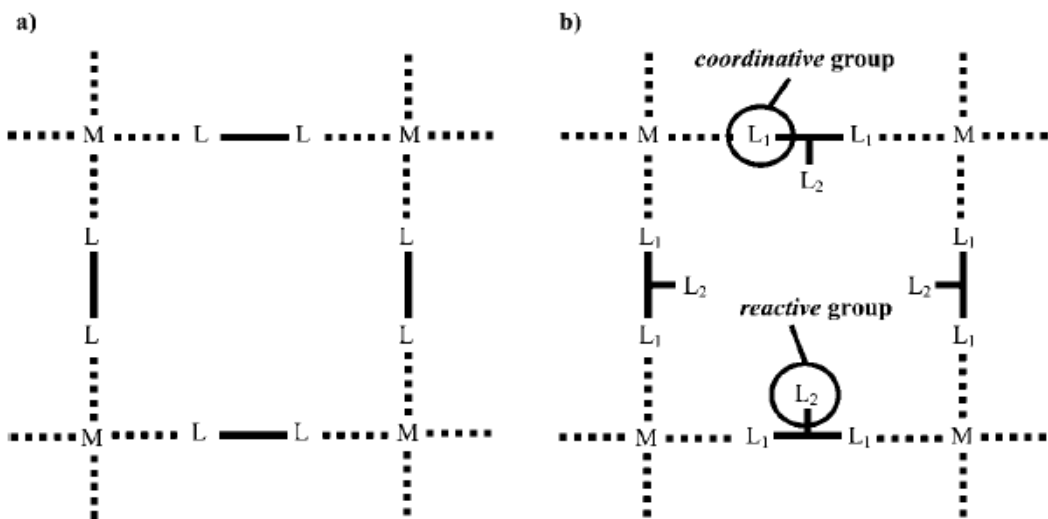


Figure 2.6 Representation of (a) a “Classic” MOF with an Organic Spacer Having Only Coordinative Groups (L) and (b) a MOF with Both *Coordinative* (L1) and *Reactive* (L2) Functional Groups

2.4 MIL-53 (Al)

The metal organic frameworks designated as MIL-n (Materials of the Institute Lavoisier) series was first synthesized by Ferey’s group in 2002.

MIL-n type MOF materials are promising candidates for H₂, CH₄ and CO₂ adsorption. Among the MIL-n materials, MIL-53 (Al), system has been found to adsorb large amounts of gases such as CH₄ and CO₂. The MIL-n type nanoporous materials are exciting due to their simple structure and higher thermal stability compared to other MOFs. Due to their “breathing” character upon adsorption of water and carbon dioxide these materials have become much interesting. In another words, MIL-53 (Al) is able to adjust its cell volume in a reversible manner to optimize interactions between the guest molecules and the framework, with no evidence of bond breaking. MIL-53(Al) provides several advantages compared with other MOFs such as high thermal stability, high surface area, high humidity resistance, and is synthesized using chemical substances available but not very cheap. The structure of MIL-53 material is built up from infinite chains of corner-sharing MO₄(OH)₂ octahedra (M = Al³⁺) interconnected by benzenedicarboxylate (BDC) units. This results in a 3D metal–organic framework containing 1D diamond-shaped channels with pores of free diameter close to 8,5 Å. The chemical formula of the MIL-53 material is Al(OH)(O₂C–C₆H₄–CO₂). ³⁶⁻³⁷

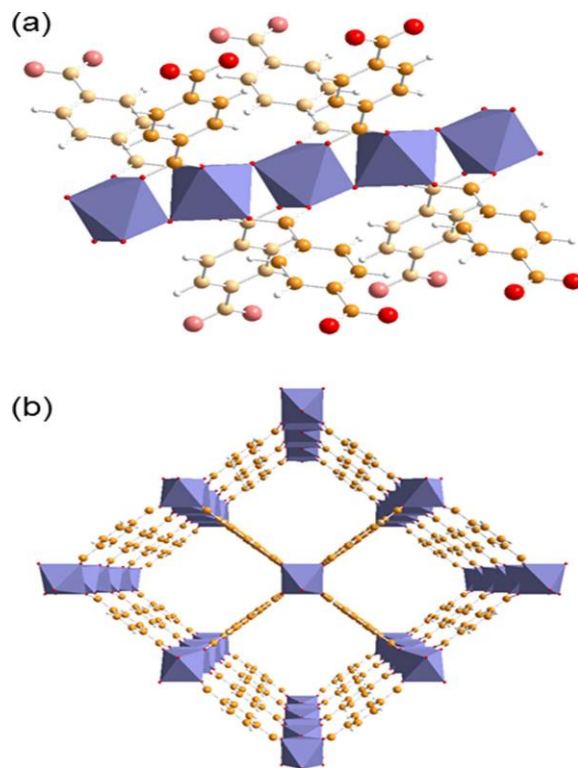


Figure 2.7 The MIL-53 structure. (a) shows the infinitely extending corner-shared chains of $\{MO_6\}$ (in purple) with cross linking benzene-1,4-dicarboxylates (oxygen red, carbon orange, hydrogen atoms white), and (b) shows the structure viewed parallel to the inorganic chains.

Metal-organic framework MIL-53(Al) was synthesized by a hydro(solvo)thermal method using aluminum chloride as the aluminum source, 1,4-benzenedicarboxylic acid (BDC) as the organic ligand, and deionized water.

In the presence of water, the MIL-53 (Al) solids exhibit an original breathing phenomenon upon hydration–dehydration which involves 5.2 Å atomic movements (Figure 2.8).

In the hydrated form (Figure 2.8, left) the pores are slightly deformed owing to hydrogen-bond interactions between the hydrogen atoms of the water molecule and the oxygens of the carboxylate and the μ_2 -hydroxo group. The water is rapidly removed upon heating to give a structure with the more open porosity (Figure 2.8, right).

Hydrogen-bonding interactions between water molecules trapped within the channels and the carboxylate groups of the BDC linkers are responsible for the dynamic switching of the structure.^{22,38}

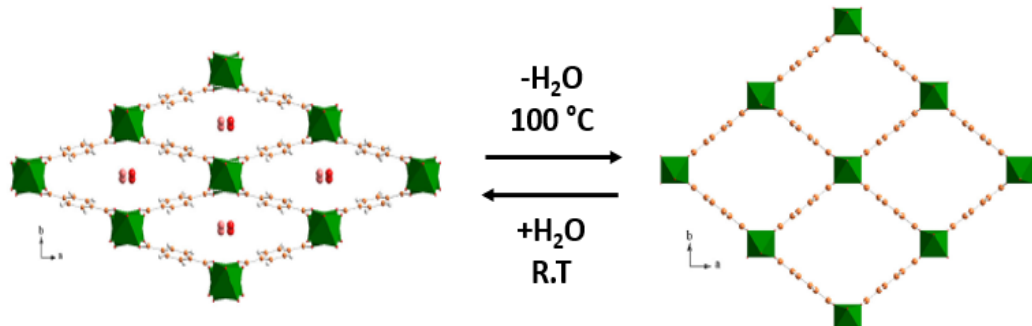


Figure 2.8 Hydration and dehydration process occurring in MIL-53(Al). Left: MIL-53_{LT} (hydrated); right: MIL-53_{HT} (dehydrated).

The difference between the open and closed structure of MIL-53 is due to the interaction between the inorganic chain and the carboxylate groups of the benzene-1,4-dicarboxylic linkers. The connection between a dicarboxylate and metal centers illustrating the flexible part of the structure; thus, the extent of breathing can be expressed by the dihedral angle between two planes, with the most expanded form showing a dihedral angle of 180° . The presence of water in the pores allows for strong hydrogen bonds between the framework and the guest molecules: this is evidenced by the short O–O contacts between water and framework hydroxide groups, as well as between water molecules, Figure 2.9. Two types of hydrogen bonding were present, between the water and carboxylate oxygens and between the water and bridging hydroxides; and it is the latter that contribute more to the pore closing effect upon hydration of the large-pore form.³⁷

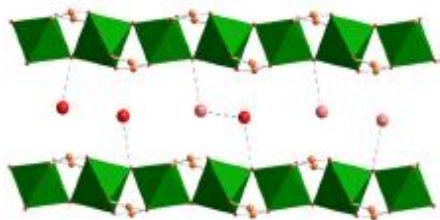


Figure 2.9 Hydrogen bonding interactions between water molecules and between water molecules and the framework hydroxide. $\{\text{AlO}_6\}$ octahedral are green with benzene-1,4-dicarboxylate atoms coloured: oxygen red or pink (each is 50% occupied on average), carbon orange, hydrogen atoms white.

MIL-53 (Al) can be used as a support material in catalysts thanks to its particular characteristics which are summarized below:

- Porous structures and unsaturated coordination sites of MOFs can limit nanoparticle aggregation and migration leading to high nanoparticle dispersion.
- The unsaturated MOF coordination sites increase activity in catalytic reactions.
- Huge surface area, high thermal stability, and thanks to its 1D channels the reaction and product molecules can arrive or leave the surface of the catalyst without problems.³⁹

2.5 Dry reforming of methane

The dry reforming of methane (DRM) is a chemical process that consists of converting methane and carbon dioxide, identified as the world's most abundant greenhouse gases (GHG), to syngas (hydrogen and carbon monoxide), with a H₂/CO molar ratio of 1.

One of the obstacles encountered in the application of this process is rapid deactivation of the catalyst, which is mainly due to coke accumulation and sintering of both the support and the active metal particles. Furthermore, the long reaction time and the need for pure CO₂ make DRM an unfamiliar process that still needs further development.

The catalysts based on noble metals such as Rh, Pt, Pd or Ru are reported excellent performance in catalyst stability and activity; these catalysts are less sensitive to coking than the nickel-based catalysts. Considering the high cost and limited availability of noble metals, however, it is more profitable to develop a Ni-based catalyst, which is resistant to coke accumulation and exhibits long-term stability.⁴⁰ To avoid nickel sintering and the carbon deposition various strategies have been developed:

- 1)addition of a small amount of a second metal usually noble metals

- 2) variation of support type
- 3) strengthening the interaction between Ni and its support

Therefore, it can be assert that the performance of catalysts used for the dry reforming of methane strongly depend on the selection of active metals, supports and promoters.⁴¹

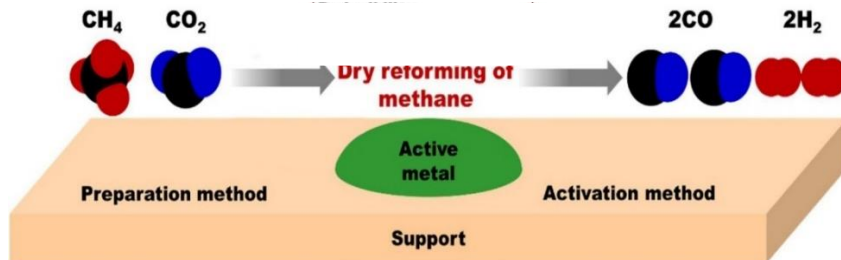
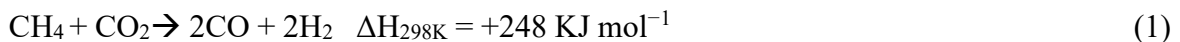


Figure 2.10 Schematic representation of DRM reaction over catalyst

2.5.1 Thermodynamics

The reaction governing DRM is:



CH_4 and CO_2 are very stable molecules with high dissociation energy:

435 ($\text{CH}_3\text{-H}$) and 526 (CO-O) kJ mol^{-1} , respectively. DRM is an endothermic reaction and requires high temperatures, generally between 630-1000 °C, to reach the desired conversion levels. Four moles of products are formed from two moles of reactants, so the reaction is favored by low pressure. Higher pressures reduce conversion at a constant temperature

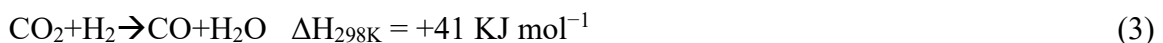
because of the increase in moles that occur during the reaction (Le Chatelier's principle). Higher temperatures increase conversion at a constant pressure because the reaction is endothermic (higher chemical equilibrium constant at higher temperature). Furthermore, it has been noted that a $\text{CO}_2 / \text{CH}_4$ molar ratio higher than the stoichiometric requirement of 1 can also lead to high syngas yields.

Compared to auto thermal (ATR) and steam reforming (SRM), the dry reforming of methane is the most endothermic reaction.



This can be attributed to the fact that CO_2 , the oxidizing agent used in DRM, is the most stable compared to oxygen and steam used in ATR and SRM respectively. Although DRM is mainly governed by the reaction between CH_4 and CO_2 (reaction 1), several other reactions can also occur during the process.

On the other hand, the equilibrium for the production of synthesis gas is generally influenced by the simultaneous occurrence of the reverse water gas shift (RWGS) reaction.



This results in higher CO_2 conversion than that of CH_4 in equilibrium. In practice, this is advantageous for producing synthesis gas with a H_2/CO ratio of 1 or below 1.

Apart from RWGS, the formation of carbon is the most important reason for fatal catalyst deactivation during DRM. As shown in Fig 2.11, the carbon formed during DRM is primarily attributed to two reactions:



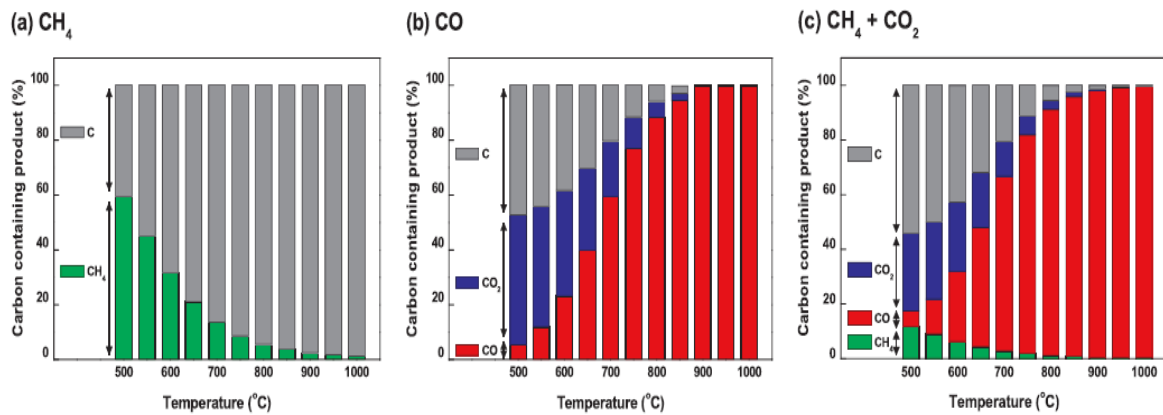


Figure 2.11 Carbon containing product for the catalytic reactions: (a) CH_4 decomposition (CH_4 100%), (b) Boudouard reaction ($\text{CO}=100\%$), (c) Dry reforming of methane (CH_4 50% and $\text{CO}_2=50\%$).

Wang et al. reported that CH_4 decomposition occurs above 557 °C, while the Boudouard reaction occurs below 700 °C. They found that carbon is formed from CH_4 decomposition or the Boudouard reaction in the temperature range 557 to 700 °C and suggested that the optimum temperature at the feed ratio of $\text{CO}_2/\text{CH}_4=1:1$ is between 870 and 1040 °C, considering the conversion and carbon formation. Several researchers have conducted thermodynamic simulations for various temperatures, CO_2/CH_4 ratios, pressures, additional oxidant and consideration of various carbon formation reactions. They commonly concluded that the operation of DRM at high temperatures above 850 °C and low pressures is required to attain high conversion. Moreover, minimizing the yield of carbon formation is particularly essential to operate the DRM process stably. However, it is difficult to generalize the formation of carbon by calculating thermodynamically the operation condition, because it is strongly dependent on the type of catalyst. Thus, DRM studies were conducted on the aspects of the catalysts.⁴¹⁻⁴²

2.5.2 Coke formation

The high temperatures required in dry reforming of methane lead to the deposition of carbon on the catalysts. This happens because, at these temperatures, enough energy is reached to split the C-H bond of the methane molecules. It is therefore desirable to understand the conditions at which carbon forms to minimize its formation. As previously stated, most of the catalysts used in this chemical process are made up of nickel deposited on aluminum oxide supports. This type of catalyst produces reactions that lead to the formation of carbon, resulting in a loss of catalyst activity. These deposited cokes may have different structure orders, morphologies, and reactivity, depending on the specific reaction conditions and structures of the catalyst. There are three types of coke that might be formed in the methane reforming reactions on supported metal catalysts: pyrolytic coke, whiskers and gum. Gum is formed at lower temperatures while coke and whiskers are more commonly formed at high temperatures.

The most common deposition of carbon on nickel catalysts is whisker carbon. This type of deposition occurs at higher temperatures, low water content and is strongly influenced by the presence of aromatics. Whisker carbon formation can completely destroy a nickel-based catalyst. Whisker carbon is filamentous carbon with a nickel crystallite at the end. It is formed by decomposition of methane (4), Boudouard reaction (5), higher hydrocarbons or carbon monoxide.

The mechanism of whisker growths is tied to the individual nickel crystallite. In gas mixtures where the steam to higher hydrocarbons ratio is too low and the temperature above a certain limit, graphene layers grow on the nickel crystallite pushing it out. This growth continues until it bursts the catalyst tablet, which deteriorates to dust. At some point, the amount of dust formed has reached a critical level and the pressure drop across the catalyst bed starts to increase. Significant formation of carbon will result in excessive pressure drop build-up and subsequently plant outage for replacement of catalyst.⁴³⁻⁴⁴

2.5.3 Catalysts and catalytic property

To date, the methane dry reforming reaction is not considered a mature chemical process that can be developed on an industrial level. The main problem is to make a catalyst that is economical, has high activity and thermal stability, and is resistant to carbon deposition. Furthermore, the catalyst must guarantee a high surface area and dispersion, and the metallic particles present must be of small size.

DRM has been investigated over supported metal catalysts based on noble (Rh, Ru, Pd, and Pt) and non-noble (Ni and Co) metals. Noble metals have attracted attention for their superior stability and activity, for their high application temperatures ($>700^{\circ}\text{C}$), and for their increased resistance to carbon deposition. However, they have the major disadvantage of being expensive and not very available. In this perspective, non-noble metals (Co and especially Ni) have become an alternative for industrial application due to their low cost, high catalytic activity, and availability. The disadvantages in using these metals are nickel sintering and carbon deposition.⁴⁵

It is therefore clear that many variables can be controlled and modified, such as support, promoter, calcination, temperature, method of preparation and particle size, to try to minimize the aforementioned disadvantages.

The catalyst consists of two parts: the active species (Ni) and the support. The active species is the component that actually determines the catalytic activity, while the support, which is the most present compound, has several functions, including:

- provide a high surface area for the dispersion of active metals
- improve mechanical strength
- increase heat exchange capacity
- ensure stability, especially when operating at high temperatures

A good support will maintain high nickel dispersion (thereby high coke resistance) and will be resistant to sintering during the high temperature reforming reaction.⁴⁶

There are two types of promoters: structural and chemical. The first ones improve the structural properties of the catalysts trying to avoid or delay the sintering of the active species. The second ones work to provide additional new active sites or to avoid the formation of carbon deposition by the addition of alkaline and the earth metal.⁴²

The catalyst preparation methods have strong influence over physico-chemical properties and performance of catalyst. The proper choice of preparation method imparts certain textural properties, support activity, and enhanced metal-support interaction that gave rise to higher catalytic activity and lower carbon deposition.⁴⁷

Calcination is a critical step in controlling the size of nickel which in turn influence catalyst stability and activity. Calcination of deposited precursor will be important for the complete

decomposition of salts and it is believed that calcination of catalyst creates specific transformation and solid-state reactions which include: decomposition of precursor solid state reaction of the support oxide and support and reaction between supported oxide and support.⁴⁸

The size, shape, structure, and surface composition have significant effects on the coke resistance of Ni catalysts, of which the size effect is the most important.

The studies on the composition and controllable shape and structure are exactly for the size control. If one can limit (or keep) the Ni particle size below several nanometers (<15 nm) during the reforming reactions, the coke formation will be totally inhibited.

Other than developing the Ni-based catalyst with some modifying agents during the catalyst preparation, incorporating the Ni particles within the mesoporous support could also increase the conversion of reactants and yield of products by avoiding the sintering of metal particles and strengthening the metal-support interaction. This is due to the high specific surface area of mesoporous materials that can improve the dispersion of Ni particles onto the supported catalyst.⁴⁹ The purpose of this work is to synthesize MIL-53 (Al), which will then be used as a sacrificial template to prepare a Ni/alumina-based catalyst particularly stable and active in the reaction of dry reforming of methane. In my novel green approach, the waste polyethylene terephthalate (PET) bottle material has effectively been used as the starting precursor instead of terephthalic acid for the synthesis of terephthalate based nanoporous trivalent metal-organic frameworks (MOFs) namely MIL-53(Al).

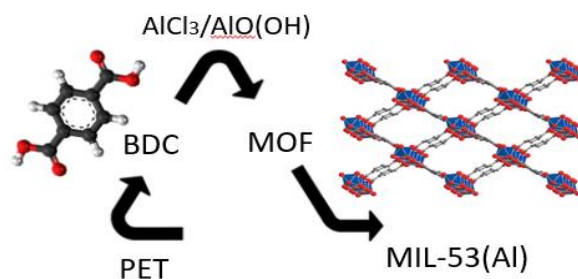


Figure 2.12 Summary of catalyst design tradeoffs

2.6 Poly (ethylene terephthalate)

Poly (ethylene terephthalate) is a thermoplastic polyester, it consists of more than 85 wt% terephthalic acid in ester form which can be hydrolyzed to yield the carboxylic acid or carboxylate. Terephthalic acid is one of materials which can be used as acid catalyst. Basically, the advantages of BDC when compared to conventional acids are high stability, insolubility in water at room temperature (only about 0.0015 g/100 g) and exponential increase of its solubility with temperature.⁵⁰

In recent years, eco-synthesis of functional materials has become increasingly important in point of energy saving and environmental protection. Among all the energy and environmental issues, disposable poly(ethylene terephthalate) (PET) bottles have received much attention. From statistics, consumption of PET reaches over 24 (~ million tons 62.8 billion bottles) worldwide each year and is still increasing.⁵¹

PET bottles cause serious environmental problems because they take a long time to degrade. Chemical recovery has long been tried, but remains a process not yet developed due to complicated procedures and low efficiencies in the recovery of the two monomers that make up it (ethylene glycol and terephthalic acid). In recent years, a way is being sought to use PET waste directly as a starting reagent for the preparation of chemical materials. With this background in mind, PET was used as a starting material for the preparation of nanoporous materials. In particular, PET waste was used as a source of terephthalic acid for the preparation of MIL-53(Al). This would achieve veritable elimination of the waste while creation of useful materials at the same time.⁵²

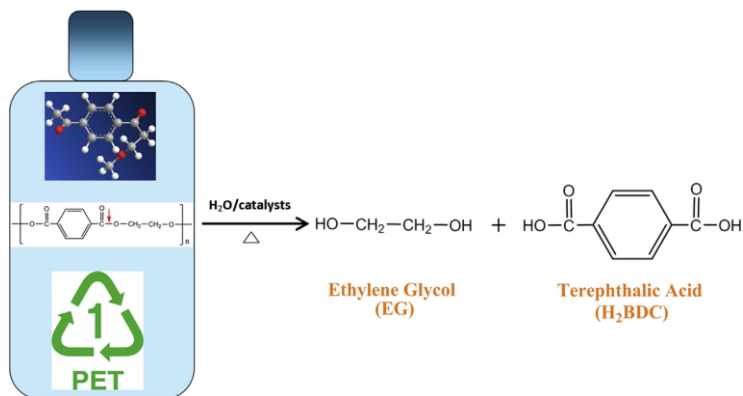


Figure 2.13 The catalysed depolymerization of PET to BDC and EG (article:green synthesis of chromium-based MOF)

3. Methods and materials

In my novel green approach, the waste polyethylene terephthalate (PET) bottle material has effectively been used as direct source of BDC acid linker for the synthesis of MIL-53. To do these two different approaches were used: one step synthesis and two steps synthesis. In the one step synthesis the waste PET is used directly, together with a source of aluminum and water as a solvent, to synthesize MIL-53(Al) in hydrothermal conditions. In the two steps synthesis the waste PET was first hydrolyzed to yield the sodium salt; the salt was then acidified with sulphuric acid to precipitate out terephthalic acid. In the second step we use terephthalic acid which we synthesized in the first step as a reagent together with an aluminum source (bohemite or AlCl₃ exahydrate) to synthesize MIL-53.

3.1 MIL-53(Al) synthesis

Hydrothermal synthesis refers to the synthesis of substances via chemical reactions in a sealed and heated solution above ambient temperature and pressure. To increase single crystals with this technique, it is necessary to use an apparatus consisting of a steel pressure vessel, called autoclave. By changing the characteristics of the initial solutions (pH, solvents, ion concentration) and the process conditions (temperature, duration, agitation mode) it is possible to effectively control the shape and size of the nanoparticles and the crystalline phases obtained. The peculiarity of this process lies in the fact that under hydrothermal conditions water can be considered as an even more effective solvent, which can also dissolve non-polar entities. In this research only Teflon liners are used. The parts of the autoclaves are shown in the Figure 3.1.



Figure 3.1 (a) The parts of the autoclaves, (b) the entire setup the autoclave

3.1.1 One step synthesis of MIL-53(Al)

Clear plastic PET bottles were collected from domestic waste as the raw material. Labels were removed and the bottles were washed with water and soap, and then dried. PET flakes used for hydro(solvo)thermal synthesis were obtained by cutting the bottles into pieces with scissors. MIL-53(Al) was synthesized by heating a reaction mixture of $\text{AlCl}_3 \cdot 6\text{H}_2\text{O}$, PET flakes and DI water, in a 50 ml Teflon-lined steel autoclave and heating it in a common oven for 26 h at 220°C. In this type of synthesis PET is used directly, and what happens is an *in situ* hydrolysis. PET is depolymerized in the monomers that constitute it thanks to the presence of hydrochloric acid (deriving from the use of AlCl_3 as an aluminum source).

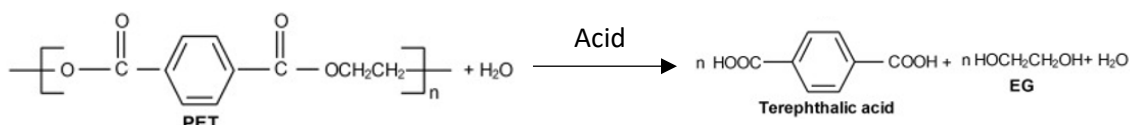


Figure 3.2 In situ hydrolysis of PET

After the completion of the reaction, the autoclave was cooled down to room temperature naturally. The solid was recovered by vacuum filtration and washed with DMF, deionized water and then with ethanol to ensure full removal of unwanted residues. After that, the white powder was dried. After removing the white powder from the filter paper, about 50 ml of DMF are added and then the solution is stirred for about 5 h. The solid was recovered by filtration, washed as previously reported and dried. In the end, the excessive 1,4-benzenedicarboxylic acid adsorbed in the pores was removed by heat treatment at 330°C for three days in air. In this way it has been achieved the activated MIL sample. In order to compare the results and to be sure that pure MIL-53 was obtained, MIL-53 was synthesized under traditional conditions. In this case I use commercial BDC instead of PET flakes to synthesize MIL-53, under the same conditions of temperature, time and pressure.

3.1.2 Two steps synthesis of MIL-53(Al)

In order to reduce even more the economic impact, we try to use boehmite as a source of aluminum instead of AlCl_3 . To do so we couldn't apply one step synthesis which require the use of AlCl_3 and consequentially the presence of acid conditions to hydrolyze PET. So we develop two step synthesis, in which the first step is the alcoholysis of PET that leads to pure BDC and the second step is the synthesis of MIL-53 in hydrothermal conditions, using terephthalic acid synthesized in the first step. Terephthalic acid (BDC) is a versatile ligand used as a linker with several metal ions to assemble a large number of MOFs with varying stoichiometries. The purity level of BDC for MOF synthesis is rather stringent as even traces

of impurities can hinder the coordination process. Interestingly, high purity BDC can easily be obtained by alkali decomposition of polyethylene terephthalate.

Alcoholysis of PET (2g) was performed in the presence EG (5 ml) at molar ratios of PET:NaOH (1:2.25) in a traditional oven over a period of 1h at 160°C .The reaction products were solubilized in water and precipitated (what is precipitated is terephthalic acid) by addition of 2M H₂SO₄. The precipitate was filtered and purified by a second dissolution-precipitation step. For this purpose, 0.2M NaOH was added dropwise to the precipitate till the pH increased to 7, followed by filtration, and addition of 2M H₂SO₄ to ensure precipitation. The precipitate was centrifuged, and water was added three or four times, with the aim of obtaining a sample free of impurities, and of Na₂S salt which has formed during the reaction. Finally, the precipitate was dried at 80°C. The BDC separated was dissolved in dimethyl sulfoxide, and its purity examined by the H NMR analysis to detect the EG residue if remained in the form of oligomers or hydroxyethyl terephthalates.

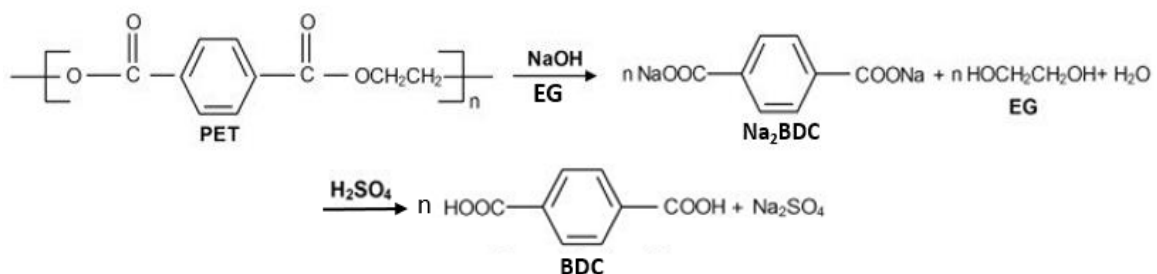


Figure 3.3 Alcoholysis of PET

After obtaining pure terephthalic acid, this reagent is placed together with an aluminum source (AlCl₃ or AlO(OH)) and deionized water in a 50 ml Teflon-lined steel autoclave and heating it in a common oven for 26 h at 220°C. The procedure showed for the one step synthesis was also followed in this case, up to obtain the activated MIL sample.

3.2 Catalyst preparation

The strategy followed for catalyst preparation is depicted in the Figure 3.2. After hydrothermal synthesis and activation at 330 °C (solvent removal) of the parent MIL-53(Al), a cationic nickel precursor is impregnated within the pores by incipient wetness impregnation. Prior to the impregnation treatment, the sample was first dehydrated at 80°C in an oven overnight, and then thermally treated at 200°C for 15h to be sure to have removed the water contained within the pores. The procedure consisted in adding dropwise a Ni(NO₃)₂*6H₂O aqueous solution with a volume equal to the pore volume of the MOF support (as estimated from N₂-sorption analysis). The solid obtained is hereafter denoted Ni/MIL-53(Al). The product from the impregnation was dried at 200 °C for 15 h, followed by calcination in air at 500 °C for 5 h (heating rate 0.5 °C/min) to give Ni²⁺@Al₂O₃, that is finally thermally treated under hydrogen at 800°C to form the reduced nickel nanoparticles that constitute the active phase for DRM.

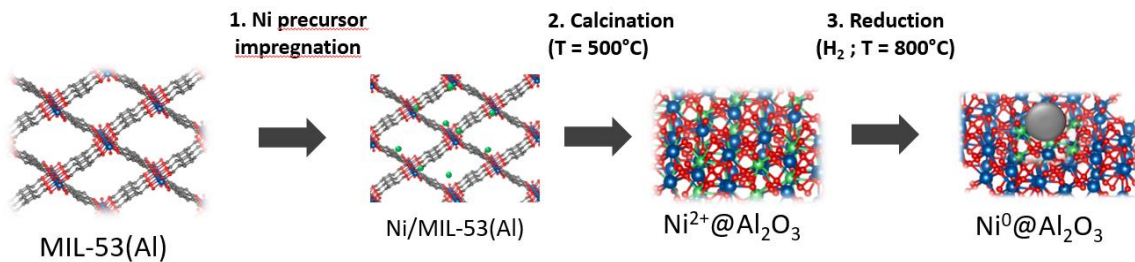


Figure 3.4 Scheme of nickel-alumina-based catalyst preparation

3.3 Physicochemical characterization techniques

The MIL-53 (Al) products were characterized using a battery of analytical techniques: X-ray diffraction, Thermo gravimetric analysis (TGA), N₂ physisorption, transmission electron microscopy (TEM), nuclear magnetic resonance (NMR), temperature programmed reduction (TPR) and scanning electron microscopy (SEM).

3.3.1 X-ray diffraction

X-ray diffraction (XRD) is a powerful non-destructive technique which reveals information about the crystal structure and orientation, chemical compositions, and physical properties of materials and thin films. The X-rays are generated by a cathode ray tube, filtered to produce monochromatic radiation, collimated to concentrate, and directed toward the sample. The interaction of the incident rays with the sample produces constructive interference (and a diffracted ray) when conditions satisfy Bragg's Law: (The analysis is carried out by engraving on the sample a monochromatic X-ray beam, which is diffracted only in particular directions of space, depending on the crystalline phases present following the Bragg's law)

$$n\lambda = 2d \sin\theta \quad (\text{Eq 3.1})$$

Where:

d = interplanar spacing

θ = diffraction angle

λ = wavelength of X-ray

n = order of diffraction

A diffracted beam is formed by a large number of X-rays diffused in phase between them; these reinforce each other by increasing the value of the diffracted intensity. The device that exploits this principle is the diffractometer, which is composed of: an X-ray source, a system of monochromators and collimators, a detector and a computer equipped with software to interpret the signal received by the detector. The result obtained from the program is a graph that shows the trend of the intensity of the diffracted radiation as a function of the angle 2θ to which the detector is positioned; this graph is called pattern and is characteristic of each crystal. Figure 3.5 shows the diffractometer scheme.

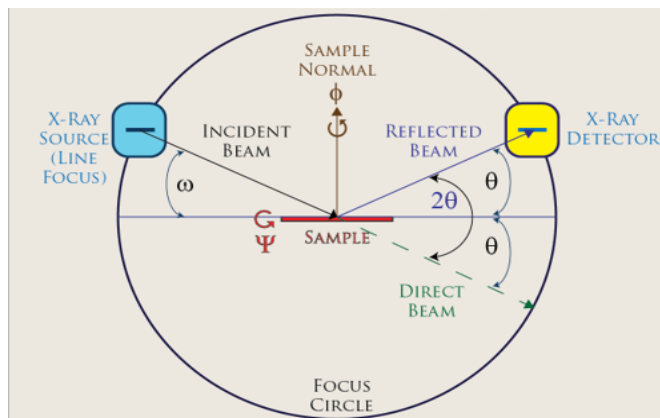


Figure 3.5 Powder X-Ray Diffraction geometry and conventions used in PAN alytical X-Pert Pro Powder at Florida State University Chemistry & Biochemistry Department (CSL 1011)

Powder XRD patterns were recorded on a BRUKER type D8 diffractometer equipped with a Cu K α irradiation source ($\lambda= 1.5405$ nm) and operating at 30 kV and 10 mA. The acquisitions were done in a 2 θ range from 5 to 90°. Crystalline phase identification was based on comparison with standard powder XRD files published by the international center for diffraction data (ICDD). The crystallite size D (in nm) was estimated from X-ray line broadening using the Scherrer's formula $D=K\lambda/\beta\cos\theta$ where λ is the X-ray wavelength, $K=0.9$ is a costant, β is the full-width half-maximum of the Bragg diffraction angle θ , and θ corresponds to the peak position.⁵³



Figure 3.6 D8 Advance X-Ray Diffractometer

3.3.2 Thermo Gravimetric Analysis

The Thermogravimetric Analyzer (TGA) is an essential laboratory tool used for material characterization. Thermogravimetric Analysis is a technique in which the mass of a substance is monitored as a function of temperature or time as the sample specimen is subjected to a controlled temperature program in a controlled atmosphere. It can be used in the determination of the thermal stability and decomposition products of a material.

A TGA consists of a sample pan that is supported by a precision balance. That pan resides in a furnace and is heated or cooled during the experiment. The mass of the sample is

monitored during the experiment. A sample purge gas controls the sample environment. This gas may be inert or a reactive gas that flows over the sample and exits through an exhaust. Thermogravimetric analysis was performed on a TA SDT Q600 (Figure 3.5) instrument working in horizontal mode. One of the two alumina pan was filled with about 20 mg of sample while the other (reference) pan was kept empty. The analysis was carried out in air flow (50 ml/min) from room temperature to 900 °C with a ramping rate of 5 °C/min.⁵⁴



Figure 3.7 SDT Q600 Thermogravimetric Analyzer

3.3.3 N_2 physisorption

N_2 physisorption analysis is a method which relies on physical adsorption of nitrogen gas at liquid nitrogen temperature (77 K). Porous materials are well known for their capacity of adsorbing both liquid and gaseous species.

When a solid is exposed to a gaseous fluid, the gas molecules are adsorbed from the surface for a finite time, after which they are desorbed and replaced by others. The adsorbed volume depends on the pressure at which the adsorption occurs and on the nature of the gas and the solid; ideally, at pressure close to zero there are few molecules that move without a precise order; increasing the pressure, increases the gas molecules and, consequently, increases the probability that an adsorption phenomenon occurs on the surface; continuing to increase the pressure leads to a point where there is a monolayer of adsorbed particles on the surface and a further increase in pressure leads to the formation of multilayers.

This is what happens in an ideal situation where the surface is flat and infinite; in a real surface it is possible to have pores and surface roughness, and based on the behavior of the monolayer in adsorption and desorption, it is possible to obtain information on the pore structure and on how much area is due to the surface of the piece and how much to the pores.

During the adsorption phase, the pores fill by forming first a monolayer and then forming others one on the other to level the surface; this behavior does not change if there is a micro- (diameter less than 2 nm) meso- (diameter between 2 and 50 nm) or macropore (diameter greater than 50 nm). The behavior in desorption is not exactly the opposite of adsorption: the pores empty to meniscus, leaving a thin superficial monolayer which is eliminated at very low pressures, when the removal of the gas molecules has been completed.

Adsorbed amounts of gas are measured (volumetrically or gravimetrically) as a function of relative pressure (absolute/saturation pressure). The resulting isotherms reflect mechanisms

of pore filling, the physics of which can be used to infer pore volume and area distributions. The difference in behavior between adsorption and desorption described above, causes hysteresis to occur in the curve. From the adsorption isotherm it is possible to calculate the volume of the adsorbed monolayer, defined as the amount of adsorbed gas needed to cover the surface with a molecular monolayer. The adsorption isotherms that can be obtained for systems where the adsorbed is made up of a single chemical species have been classified into five different types depending on their shape, which depends mainly on the pore size of the sorbent and the temperature of the system.

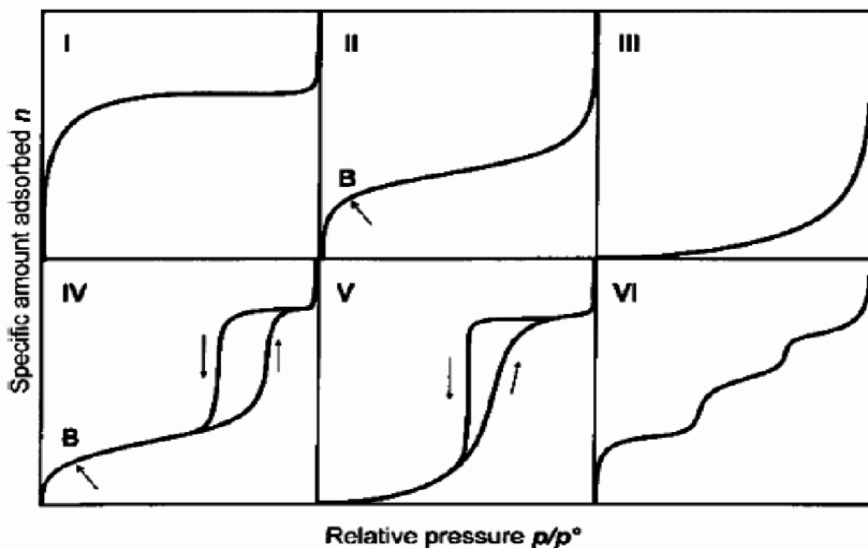


Figure 3.8 Classification of adsorption isotherms according to the IUPAC nomenclature

The isotherm of BET (Brunauer– Emmett– Teller), developed in 1938, which considers multi-layer adsorption, is used to describe adsorption on steam phase surfaces; studying the curve, it is possible to obtain a more or less accurate estimate of the surface area involved during adsorption. The BET analysis consists essentially in conducting cycles of adsorption and desorption isotherms by varying the partial pressure of nitrogen in a chamber of known volume connected to the chamber containing the sample; nitrogen is used because it has molecules with little interaction between them and a not excessive interaction with almost all materials, and this allows the multilayer physisorption of nitrogen. To the results obtained with the analysis BET mathematical models and simulations are applied, that allow to obtain information regarding the distribution of the pores in the material. Textural properties were evaluated from the nitrogen adsorption-desorption isotherms, determined at -198 ° C with a BELSORP-max apparatus. The specific areas of the samples were determined in line with the standard BET procedure, using nitrogen adsorption taken in the relative equilibrium pressure interval of 0.05–0.3. Mean pore size was calculated using the BJH method. The samples were degassed before measurements at 120 °C under vacuum for 6 h.^{55,56}



Figure 3.9 BELSORP-max apparatus

3.3.4 Transmission electron microscopy (TEM)

A transmission electron microscope (TEM) is an analytical tool allowing visualisation and analysis of specimens in the realms of microspace to nanospace. The TEM reveals levels of detail and complexity inaccessible by light microscopy because it uses a focused beam of high energy electrons. TEMs produce high-resolution, two-dimensional images, allowing for a wide range of educational, science and industry applications. It also enables the investigation of crystal structures, specimen orientations and chemical compositions of phases, precipitates and contaminants through diffraction pattern, X-ray and electron-energy analysis.

Transmission electron microscope (TEM), type of electron microscope that has three essential systems: (1) an electron gun, which produces the electron beam, and the condenser system, which focuses the beam onto the object, (2) the image-producing system, consisting of the objective lens, movable specimen stage, and intermediate and projector lenses, which focus the electrons passing through the specimen to form a real, highly magnified image, and (3) the image-recording system, which converts the electron image into some form perceptible to the human eye. The image-recording system usually consists of a fluorescent screen for viewing and focusing the image and a digital camera for permanent records. In addition, a vacuum system, consisting of pumps and their associated gauges and valves, and power supplies are required.

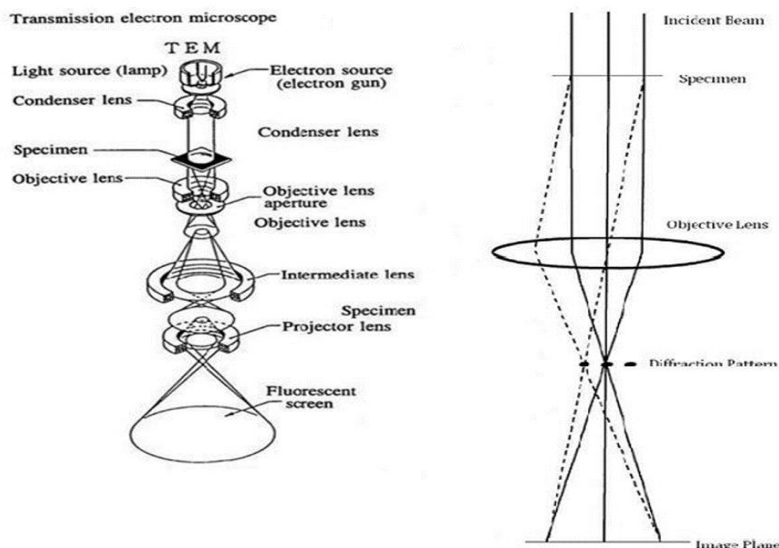


Figure 3.10 General layout of a TEM describing the path of electron beam in a TEM (on the left) and a ray diagram for the diffraction mechanism in TEM (on the right)

Transmission electron microscopy is used to produce images from a sample by illuminating the sample with electrons (i.e. the electron beam) within a high vacuum, and detecting the electrons that are transmitted through the sample. The electron transmitting microscope uses as radiation an accelerated and focused electron beam through an electromagnetic lens system. In particular, the electrons are emitted by a tungsten cathode and are accelerated towards the anode which takes the form of a disk with axial hole. If the stabilization of the high voltage is adequate, the electrons pass through the central aperture at a constant energy. The intensity and angular aperture of the beam are controlled by the condenser lens system between the gun and the specimen. The control and alignment of the electron gun are critical in ensuring satisfactory operation. The electron beam hits the sample, and parts of it are transmitted according to the thickness and transparency of the sample. The transmitted part comes into contact with the phosphorescent screen, and here the electrons are converted into light and form an image. In the regions where electrons do not pass through the sample the image is dark. Where electrons are unscattered, the image is brighter, and there are a range of greys in between depending on the way the electrons interact with and are scattered by the sample. These differences provide information on the structure, consistency, shape and size of the sample. To obtain an accurate analysis the samples must be thin enough to allow the passage of electrons and must be able to withstand the vacuum conditions. Transmission electron microscopy (TEM) observations were done on ultrathin sections of solids to correctly visualize the dispersed nickel nanoparticles (and eventual coke deposits) and their location inside or outside the porous alumina grains. The sections were prepared as follows: a few milligrams of powder were mixed with an EPON 812 embedding resin in a beam capsule. Polymerization of the mixture took place at 60 °C for 48 h, then the polymerized blocks were cut with a diamond knife in slices (50–70 nm in thick-ness) that were deposited on copper grids covered with a carbon membrane layer. TEM images were taken on a JEOL-JEM 200 electron microscope operating at 200 keV (LaB₆gun). Average metallicNi₀particle sizes were estimated using the “Comptage de Particules” LRS software considering at least 500 particles present ingrains with main elongation axis (channels) orientated parallel to the electronic beam (i.e. pore openings perpendicular to the beam).⁵⁷

3.3.5 Nuclear magnetic resonance (NMR)

Nuclear Magnetic Resonance (NMR) spectroscopy is an analytical chemistry technique used in quality control and research for determining the content and purity of a sample as well as its molecular structure. An NMR instrument allows the molecular structure of a material to be analyzed by observing and measuring the interaction of nuclear spins when placed in a powerful magnetic field. When a nucleus that possesses a magnetic moment (such as a hydrogen nucleus ¹H, or carbon nucleus ¹³C) is placed in a strong magnetic field, it will begin to precess, like a spinning top. If the sample placed in this magnetic field is irradiated with radio waves at the same frequency as the precession frequency, an NMR spectrum can be obtained. The precise resonant frequency of the energy transition is dependent on the effective magnetic field at the nucleus. This field is affected by electron shielding which is in turn dependent on the chemical environment. As a result, information about the nucleus' chemical environment can be derived from its resonant frequency. In general, the more electronegative the nucleus is, the higher the resonant frequency. This is because the precise resonant frequency shift of each nucleus depends on the magnetic field used. The effective magnetic field is also affected by the orientation of neighboring nuclei.

This effect is known as spin-spin coupling which can cause splitting of the signal for each type of nucleus into two or more lines. The number of splitting indicates the number of chemically bonded nuclei in the vicinity of the observed nucleus. The basic arrangement of an NMR spectrometer is displayed below. A sample (in a small glass tube) is placed between the poles of a strong magnetic. A radio frequency generator pulses the sample and excites the nuclei causing a spin-flip. The spin flip is detected by the detector and the signal sent to a computer where it is processed.⁵⁸

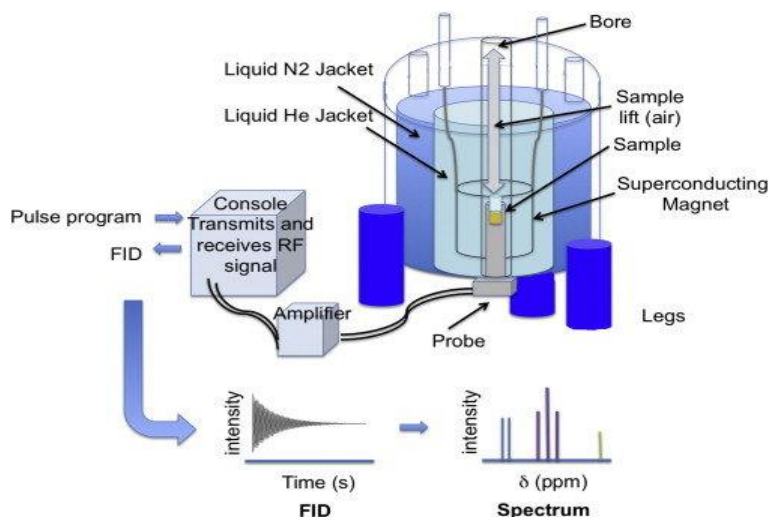


Figure 3.11 Simplified diagram of a nuclear magnetic resonance spectrometer

The following information can be obtained from an NMR spectrum:

- 1) Chemical shift: information about the composition of atomic groups within the molecule.
- 2) Spin-Spin coupling constant: information about adjacent atoms.
- 3) Relaxation time: information on molecular dynamics.
- 4) Signal intensity: quantitative information, e.g. atomic ratios within a molecule that can be helpful in determining the molecular structure, and proportions of different compounds in a mixture.

Liquid phase ^1H NMR spectra were recorded on a Bruker Avance 400 MHz spectrometer equipped with a BBI 5 mm probe, and using DMSO as solvent.



Figure 3.12 Bruker Avance 400 MHz spectrometer

3.3.6 Temperature-programmed reduction

Temperature programmed reduction is used to determine the reducibility of the catalysts. In this method, reducible catalysts are exposed to flow of reducing gas mixture typically H_2 in

Ar. During the analysis a metal oxide reacts with hydrogen to form a pure metal, according to the chemical reaction show here: $M_xO_y + yH_2 \rightarrow xM + yH_2O$.

The theory of this analysis is based on changing the thermal conductivity of gases. Argon, which has a very low relative thermal conductivity, is mixed in a fixed proportion with hydrogen, the reducing gas with a much higher thermal conductivity. When the mixture of hydrogen and argon begins to flow on the sample, a reference reading is established from the detector, generally at a low temperature. By increasing the temperature, the hydrogen atoms in the gas stream react with the sample, forming water molecules that are removed from the gas stream by a cold trap. As a result, the amount of hydrogen in the argon / hydrogen gas mixture inside the analyzer decreases and the proportion between the two gases moves in the argon direction, as does the thermal conductivity of the mixture. A thermal conductivity detector (TCD) is used to measure changes in the thermal conductivity of the gas stream. The TCD signal is then converted into a concentration of active gas using a level calibration. The total amount of H_2 consumed is determined by the area under the peak and is used to calculate the degree of reduction and average oxidation of the solid material after reduction.^{59,60}

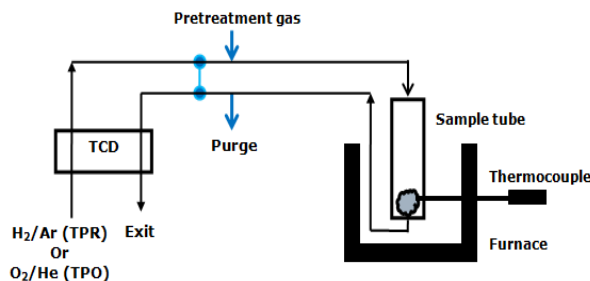


Figure 3.12 Schematic diagram for TPR/TPO analysis

From TPR curves the following information can be obtained:

- 1) Reduction peak temperature indicates the ease of reduction and degree of interaction between different species present in the catalyst sample. A higher reduction temperature indicates higher difficulty in reduction which can be attributed to the greater degree of interaction between the active metal and support.
- 2) Multiple peaks indicate the presence of metal in different forms on the support having different level of interaction between species and support.
- 3) The extent of reduction can be calculated as follows:

$$\text{Extent of reduction} = \frac{\text{actual amount of hydrogen consumed}}{\text{theoretical amount of hydrogen consumed assuming complete reduction}}$$

The actual amount of hydrogen consumed is calculated from the area under the curve and the theoretical amount is calculated from stoichiometry of reduction equation.

Catalyst reduction behavior was examined by temperature-programmed reduction (H_2 -TPR), and the experiments were conducted on a Micromeritics AutoChem 2910 instrument. The experiments were carried out in a quartz tube reactor using 50-70 mg calcined catalysts. To identify the reduction temperature and H_2 consumption of catalysts, the reducing gas, a mixture of 5% H_2 diluted by Ar, was fed via a mass flow controller at 25 ml/min and then the sample was heated from 25°C to 900°C at a constant heating rate of 10 °C/min. The signal of hydrogen consumption ($NiO_{(s)} + H_2_{(g)} \rightarrow Ni^0_{(s)} + H_2O_{(g)}$) was detected by a thermal conduction detector (TCD). The effluent of reactor passed through a 5 Å molecular sieve trap to remove produced water, before reaching TCD. The consumption of H_2 was

quantitatively measured by integrating the area of the TCD curve versus temperature and referring it to a calibration curve.



Figure 3.13 Micromeritics AutoChem 2920 instrument

3.3.7 Scanning Electron Microscopy

Scanning electron microscopes offer several unique advantages and they have evolved into complexly integrated instruments that often incorporate several important accessories. Their principle advantage stems from the method of constructing an image from a highly focused electron beams that scans across the surface of a specimen. Primary limitations of this technique were the restrictions it imposed on samples by requiring a high vacuum sample environment. Samples had to be clean, dry and electrically conductive. SEM uses a focused beam of high-energy electrons to generate a variety of signals at the surface of solid specimens. The signals that derive from electron-sample interactions reveal information about the sample including external morphology, chemical composition, and crystalline structure and orientation of materials making up the sample. All SEM's consist of an electron column, that creates a beam of electrons; a sample chamber, where the electron beam interacts with the sample; detectors, that monitor a variety of signals resulting from the beam-sample interaction and a viewing system, that constructs an image from the signal. An electron gun at the top of the column generates the electron beam; an electrostatic field directs electrons, emitted from a very small region on the surface of an electrode, through a small spot called the crossover. The gun then accelerates the electrons down the column toward the sample with energies typically ranging from a few hundred to tens of thousands of electron volts. Near the bottom of the column, a set of scan coils deflects the beam in a scanning pattern over the sample surface. As the beam electrons penetrate the sample, they give up energy, which is emitted from the sample in a variety of ways. Each emission mode is potentially a signal from which to create an image. Scanning Electron Microscope (SEM) was used to study the morphology of the obtained MIL-53 samples. SEM micrographs were registered on a Hitachi SU-70 SEM-FEG microscope with an electron acceleration tension of 7 kV.⁶¹

3.4 Catalytic measurements

3.4.1 Description of the equipment

Catalytic activity and stability tests were performed using a Hastelloy-X tubular reactor (PID Eng. & Tech). The Hastelloy X reactor (Figure 2.8) equipped with a porous plate and a thermocouple has a length of 305 mm, an external and internal diameter of 14.5 and 9 mm

respectively, an internal volume of 20 mL, a maximum recommended temperature of 1200 °C, and a maximum recommended pressure of 100 bars.

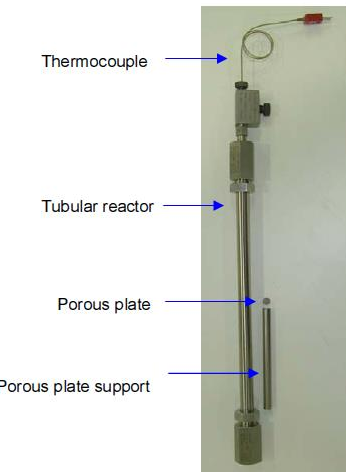


Figure 3.14: Hastelloy X Reactor

The apparatus is composed mainly of a micro activity reference unit. It is formed of a combined unit composed of a hot box, a reaction system, and valves and control elements. Gilson HPLC pump is sometimes used to feed liquid inside the reactor (not used in our study). Moreover, a computer equipped with a remote control system includes communications through Ethernet (Figure 3.15)

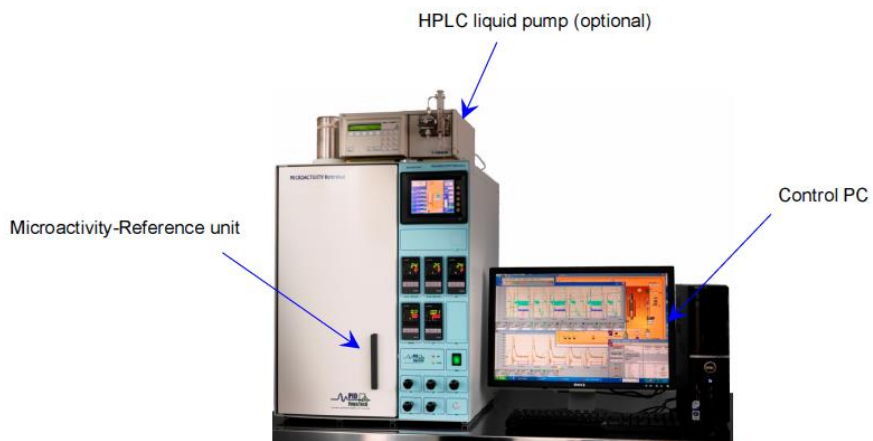


Figure 3.15: General View of the Apparatus

Concerning the reaction system, the catalyst bed is settled on a quartz wool inside a fixed bed tubular reactor. There exists an up-down flow where the reactants mixture are fed in the upper part of the reactor and the products are retained from the lower part. Before entering the reactor system, the reactants gas stream (the gases involved in this study are CH₄, CO₂, CO, H₂ and Ar) passes through a line shut off valve. Electrical forced convection heaters are present in the hot box to heat the gaseous flows to about 120 °C and avoid any condensation. Then, the preheated stream merges to a 6-port valve controlled by a touch screen. This stream can either flow toward the reactor or rerouting toward the system and by-passing the reactor.

At the reactor outlet, the products go through the 6-port valve to pass from the hot box to the liquid-gas separator (Peltier) which separates both liquid and gas phases. While liquid products are removed, the outlet gases are again introduced to the hot box and the pressure

is controlled by passing these gases to a micrometric regulating valve. At the end, the product gases go out of the hot box to the micro-GC (Figure 3.16).

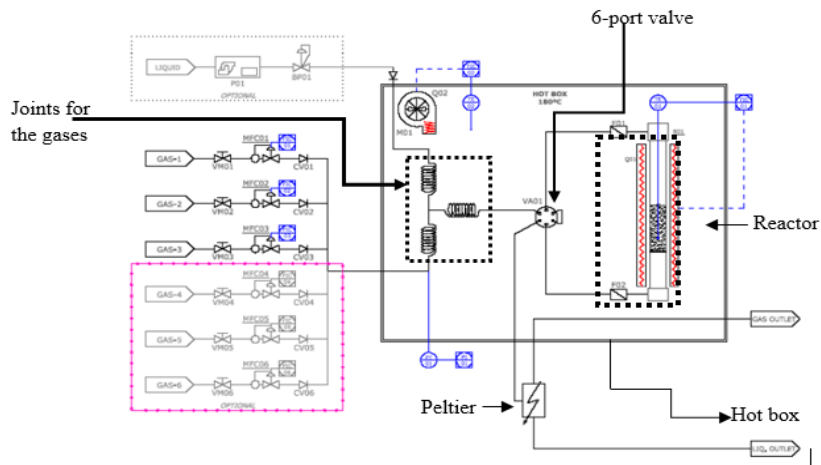


Figure 3.16: Reactor System

The products are analyzed by INFICON 3000 Micro-GC equipped with a thermal conductivity detector and containing 2 molecular sieve columns (column A) in parallel and a plot U column (column B). Column A detects by adsorption H₂ (retention time: 0.8 minutes), CH₄ (retention time: 2.2 minutes) and CO (retention time: 3.2 minutes) and column B adsorbs CH₄ (retention time: 3.3 minutes) and CO₂ (retention time: 0.65 minutes). It is important to know that the values of retention times are obtained based on our experimental conditions that will be mentioned in the next paragraph. Using different experimental parameters or conditions will result in a change in the retention times.

3.4.2 Catalytic test conditions

A leak test and a pretreatment should be performed before starting the reaction. The leak test is important to ensure no leakage system or the test cannot be run. This is done by using helium as inert gas.

The catalytic tests were conducted at atmospheric pressure in a continuous U-shaped fixed bed flow reactor in quartz. 20 mgs of powder were loaded on a quartz wool plug. This mass was chosen to provide information about intrinsic kinetics and diffusion limitations since at low mass quantity both low conversion levels and absence of transport effects are guaranteed. Prior to the catalytic reaction, catalysts pretreatment is applied where each sample was thermally reduced in situ at 800 °C for about 2 hours in a 5% H₂/Ar flow (30 ml·min⁻¹). In this step, nickel oxide NiO is converted to Ni⁰ through the following equation:



The conversion of NiO to Ni⁰ is a vital step in order to avoid CH₄ oxidation and loss of reactants. After cooling down the temperature to around 200 °C, the reactants were introduced (molar ratio CH₄/CO₂=1:1 with CH₄ and CO₂ volumetric flow rate of 32 and 28 ml/min respectively) at total gas hourly space velocity of 180 L·g⁻¹·h⁻¹ for 20 mg loading and the reaction temperature was increased (5 °C·min⁻¹) from 200 °C up to 800 °C. For stability measurements, the reactor was cooled to 650 °C and the temperature was maintained at this value for 12 h on stream where conversion and selectivity were measured. The reactants (CH₄ and CO₂) and main products (H₂ and CO) were then analyzed on the INFICON 3000 Micro Gas. The conversions of methane, carbon dioxide and H₂/CO ratio corresponding for the activity and stability test are calculated as follows:

$$\text{CH}_4 \text{ conversion \%} = \frac{(\text{CH}_4\text{(in)} - \text{CH}_4\text{(out)})}{\text{CH}_4\text{(in)}} \times 100 \quad (\text{Eq. 3.3})$$

$$\text{CO}_2 \text{ conversion \%} = \frac{(\text{CO}_2\text{(in)} - \text{CO}_2\text{(out)})}{\text{CO}_2\text{(in)}} \times 100 \quad (\text{Eq. 3.4})$$

$$\text{H}_2/\text{CO} = \frac{\text{H}_2 \text{ generation rate}}{\text{CO} \text{ generation rate}} \quad (\text{Eq. 3.5})$$

where $(\text{CO}_2)_{\text{in}}$ and $(\text{CH}_4)_{\text{in}}$ are the inlet flow rates of CO_2 and CH_4 respectively, and $(\text{CO}_2)_{\text{out}}$ and $(\text{CH}_4)_{\text{out}}$ are the outlet flow rates.

4. Results and discussion

It has been revealed from thermodynamic approximations that the weakest chemical bond in the PET chain is the ester link, pointed out by the red arrow in Figure 4.1. Therefore, less energy is needed to break this bond and as such the attack mechanisms of the degrading agents largely focus on this bond. The two different types of synthesis of MIL-53 (Al) focus on the hydrolysis of this bond.

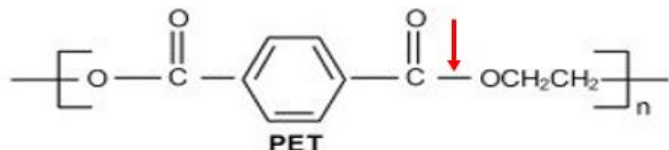


Figure 4.1 Hydrolysis of the PET ester bond

4.1 One step synthesis

The following results refer to different samples:

- Sample MIL-53-BDC: synthesized by commercial BDC
- Sample MIL-53-PET: synthesized using PET as a source of BDC

4.1.1 As-synthesized MIL-53(Al)

To synthesize MIL-53(Al) in one step terephthalic acid, aluminum chloride and water are needed. The presence of AlCl_3 increases the rate of hydrolysis because HCl is generated in situ when the aluminum chloride is hydrolyzed. BDC from PET hydrolysis can further combine with aluminum ions to form MIL-53(Al). The MOF formation also speeds up the hydrolysis reaction as it removes dissolved BDC from solution, preventing the formation of BDC precipitates on the polymer surface. Although PET hydrolysis is the first step of the reaction, MOF crystallization starts as soon as a sufficient concentration of free terephthalic acid is generated. After 26 h, under conditions of high temperature (220°C) and pressure, all the PET reacted and MIL-53 (Al) was synthesized with a 35% yield. To compare the results obtained using PET as a source of BDC, MIL-53 (Al) was synthesized using commercial BDCs in the same conditions of temperature, time and pressure. In this case the yield is higher and equal to 67%.

After synthesis in hydrothermal conditions, the parent MIL-53 sample is characterized by an X-ray diffractogram (Figure 4.2). The diffraction pattern clearly indicated that the

material is well crystalline, and the peaks obtained are in good agreement with the literature pattern of MIL-53(Al) framework. The XRD pattern of MIL-53(Al) synthesized from PET (red line) shows main diffraction peaks at $2\theta = 9.02^\circ, 10.44^\circ, 15.37^\circ, 18^\circ, 21.44^\circ, 27.05^\circ$. Similarly, the characteristic diffraction peaks of MIL-53(Al) synthesized from commercial BDC (green line) were found at $2\theta = 8.99^\circ, 10.39^\circ, 15.27^\circ, 17.94^\circ, 21.42^\circ, 26.96^\circ$. We can therefore conclude that it is possible to use PET as a source of terephthalic acid for synthesize pure MIL-53(Al).

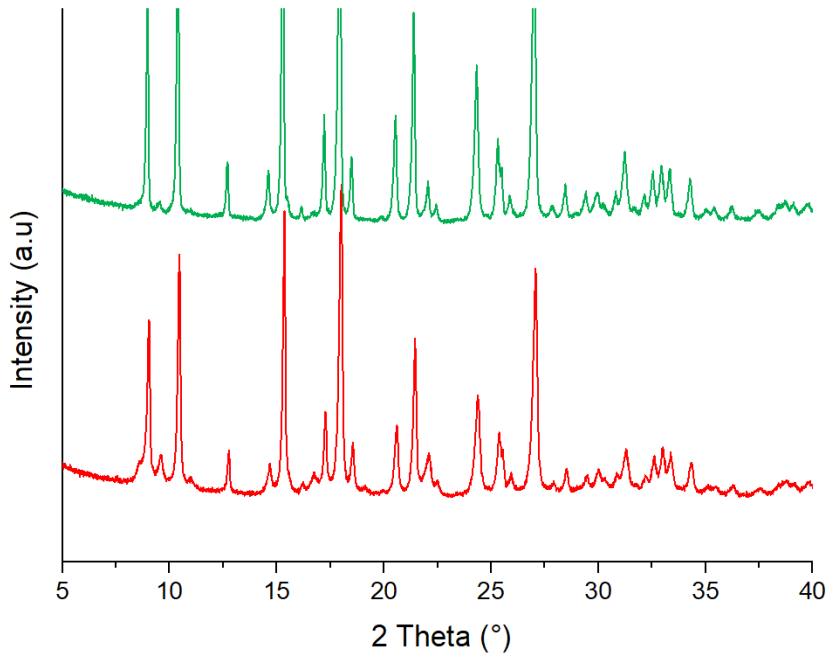


Figure 4.2 X-ray diffraction pattern of: as-synthesized MIL-53(Al) from PET (red line), as-synthesized MIL-53(Al) from BDC (green line)

The pores of MIL-53-as-synthesized (MIL-53-as) are occupied by unreacted BDC molecules, and by other impurities like DMF (Figure 4.3).

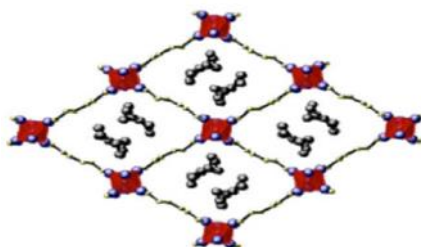


Figure 4.3 Structures of as-synthesized MIL-53

The TG curve of MIL-53 as (figure 4.4) shows two weight drops between room temperature and 900°C . The first weight drops from 330 to 430°C is due to the DMF molecules and other impurities within the pores. The second weight drop is due to the decomposition of BDC linkers from the framework when the temperature is between 500 and 600°C . Above 600°C , the MIL-53 crystals are transformed into Al_2O_3 . The total weight of Al_2O_3 could include two kinds of sources: one is derived from the MIL-53 phase transformation and the other is resulting from the unreacted AAO. MIL-53(Al) has better stability compared with most other metal-organic frameworks decomposed at 350°C , which is beneficial DRM.

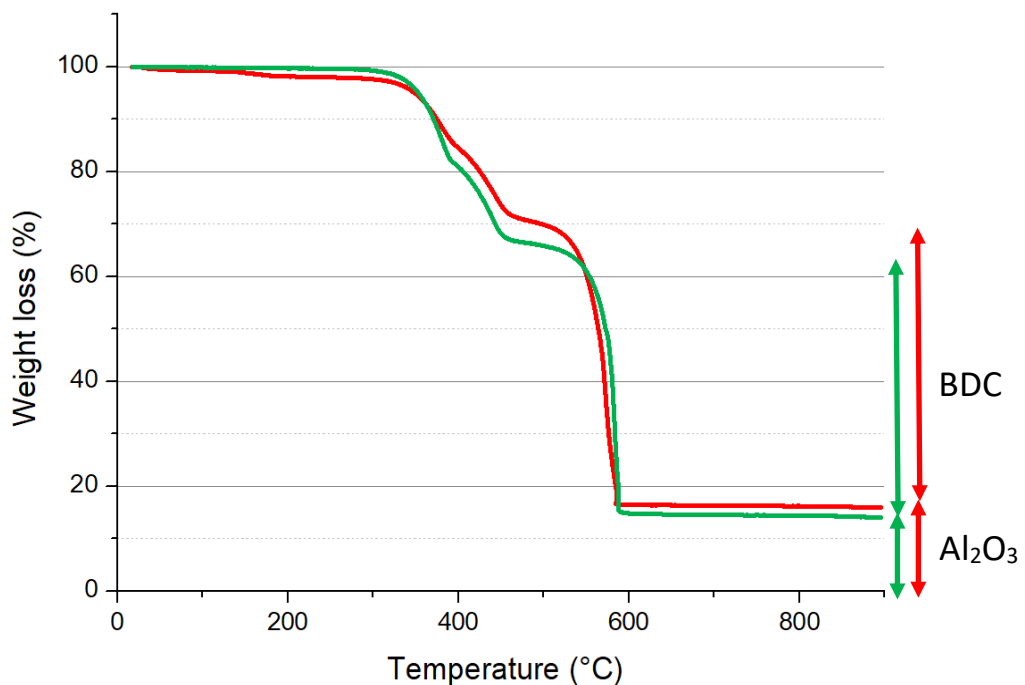


Figure 4.4 TGA curves of: as-synthesized MIL-53(Al) from PET (red line), as-synthesized MIL-53(Al) from BDC (green line)

The chemical formula of MIL-53(Al) is $\text{Al}(\text{OH})(\text{O}_2\text{C}-\text{C}_6\text{H}_4-\text{CO}_2)$, so in theory the ratio between the number of mole of Al and BDC it must be equal to one. From TGA curve is possible to know the quantity of BDC and of Al_2O_3 and consequentially calculate the ratio (table 4.1).

	BDC weight loss (%)	Al_2O_3 weight loss (%)	$n_{\text{Al}} / n_{\text{BDC}}$
MIL-53-as-PET	52	18	1,13
MIL-53-as-BDC	42	15	1,16

Table 4.1 Data related to TG curves

From the table we can observe that the ratio is around one in both case, so we can conclude that we got pure MIL-53 and that there is no more PET unreacted.

4.1.2 Activated MIL-53(Al)

The as-synthesized form contains DMF molecules and unreacted BDC insides the pores. These two molecules can be removed by heating MIL-53-as at 330 °C for 72 h. The resulting structure is referred to as MIL-53-high-temperature (MIL-53-ht), which has empty, open pores of 8.5 Å x 8.5 Å in diameter (Fig 4.5 left). Upon cooling in air, the structure absorbs water leading to the third form, MIL-53-low-temperature (MIL-53-lt), having smaller or closed pores with dimensions of 2.6 Å x 13 Å (Fig 4.5 right). This hydrated form of MIL-53 has contracted pores due to the H-bond interactions between the hydrogen atoms of the absorbed water molecules and the oxygen atoms of the carboxylate functionalities of the linker and the OH-groups associated with aluminum. The absorbed water can be removed by heating, resulting in the MIL-53 open-pore (MIL-53-ht) structure.

This transition is fully reversible when water is evacuated from the pores, and no bond breaking, or phase transition is observed in the process.

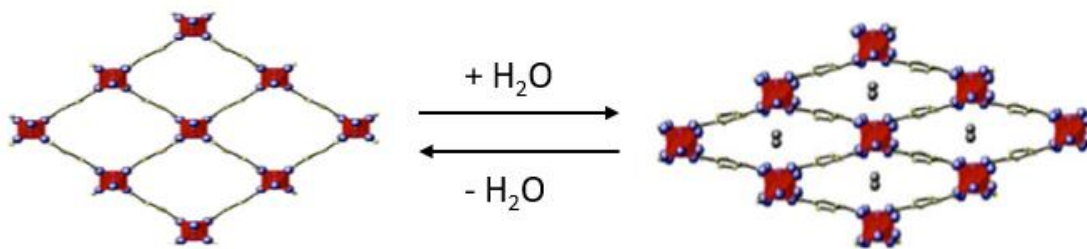


Figure 4.5 Structures of MIL-53-ht on the left, and MIL-53-lt on the right

MIL-53 is a flexible framework, implying pore size variations upon guest adsorption (so-called “breathing behavior”) with an amplitude that depends on the size of the guest molecules and on the strength of their interaction with the framework. So for each form or each guest exists a specific XRD pattern. After activation at 330 °C (to eliminate all molecules trapped in the pores), the diffractogram changes to a completely different one, in accordance with the dynamic nature of the MIL-53 structure. One can note however that the new PXRD pattern is not composed of peaks belonging to the large pore form of MIL-53 only (indicated by black triangles) as should be expected in the absence of trapped molecules, but is also contains peaks related to the narrow pore form (indicated by black spheres) as well as reflections belonging to an intermediate state between the open and closed forms (indicated by black diamonds). Average crystallite size was estimated using the Scherrer equation, is in the range of 210–635 nm for the activated MIL-53-BDC sample and in the range of 160–550 nm.

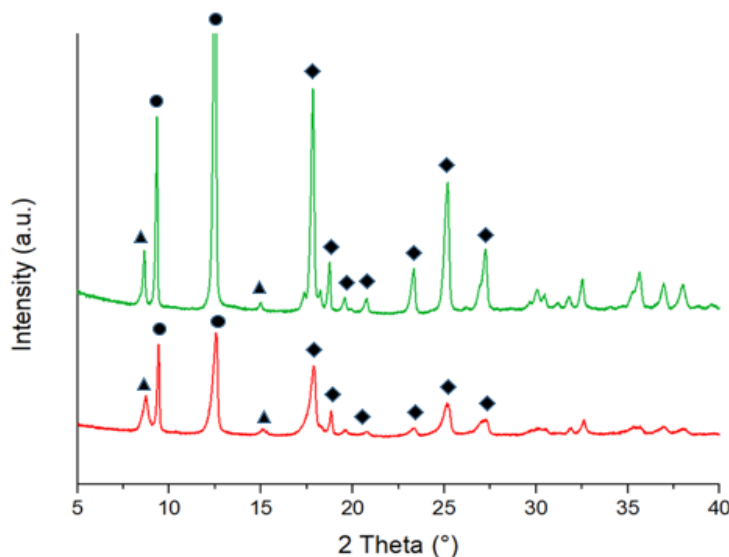


Figure 4.6 X-ray diffraction patterns of: activated MIL-53-PET (red line) and activated MIL-53-BDC

The thermal behavior of activated MIL-53 is characterized by two weight losses (Figure 4.7). The first, from 25°C to 100°C, is assigned to the dehydration process, and corresponds to the removal of one equivalent of water molecules from the pores of MIL-53-lt (8 wt.%). The second weight loss (about 70 wt.%) from 500 to 560 °C corresponds to the

decomposition of structural BDC linkers from the framework. At 900 °C, the final residue is again Al₂O₃ (about 22wt.%).

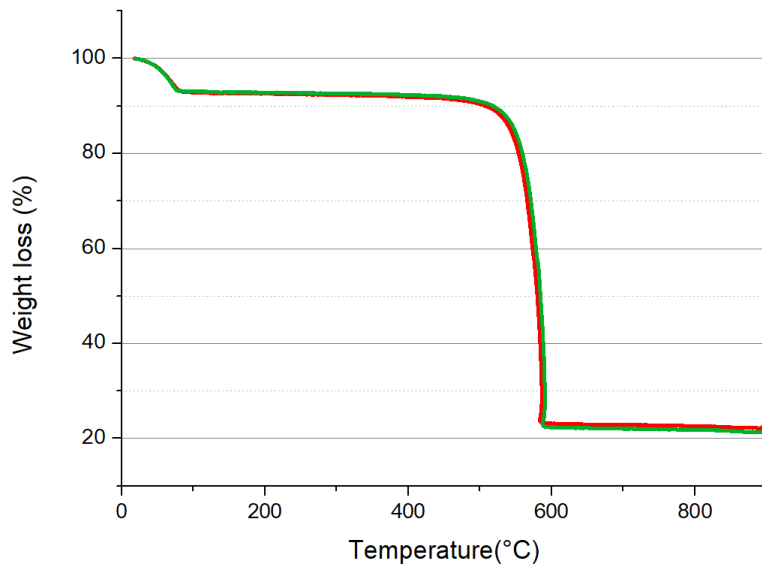


Figure 4.7 TGA curves of: activated MIL-53(Al) from PET (red line), activated MIL-53(Al) from BDC (green line)

The nitrogen adsorption–desorption isotherm measurements on MIL-53(Al) samples exhibited Type I isotherms, which were characteristic of a microporous material. According to figure 4.7, N₂ sorption isotherms were reversible and did not show any hysteresis upon desorption. The major uptake of N₂ in the adsorption/desorption isotherms occurred at relatively low relative pressure and reaches the plateau.

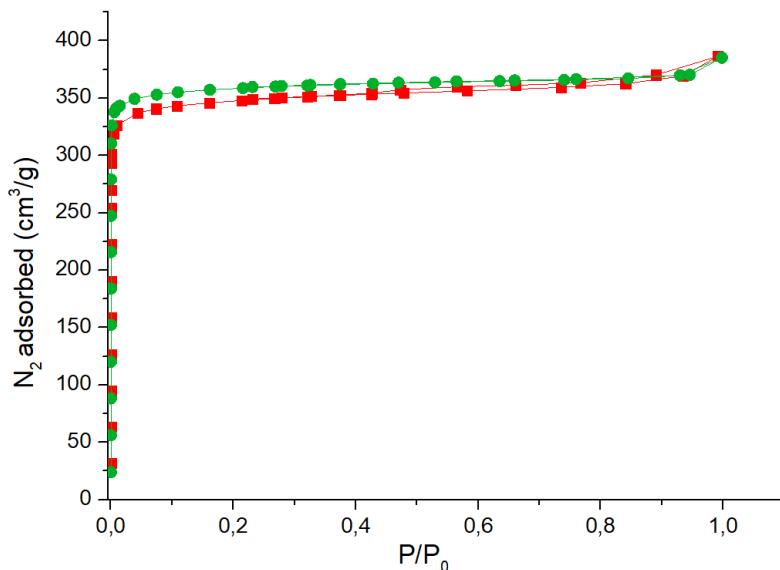


Figure 4.8 N₂ physisorption isotherms after activation at 330°C of: activated MIL-53-PET (red line) and activated MIL-53-BDC

The BET surface area, pore volume and pore diameter have also been calculated by using the N₂ adsorption isotherm. The studied MOFs, MIL-53-PET and MIL-53-BDC have

shown the BET surface area of 1402,5 m²/g and 1397,6 m²/g, pore volume of 0,59 cm³/g and 0,58 cm³/g, and pore diameter of 1,68 nm and 1,67 nm respectively.

Figure 4.8 shows the SEM images of those samples. From SEM images it can be noted that in both cases large crystals are obtained, but with a more defined shape when commercial BDC is used. It was however noted that the crystal sizes of the MIL-53(Al) synthesized from the PET were relatively bigger than those obtained from the commercial BDC. This observation complemented the differences in relative crystallinity observed from the XRD analysis shown in Fig 4.6.

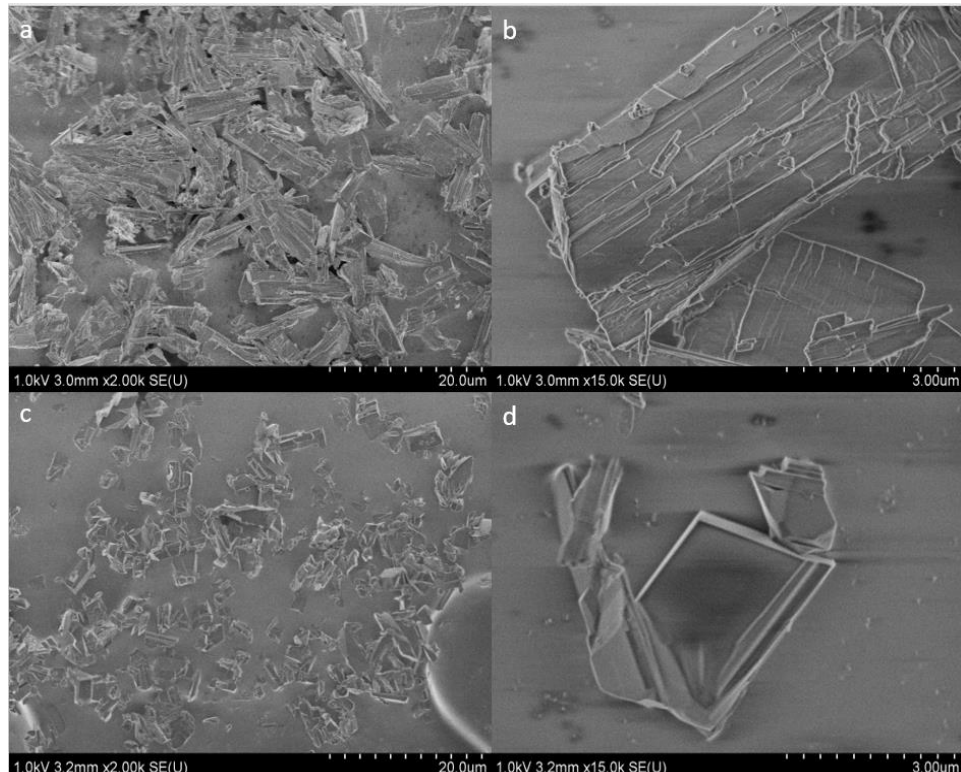


Figure 4.9 Representative scanning electron microscopy images of: (a) and (b) Activated MIL-53-PET, (c) and (d) Activated MIL-53-BDC

It can therefore be confirmed that it is possible to synthesize MIL-53 (Al) using waste PET as a source of terephthalic acid. So from now on I will focus my attention on the MIL-53 synthesize using PET.

4.1.3 Impregnated MIL-53(Al)

In this study, nickel nitrate (Ni^{2+}) is used as metal precursor. In the case of incipient wetness impregnation, the pores of the support (know from N_2 physisorption on activated samples) are filled with a volume of aqueous precursor solution that is equal to the pore volume, and deposition of Ni^{2+} on the surface occurs during drying and calcination. Nickel catalysts of 2 wt.% Ni are prepared, and the samples are calcined at 500°C to explore the possibility of the formation of nickel oxide and stoichiometric/non-stoichiometric nickel aluminates. After nickel impregnation it can observe from N_2 physisorption a loss of pores volume at low relative pressure ($P/P_0=0,2$), due to the presence of Ni^{2+} inclusion within the pores. Accordingly, the BET surface area decreases from 1402,5 m²/g to 1106,1 m²/g, the microporous volume decreases from 0,58 cm³/g to 0,50 cm³/g and the pore diameter increase to 1,82 nm.

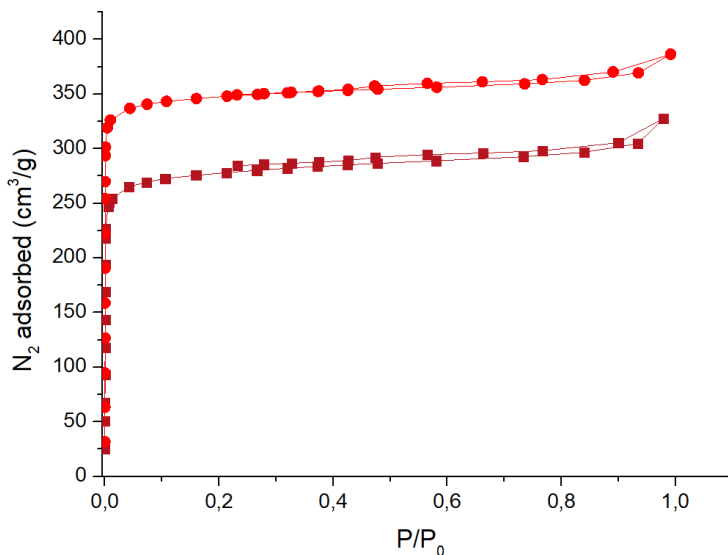


Figure 4.10 N_2 physisorption isotherms of: activated MIL-53-PET (light red line) and impregnated MIL-53-PET (dark red line)

To be sure that nickel is within the pores and not blocking only the entrance of the surface, the PXRD after Ni impregnation is checked. Because MIL-53 displays structural flexibility; indeed, the MIL-53 structure which is fully open after activation at high temperature drastically change under molecular adsorption because the pore size adjusts to the guest molecules, and these phenomena has a direct consequence on PXRD.

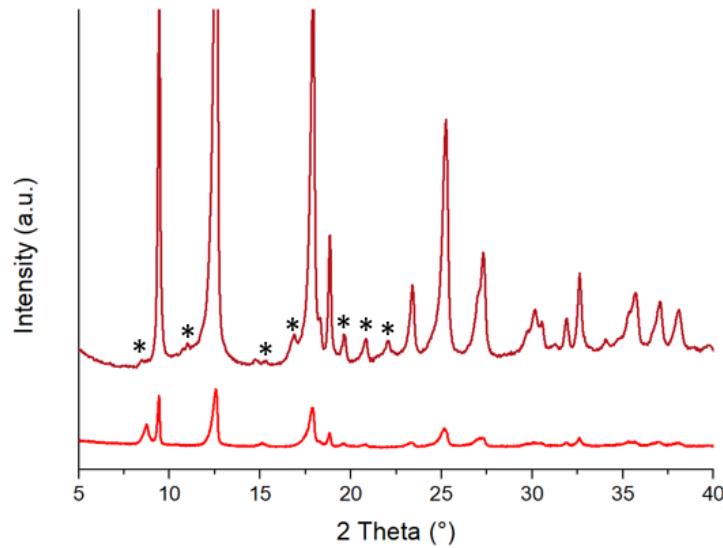


Figure 4.11 X-ray diffraction patterns of: activated MIL-53-PET (light red line) and impregnated MIL-53-PET (dark red line)

The appearance of new unattributed peaks (indicated by black stars) cannot be attributed either to the closed form or to the open form, but to an intermediate form. This local structural distortion is induced by the interaction of the structure with occluded nickel cations within the pores, as well as in MIL-53 by interaction with adsorbed organic molecules.

The intimate mixing between the nickel precursor species and the porous network in Ni/MIL is furthermore evidenced by thermogravimetric analyses that shows a weight loss of about 15% between 200°C and 450°C which corresponds to the decomposition of the nitrate salts into NO_x (NO, NO₂, etc). In view of these TG profiles, we decided to set the calcination temperature of impregnated MIL-53 during sample reparation at 500°C, a temperature high enough to degrade the linkers but guaranteeing as well the development of the porosity and the large surface area of the pure mineral phase.

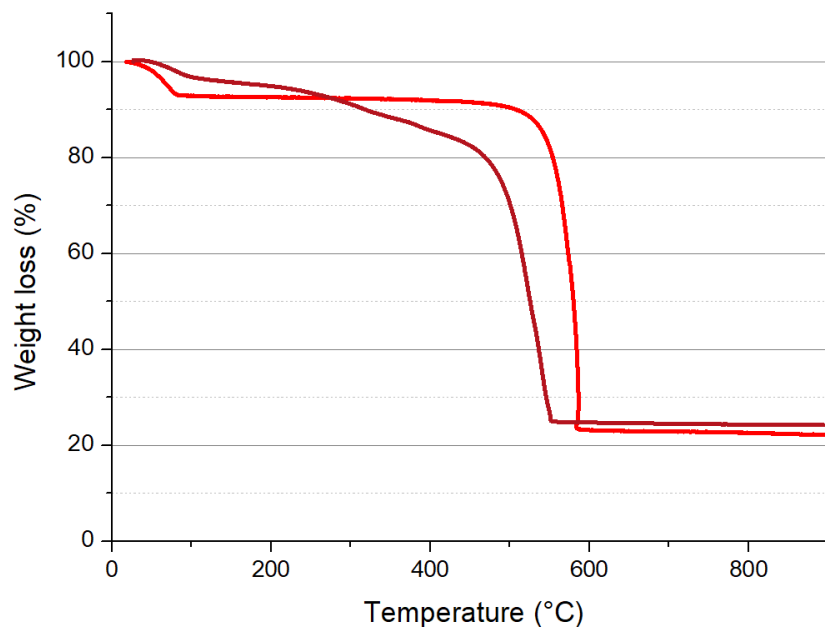


Figure 4.12 TGA curves of: activated MIL-53(Al) from PET (light red line), impregnated MIL-53(Al) from PET (dark red line)

Hence, all data agree on the fact that the linkers degradation is displaced towards a significantly lower temperature after nickel impregnation, giving the following scenario during heating of Ni/MIL:

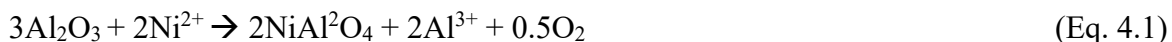
- 1) the temperature increases up to 150°C leads to the dehydration of the hexahydrate nickel nitrate used as a nickel precursor according to the equation $\text{Ni}(\text{NO}_3)_2 \cdot 6\text{H}_2\text{O} \rightarrow \text{Ni}(\text{NO}_3)_2$, the theoretical mass loss of 59% for this event being close to the 50% measured by TG;
- 2) this is followed between 200 and 400 °C by nitrates decomposition into NO_x with simultaneous formation of a NiO-based phase (for the sake of neutrality preservation) then, strongly adsorbed NO_x oxidizers remaining within the pores in close proximity with the organic linkers promote their decomposition, decreasing the temperature at which occurs.

4.1.4 Calcined MIL-53(Al)

The reducible NiO species are usually divided into three types: α , β and γ . The peak located in the low temperature region (300–550 °C) was assigned to α -type NiO species, which were free nickel oxides species having a weak interaction with the support. The mild-temperature peak (550–700 °C) represented β -type NiO species with a stronger interaction with alumina than α -type NiO. Finally, the high-temperature peak (>700 °C) was related to γ -type NiO species which were ascribed to the stable nickel aluminate phase with a spinel structure. After calcination at 500 °C, it is possible to observe from XRD pattern (Fig. 4.13) the presence of new peaks due to the formation of Ni aluminate (indicated by black stars). The XRD pattern of the calcined samples shows main diffraction peaks at $2\theta = 44,39^\circ$ and

63,73°. It doesn't contain any peak attributable to a crystalline NiO, confirming the assumption of an intimate mixing between Ni and the oxide support. The formation of NiAl₂O₄ is due to the counter-diffusion of Ni²⁺ and Al³⁺ through aluminate structure. The following reactions describe the formation of nickel aluminate phase. The decomposition of Al₂O₃ to Al³⁺ and O₂ occurs at the interface of Al₂O₃ (Equation 4.1). In addition, the movement of oxygen to the interface of NiO results in the occurrence of reaction with Al³⁺ to form NiAl₂O₄ spinel (Equation 4.2).

At Al₂O₃ interface:



At NiO interface:

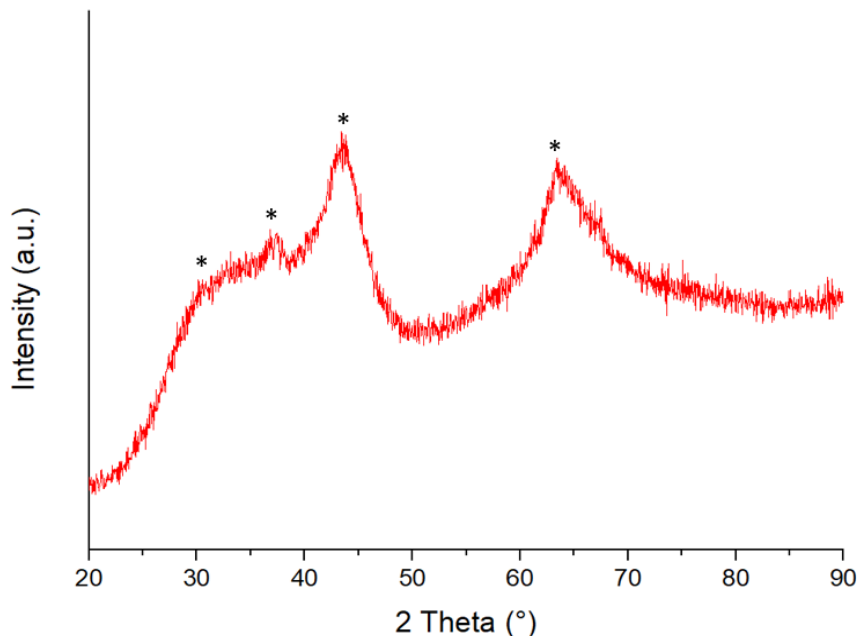


Figure 4.13 X-ray diffraction patterns of: calcined MIL-53-PET (red line)

H₂-TPR experiments were carried out in order to investigate the reducibility of the nickel species and the metal–support interactions. It is believed that reducibility of NiO species, in supported nickel catalysts, is highly affected by the nature of metal–support interaction. Generally, the reduction peak of NiO species shift towards higher temperatures due to higher metal-support interaction. The dispersion of Ni²⁺ in the form of the cubic spinel NiAl₂O₄ is also demonstrated by the temperature programmed reduction profile (Fig. 4.14) of calcined MIL-53-PET that contain a main peak at high temperature of about 870°C, revealing some inclusion of nickel within the oxide matrix that interacts strongly with the support (MSI). From TPR profile is possible to see a small shoulder in a range between 700 and 760 °C, which could indicate the presence of a second population interacting less strongly with the alumina support (most probably nickel oxo-clusters on the external surface of the alumina grains).

In view of these TPR profiles, it has been decided to set the reduction temperature of calcined MIL-53 at 800°C.

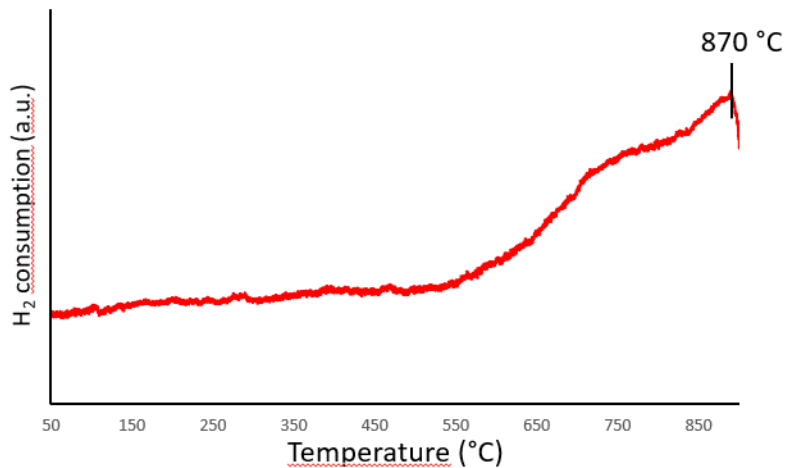


Figure 4.14 H₂-TPR profiles of calcined MIL-53-PET

In order to visualize the textural aspects derived from the preparation method and Ni loading the reduced samples were also investigated by scanning electron microscopy. From SEM images (Fig. 4.15) it can be seen that MIL-53 crystals were transformed in to stacked layer of Al₂O₃, while keep the same morphology.

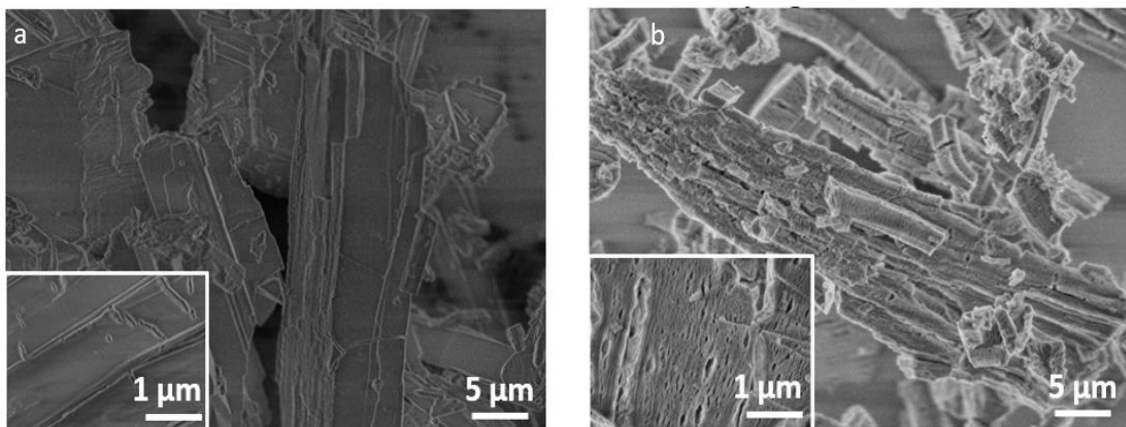


Figure 4.15 Representative scanning electron microscopy images of: (a) Impregnated MIL-53-PET, and (b) Calcined MIL-53-PET

Such morphology is in line with that deduced from the N₂ isotherm that displays features typical of layered mesoporous materials, namely a progressive increase of the adsorbed N₂ volume, observed here at P/P₀ higher than 0.7, and a slit-type hysteresis spread over P/P₀ values, ranging here from 0.7 to 1 and revealing a relatively polydisperse size distribution of large mesoporous. From Fig. 4.16, the N₂ isotherm of two samples is a type IV isotherm, and type IV isotherms are typical for mesoporous materials according to the IUPAC classification.

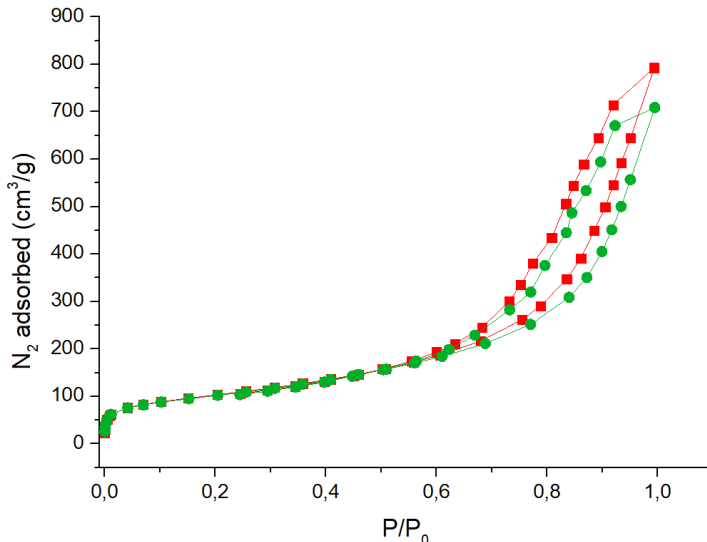


Figure 4.16 N_2 physisorption isotherms of: calcined MIL-53-PET (light red line) and calcined MIL-53-BDC (green line)

The good structural properties of the samples can also be seen from the surface area values, pore volumes and pore diameters deduced from the isotherms, reported in the following table.

	Specific area (m ² /g)	Pore volume (cm ³ /g)	Pore diameter (nm)
Calcined MIL-53-PET	356,36	1,124	12,612
Calcined MIL-53-BDC	351,88	0,988	11,237

Table 4.2 Data related to N_2 isotherms after calcination at 500 °C

The BET specific area is still high, even if much smaller than in the activated MIL-53 material due to the organic linkers removal, and the microporous volume and pore size is higher than in the impregnated MIL-53. Generally, the catalysts with high BET surface area can provide large contact area for the reactants, consequently resulting in high reaction activity.

4.1.5 Reduced MIL-53(Al)

Previous to catalytic tests, all the prepared nickel-alumina materials were treated under a flowing H_2 atmosphere to obtain the reduced Ni° active phase for DRM. The H_2 consumption during TPR was used to estimate the amount of reducible Ni^{2+} in all nickel containing samples. For all them the content is close to expected 5 wt%.

The PXRD patterns of the sample reduced at 800°C is showed in Figure 4.17 to those before reduction. The reduction of $\text{Ni}^{2+}@\text{Al}_2\text{O}_3$ to $\text{Ni}^\circ@\text{Al}_2\text{O}_3$, leads to the formation of new diffraction peaks at $2\theta=44.7^\circ$, 51.56° , 67.15° and 76.37° . Bands attributable to an alumina-based phase are still present but they are slightly shifted (compare to those before reduction) towards positions characteristic of pure $\gamma\text{-Al}_2\text{O}_3$ attesting of the extraction of the Ni species from oxide matrix towards the pore surface. Application of Scherrer equation to the Ni° reflection at $2\theta=51.56^\circ$ leads to a mean Ni° nanoparticles size of 20.29 nm, and at $2\theta=76.37^\circ$ leads to a mean Ni° nanoparticles size of 6.39 nm. The lower size was attributed to the

reduction of the aluminate phase whereas the larger size was related to the reduction of NiO (α - and β -type species), as revealed by H₂-TPR analysis.

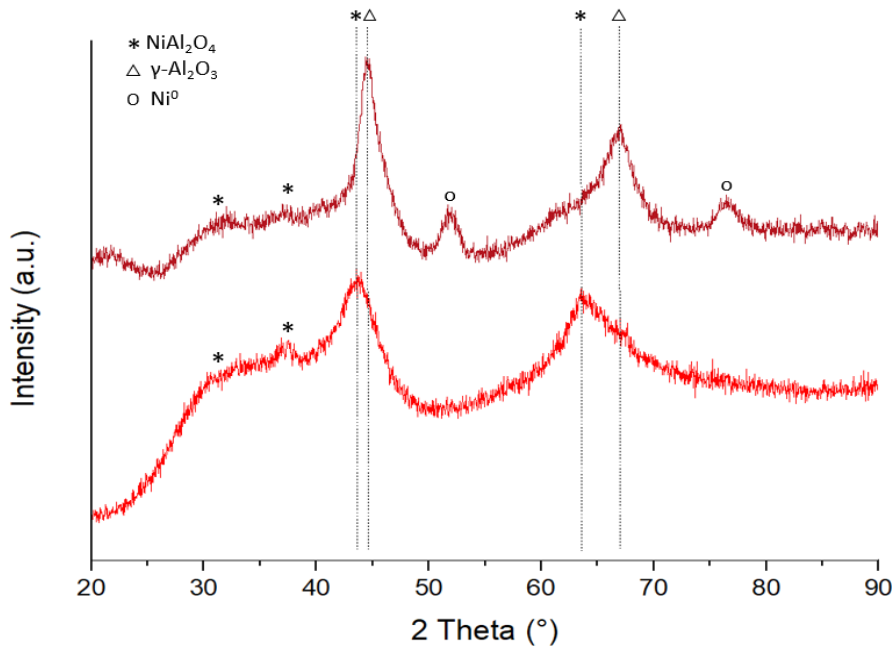


Figure 4.17 X-ray diffraction patterns of: calcined MIL-53-PET (light red line) and reduced MIL-53-BDC (dark red line)

Figure 4.18 shows the pore size distribution and adsorption/desorption isotherm of the reduced sample. The N₂ physisorption isotherm of reduced MIL-53(Al) still showing a slit-like hysteresis typical of a layered material composed of poorly organized interlayered pores. The amount of N₂ adsorbed at P/P₀>0,8 is however higher than that before reduction, indicating the formation of additional large mesopores within the material. This increase of the total pore volume and mean pore size upon reduction (table 4.3) is likely due to the exfoliation of the packed nanosheets through the transformation of the NiAl₂O₄ spinel phase into γ -Al₂O₃, and the formation of the Ni⁰ nanoparticles, which may tend to further space apart the nanosheets one from another.

	Specific area (m ² /g)	Pore volume (cm ³ /g)	Pore diameter (nm)
Calcined MIL-53-PET	356,36	1,124	12,612
Reduced MIL-53-PET	265,48	1,215	15,298

Table 4.3 Data related to N₂ isotherms after reduction at 800 °C

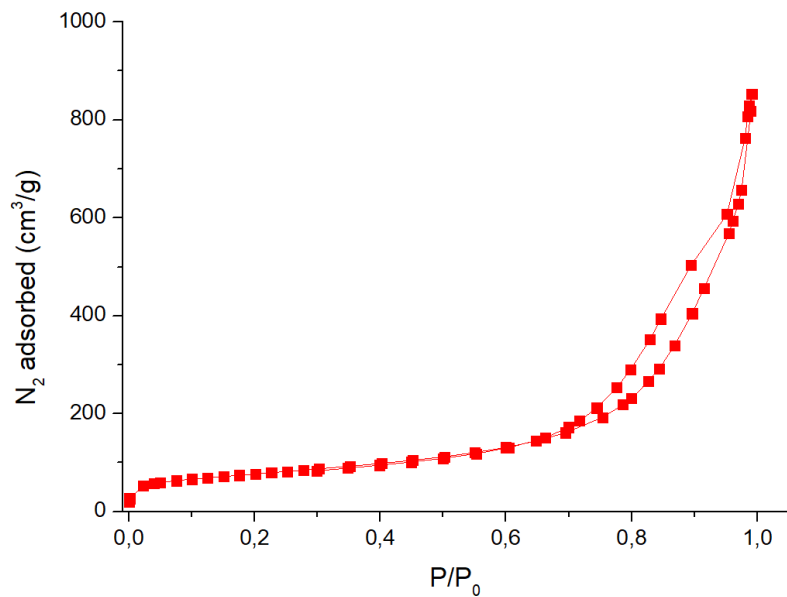


Figure 4.18 N₂ physisorption isotherm of reduced MIL-53-PET

Figure 4.19 shows typical TEM micrographs of the MIL-53 after calcination at 500 °C, and after reduction at 800 °C. The impregnation of Ni within the MOF before its calcination was not very homogeneous so that the Ni nanoparticles after reduction are mainly located on the edge of the material and not homogeneously dispersed throughout the whole sample. The not totally homogeneous dispersion of the nickel particles causes in some parts the deposition of large nickel particles (probably NiO) at the edge of the calcined MOF even before the reduction step. Still the lamellar Al₂O₃ material obtained looks nice.

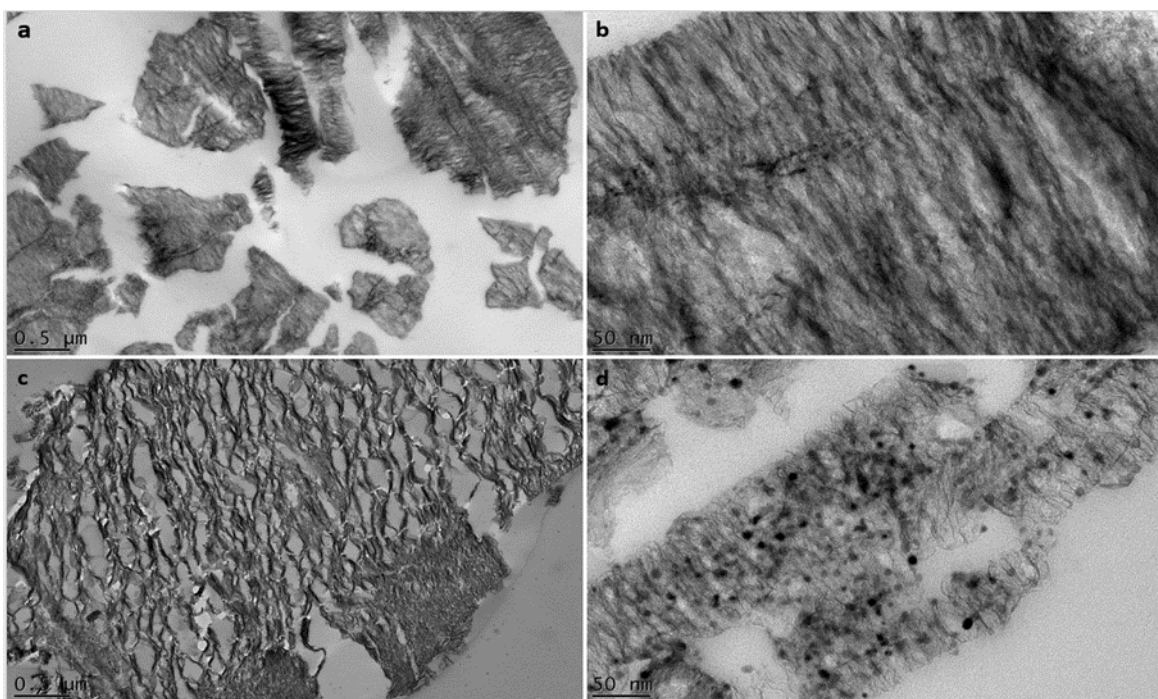


Figure 4.19 Representative Transmission electron microscopy images (a) and (b) of calcined MIL-53(Al), (c) and (d) of reduced MIL-53(Al)

4.2 Two steps synthesis

The following results refer to different samples:

-Sample MIL-53-AlO(OH): synthesized using PET and boehmite

-Sample MIL-53-AlCl₃: synthesized using PET and aluminum chloride

4.2.1 Alcoholytic of PET

Alcoholytic of PET is the first step and is usually carried out with the use of sodium hydroxide and ethylene glycol. A white powder of Na₂BDC, which was formed during the course of reaction in EG, was separated, dissolved in water, and acidified with an excess amount of sulfuric acid to obtain terephthalic acid. The BDC separated was dissolved in dimethyl sulfoxide (DMSO) and its purity examined by the FT-¹H NMR analysis to detect the EG residue if remained in the form of oligomers or hydroxyethyl terephthalates. From NMR spectrum shown in the figure 4.20 it can be seen that pure BDC was obtained, indeed there are only two peaks. The first one δ=2.52 ppm is due to the use of DMSO as a solvent, the second one δ=8.06 ppm is due to the presence of BDC.

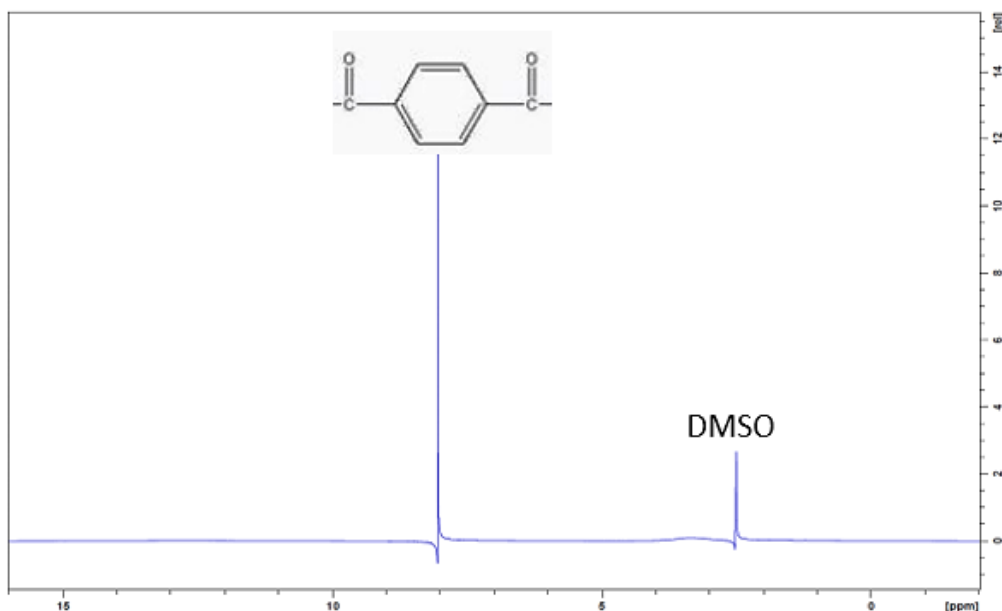


Figure 4.20 ¹H-NMR spectrum of BDC obtained from the alcoholytic of PET heated at 160°C for 1 h and precipitated by the addition of sulfuric acid.

4.2.2 Synthesis and activation of MIL-53(Al)

In the second step, the terephthalic acid obtained in the first step was used as a reagent together with an aluminum source (boehmite or aluminum chloride hexahydrate) to synthesize MIL-53 (Al). After synthesis in hydrothermal conditions, the parent MIL-53 sample is characterized by a X-ray diffractogram. The XRD patterns of the MIL-53(Al) frameworks prepared from aluminum chloride and boehmite (MIL-53-AlCl₃ and MIL-53-AlO(OH), respectively) are mostly identical and in good agreement with those of the previously reported as-synthesized MIL-53-BDC (Figure 4.21). This indicates the formation of pure MIL-53 (Al) framework.

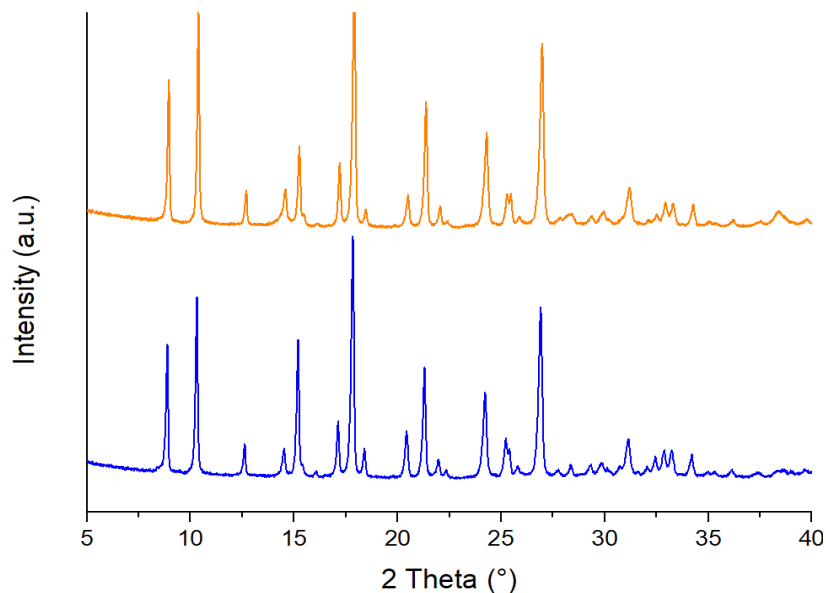


Figure 4.21 X-ray diffraction pattern of: as-synthesized MIL-53(Al) from AlCl₃ (blue line), as-synthesized MIL-53(Al) from AlO(OH) (orange line)

After activation at 330°C, the XRD patterns of the MIL-53-AlCl₃ and MIL-53-AlO(OH) shows, as in the one step synthesis, the coexistence of three different structures: large pore form, narrow pore form and intermediate form. Average crystallite size of the samples was estimated in the range of 370–600 nm using the Scherrer equation. The strong and narrow diffraction peaks indicate a high purity and good crystallinity of the synthesized materials. The activation temperature and the synthesis temperature are the most effective parameters on the crystallinity of the final products. The activation temperature had positive effect due to the higher impurities removal at high temperature. It should be noted that the presence of disordered terephthalic acid, as a major impurity, reduces the relative crystallinity of the final product because of differences in crystal structure of MIL-53(Al) before and after BDC removal.

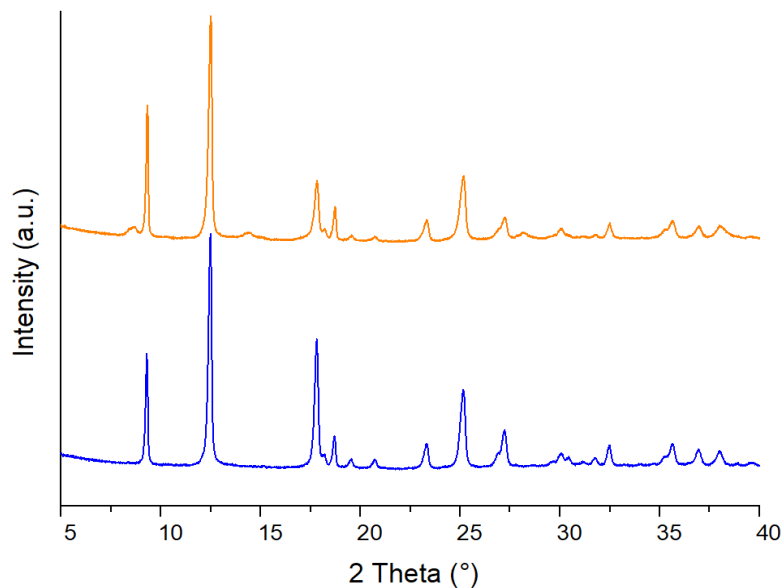


Figure 4.22 X-ray diffraction pattern of: activated MIL-53-AlCl₃ (blue line), activated MIL-53-AlO(OH) (orange line)

The adsorption and desorption isotherms of N₂ at 77K are depicted in Figure 4.23. It can be seen that N₂ sorption isotherms are reversible and do not show any hysteresis upon desorption. Obtained isotherms of all the samples could be classified as Type-I according to IUPAC classification. The major uptake of N₂ in the adsorption/ desorption isotherms occurred at relatively low relative pressure and reaches the plateau. It can also be noted that the volume adsorbed by the sample synthesized using boehmite is smaller than that synthesized using AlCl₃.

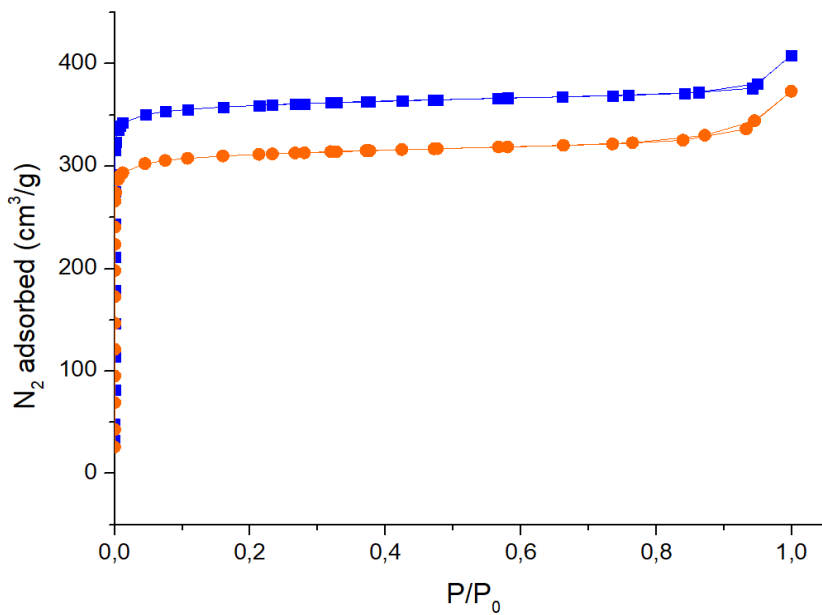


Figure 4.23 N₂ physisorption isotherms of: activated MIL-53-AlCl₃ (blue line), activated MIL-53-Al(OH) (orange line)

The obtained results from the N₂ sorption isotherms are presented in Table 4.3. It can be observed that the surface area (BET) and micropore volume of activated MIL-53-AlCl₃ sample were higher compared to activated MIL-53-Al(OH) sample. The high temperature during activation may affect the textural properties of the material which may result in lower surface area and pore volume. The high surface area and porosity are two important factors to synthesize highly stable and active catalysts for dry reforming of methane.

	Specific area (m ² /g)	Pore volume (cm ³ /g)	Pore diameter (nm)
Activated MIL-53-AlCl₃	1455,2	0,610	1,678
Activated MIL-53-Al(OH)	1262,8	0,556	1,762

Table 4.4 Data related to N₂ isotherms after activation of the parent MIL-53
4.2.3 Nickel impregnation of MIL-53(Al)

To synthesize a catalyst that is active and stable in the reaction of dry reforming of methane, it is necessary impregnate the support with a nickel precursor solution which represents the active phase of the catalyst. As shown in Figures 4.24 and 4.25, all the peaks corresponding to the activated form are still present after the Ni impregnation, even if slightly displaced

and with higher intensity after impregnation and drying at 200 ° C. Furthermore, it can be noted the appearance of new peaks (indicated by black stars), probably attributable to structural changes of the framework due to the presence of nickel cations inside the pores of MIL-53.

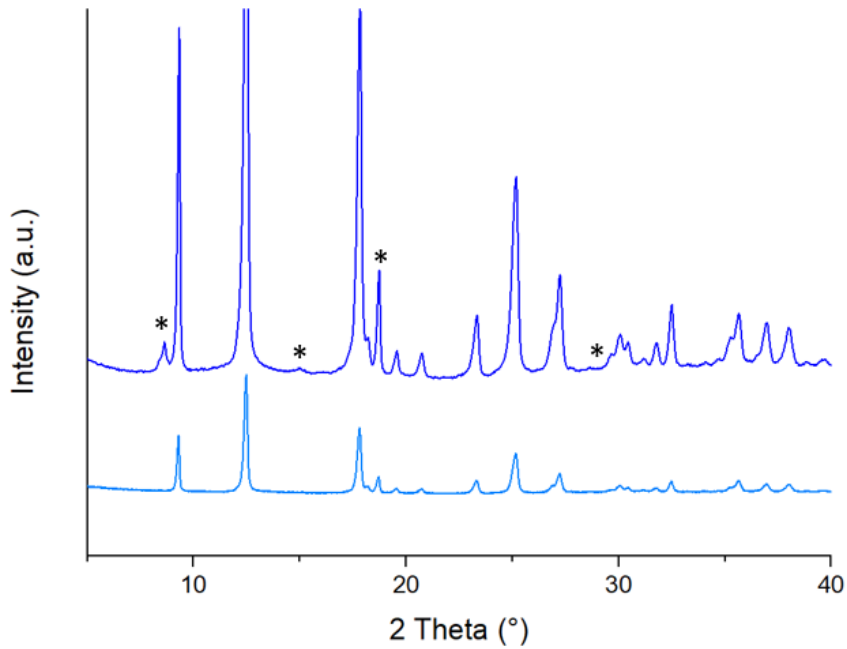


Figure 4.24 X-ray diffraction pattern of: activated MIL-53-AlCl₃ (light blue line), impregnated MIL-53-AlCl₃ (dark blue line)

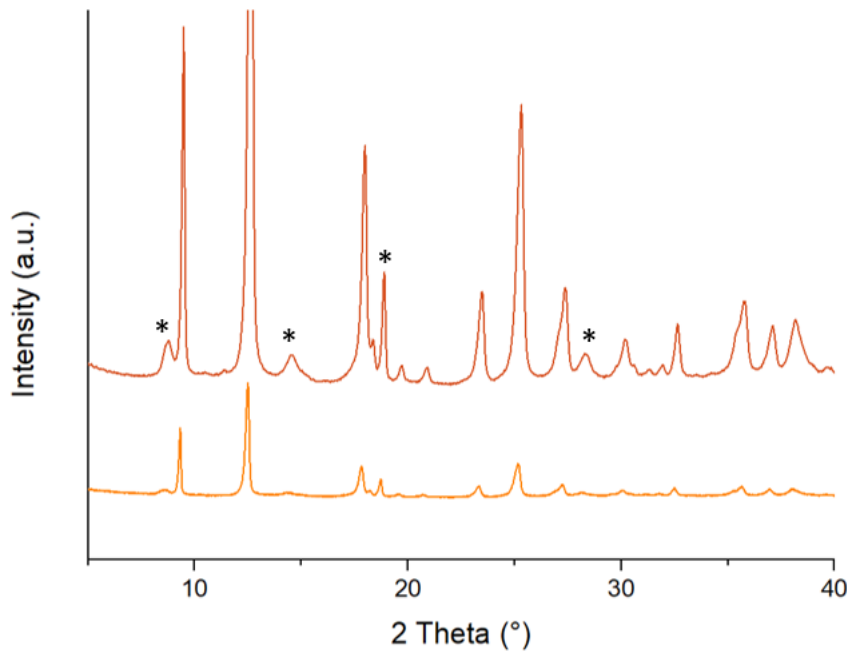


Figure 4.25 X-ray diffraction pattern of: activated MIL-53-AlO(OH) (light orange line), impregnated MIL-53-AlO(OH) (dark orange line)

N₂ physisorption was performed on activated and impregnated samples. For the sample synthetized using aluminum chloride (Figure 4.26) it can be seen a decrease of pore volume after nickel impregnation, due to the presence of nickel inside the pores and not only at the

entrance of the pores. Instead for the sample synthetized using boehmite (Figure 4.27) there is a very small loss of pores volume after nickel impregnation. This is due to the fact that the nickel particles are not present inside the pores but only on the surface of the matrix.

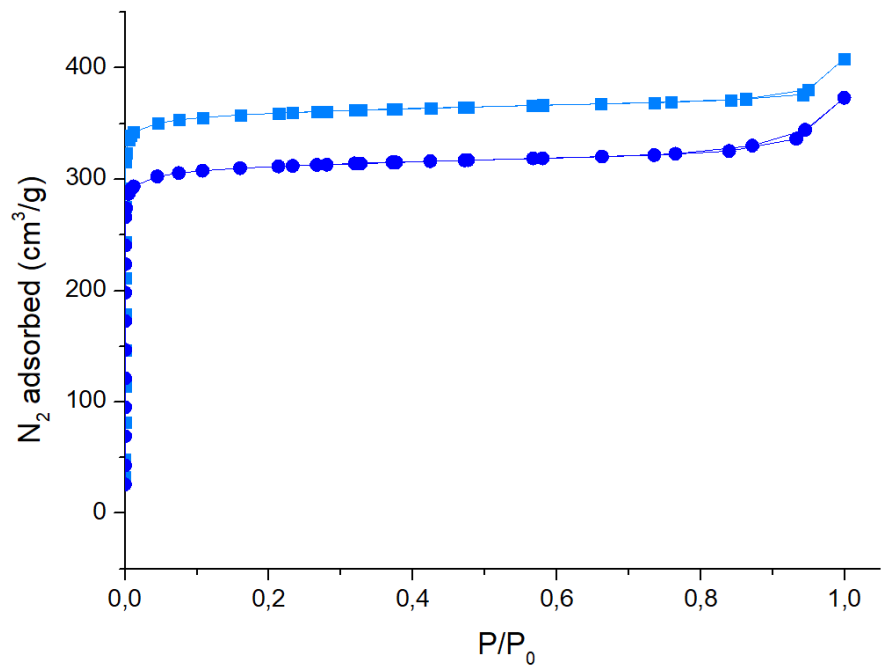


Figure 4.26 N₂ physisorption isotherms of: activated MIL-53-AlCl₃ (light blue line), impregnated MIL-53-AlCl₃ (dark blue line)

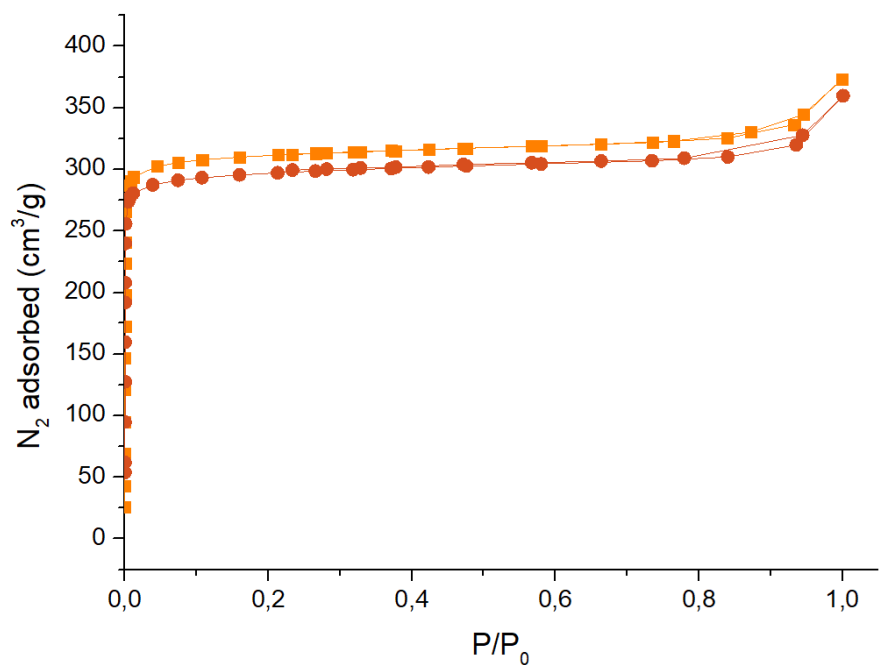


Figure 4.27 N₂ physisorption isotherms of: activated MIL-53-AlO(OH) (light orange line), impregnated MIL-53-AlO(OH) (dark orange line)

The specific surface area, pore volume and average pore size are shown in Table 4.4. From these results, it can be noted that for MIL-53-AlCl₃ the specific area and pore volume decreases while the pore size increases; this confirms the presence of nickel inside the pores.

Instead for the MIL-53-AlO(OH) the specific area and the pore volume show a very small decrease after nickel impregnation, and the pore size does not increase much; this confirms that in this case the nickel cannot penetrate inside the pores but remains blocked at the entrance of the pores.

	Specific area (m ² /g)	Pore volume (cm ³ /g)	Pore diameter (nm)
Impregnated MIL-53-AlCl₃	1236,4	0,598	1,857
Impregnated MIL-53-AlO(OH)	1202,2	0,532	1,769

Table 4.5 Data related to N₂ isotherms after Ni impregnation of the parent MIL-53

4.2.4 Calcination of MIL-53(Al)

The crystalline structure of the samples was determined by XRD. Figure 4.28 shows the XRD patterns of the catalysts obtained using two different aluminum sources after calcination at 500 °C. For MIL-53-AlCl₃ the peaks at about 36 °, 43 ° and 63 ° are attributed to the presence of nickel aluminate (NiAl₂O₄), there are no peaks due to NiO and this means that there is only one type of nickel. The size of the nickel particles is calculated with the Scherer formula obtaining a diameter less than 10 nm. For MIL-53-AlO(OH) the peak at 36 ° indicates the presence of NiAl₂O₄, while the other two peaks are slightly shifted to the right (29 = 45.5 ° and 66.5 °) and this indicates the presence of another phase attributable to gamma alumina (γ -Al₂O₃). In this case the particle diameter is about 40 nm. This further confirms that nickel is not actually present in the pores.

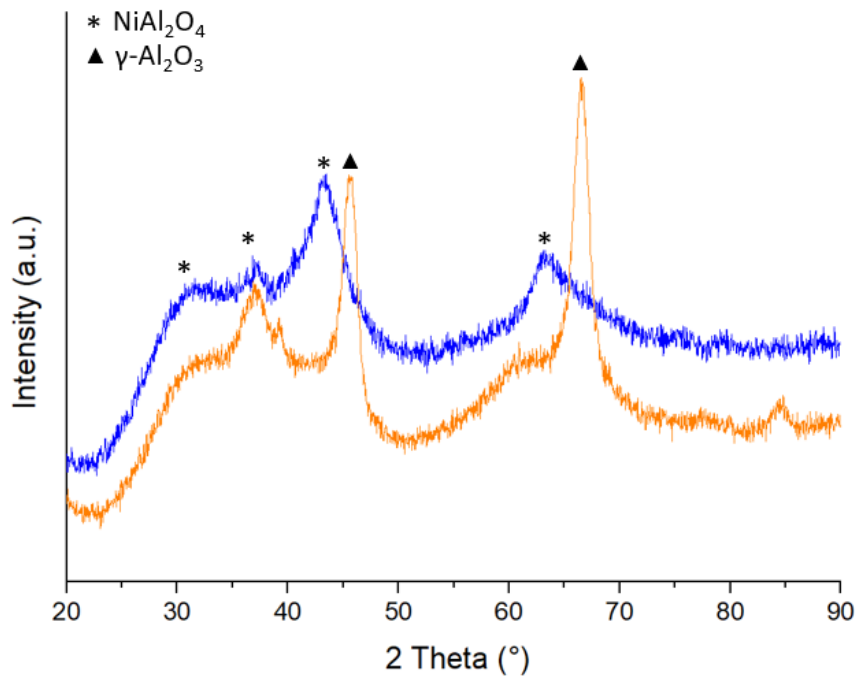


Figure 4.28 X-ray diffraction pattern of: calcined MIL-53-AlCl₃ (blue line), calcined MIL-53-AlO(OH) (orange line)

The textural properties of the calcined MIL-53(Al) were also examined by nitrogen adsorption-desorption measurements (Fig 4.29). The illustrated isotherms showed IV

isotherm with H₂ shape hysteresis loop attributed to the mesoporous powders. The results show that the amounts of N₂ adsorption is greater when aluminum chloride is used as a source of aluminum.

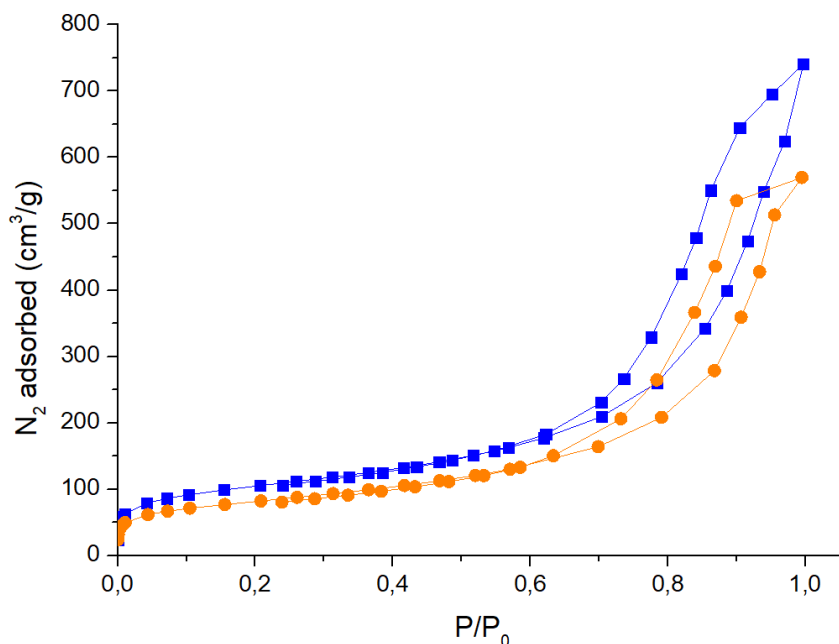


Figure 4.29 N₂ physisorption isotherms of: calcined MIL-53-AlCl₃ (blue line), calcined MIL-53-AlO(OH) (orange line)

The textural characteristics of the MIL-53 samples after calcination at 500°C for 5 h are reported in Table 4.6. It can be seen that after calcination the specific area decreases (from 1200 to about 300 m²/g) because the high temperatures cause the removal of organic linkers, and the pore volume and the pore diameter increase.

	Specific area (m ² /g)	Pore volume (cm ³ /g)	Pore diameter (nm)
Calcined MIL-53-AlCl₃	327,00	0,997	12,196
Calcined MIL-53-AlO(OH)	260,15	0,836	12,851

Table 4.6 Data related to N₂ isotherms after calcination at 500°C

5. Conclusions

During my experience at the *Laboratoire de Réactivité de Surface*, I had the opportunity to work in a very interesting and priority project and to improve my knowledge in many fields, such as synthesis of porous materials, functionalization and surface characterization and heterogeneous catalysis.

In this work we demonstrate the benefit of using the aluminum carboxylate as a sacrificial support to prepare a dry methane reforming catalyst composed of nickel nanoparticles dispersed within a porous γ -Al₂O₃ lamellar phase. The extremely high surface area of this metal organic framework material compared to other types of porous alumina supports allows for an efficient dispersion of the nickel precursors within the MOF and, in turn, for a superior dispersion and uniformity of the nickel nanoparticles after calcination.

Alkali decomposition of PET in EG was revealed to be an efficient method for the reproduction of terephthalic acid (TPA) and ethylene glycol (EG) from the recovered PET plastic wastes under mild conditions. The efficiency of monomers' reproducibility and separation is remarkably high so that the procedure seems to be usable as one of the practical methods for the recycling of PET plastics, thus contributing to the plastic waste problems.

A Ni/NiAl₂O₄-M catalyst, with a strong Ni-support interaction, was successfully fabricated by using a simple MOF-templated strategy. The strong Ni-support interaction on Ni/NiAl₂O₄-M is possibly due to the Ni²⁺ ions in the lattice of NiAl₂O₄ which may play as the nuclei for the nucleation and growth of the Ni nanoparticles and be like anchors fastening the Ni nanoparticles on the NiAl₂O₄ support. The strong Ni-support interaction on Ni/NiAl₂O₄-M results in more active H atoms which can promote the formation of the active CH* species. This suppresses the formation of the carbon deposition which has a negative effect on the catalytic reactions, thus enhancing the catalytic performance. Besides, the strong Ni-support interaction allows Ni/NiAl₂O₄-M to be highly resistant to the sintering of the Ni NPs. These findings are helpful for fabricating catalysts with strong metal-support interactions for more efficient heterogeneous catalysis.

Despite the high surface area obtained and the strong interaction between the nickel particles and the support, the TEM images on the calcined and reduced sample show that the impregnation of Ni within the MOF before its calcination was not very homogeneous so that the Ni nanoparticles after reduction are mainly located on the edge of the material and not homogeneously dispersed throughout the whole sample. The not totally homogeneous dispersion of the nickel particles causes in some parts the deposition of large nickel particles (probably NiO) at the edge of the calcined MOF even before the reduction step. This could lead to not very stable catalysts and not very high catalytic performances, so the dispersion of the nickel particles may need to be improved, perhaps by changing the impregnation method.

In summary, herein, we have successfully demonstrated that the waste polyethylene terephthalate bottle material can effectively be utilized for the synthesis of MIL-53(Al) through a simple solvothermal method. Moreover, in our ever-changing world, which is under serious threat from climate change, the value of this indigenous novel process can help to deal, at least to a small extent with one of our environmental problems and will be of great advantage both environmentally and economically. Though, this process of using waste PET for the production of many important terephthalate based MOFs requires further investigation to reach the industrial viability, the results obtained here have laid the foundation for an innovative green technology that may prove valuable to the world striving towards a greener future.

6. Abbreviations

AAO	Anodic aluminum oxide
ATR	Autothermal reforming
BDC	Benzenedicarboxylate/terephthalic acid
BET	Brunauer–Emmett–Teller
BTC	Benzenetricarboxylate
D	Crystallite size [nm]
d	Interplanar spacing
DI	Deionized water
DMF	N,N-dimethylformamide
DMSO	Dimethyl sulfoxide
DRM	Dry reforming of methane
EG	Ethylene glycol
GHG	Greenhouse gases
MIL	Materials of the Institute Lavoisier
MOFs	Metal-organic-frameworks
n	Order of diffraction
NMR	Nuclear magnetic resonance
PCPs	Porous coordination polymers
PET	Poly(ethylene terephthalate)
POM	Partial oxidation of methane
PXRD	Powder X-ray diffractograms
RWGS	Reverse water gas shift
SBUs	Secondary building units
SEM	Scanning electron microscopy
SRM	Steam reforming of methane
T	Temperature [K]
TCD	Thrmal conductivity detector
TEM	Trasmission electron microscopy
TGA	Thermogravimetric analysis
TPR	Temperature programmed reduction
XRD	X-ray diffractograms
ΔH	Enthalpy [J]
β	Full-width half-maximum

θ Scattering angle [rad]
 λ Wavelength of X-ray [nm]

7. References

- ¹ Li, X., 2005. Diversification and localization of energy systems for sustainable development and energy security. *Energ. Policy* 33 (17), 2237-2243.
- ² Noor, Z.Z., Yusuf, R.O., Abba, A.H., Abu Hassan, M.A., Mohd Din, M.F., 2013. An overview for energy recovery from municipal solid wastes (MSW) in Malaysia scenario. *Renew. Sust. Energ. Rev.* 20, 378-384.
- ³ Talyan, V., Dahiya, R.P., Anand, S., Sreekrishnan, T.R., 2007. Quantification of methane emission from municipal solid waste disposal in Delhi. *Resour. Conserv. Recycl.* 50 (3), 240-259.
- ⁴ Wuebbles, D.J., Hayhoe, K., 2002. Atmospheric methane and global change. *Earth- Sci. Rev.* 57 (3-4), 177-210.
- ⁵ Rafiu O.Yusuf, Zainura Z.Noor, Ahmad H.Amma, Mohd Ariffin Abu Hassan, Mohd Fadhil Mohd Din., 2012. Methane emission by sectors: A comprehensive review of emission sources and mitigation methods. *Renew. Sust. Energ. Rev.* 16 (7), 5059-5070.
- ⁶ Asencios, Y.J.O., Assaf, E.M., 2013. Combination of dry reforming and partial oxidation of methane on NiO-MgO-ZrO₂ catalyst: effect of nickel content. *Fuel Process. Tech.* 106, 247-252.
- ⁷ Selvarajah, K., Phuc, N.H.H., Abdullah, B., Alenazey, F., Vo, D.-V.N., 2016. Syngas production from methane dry reforming over Ni/Al₂O₃ catalyst. *Res. Chem. Interm.* 42 (1), 269-288.
- ⁸ Lucredo AF, Assaf JM, Assaf EM, 2012. Reforming of a model biogas on Ni and Rh–Ni catalysts: effect of adding La. *Fuel Process Technol.*, 102, 124–31.
- ⁹ Lunsford JH, 2000. Catalytic conversion of methane to more useful chemicals and fuels: a challenge for the 21st century. *Catal Today*. 63:165–74.
- ¹⁰ Wurzel T, Marcus S, Mleczko L. Reaction engineering investigations of CO₂ reforming in a fluidized-bed reactor. *Chem Eng Sci* 2000; 55:3955–66.
- ¹¹ San-Jose-Alonso, D., Juan-Juan, J., Illan-Gomez, M.J., Roman-Martínez, M.C., 2009. Ni, Co and bimetallic Ni-Co catalysts for the dry reforming of methane. *Appl. Catal. A: Gener.* 371 (1-2), 54-59.
- ¹² Liu, D., Quek, X.-Y., Wah, H.H.A., Zeng, G., Li, Y., Yang, Y., 2009. Carbon dioxide reforming of methane over nickel-grafted SBA-15 and MCM-41 catalysts. *Catal. Today* 148 (3-4), 243-250.
- ¹³ D. Pakhare, J. Spivey, A review of dry (CO₂) reforming of methane over noble metalcatalysts, *Chem. Soc. Rev.* 43 (2014) 7813–7837.
- ¹⁴ Z.L. Zhang, X.E. Verykios, Carbon dioxide reforming of methane to synthesis gas over supported Ni catalysts, *Catal. Today* 21 (1994) 589–595.
- ¹⁵ J.R. Rostrup-Nielsen, J.B. Hansen, CO₂-reforming of methane over transition metals, *J. Catal.* 144 (1993) 38–49.
- ¹⁶ L. Xu, H. Song, L. Chou, One-pot synthesis of ordered mesoporous NiO–CaO–Al₂O₃ composite oxides for catalyzing CO₂ reforming of CH₄, *ACS Catal.* 2 (2012) 1331–1342.
- ¹⁷ E.G. Mahoney, J.M. Pusel, S.M. Stagg-williams, S. Faraji. The effects of Pt addition to supported Ni catalysts on dry (CO₂) reforming of methane to syngas, *J. CO₂ Util.* 6 (2014) 40–44.
- ¹⁸ X. Lv, J. Chen, Y. Tan, Y. Zhang, A highly dispersed nickel supported catalyst for dry reforming of methane, *Catal. Commun.* 20 (2012) 6–11.
- ¹⁹ M.C.J. Bradford, M.A. Vannice, The role of metal±support interactions in CO₂ reforming of CH₄, *Appl. Catal. A Gen.* 50 (1999).
- ²⁰ Hong-Cai Zhou, Jeffrey R. Long, Omar M. Yaghi, Introduction to Metal–Organic Frameworks. *Chem. Rev.*, 2012, 112 (2), pp 673–674.
- ²¹ Rowsell, J. L. C.; Yaghi, O. M. *Microporous Mesoporous Mater.*, 2004, 73, 3.
- ²² Thierry Loiseau, Christian Serre, Clarisse Huguenard, Gerhard Fink, Francis Taulelle, Marc Henry, Thierry Bataille, and Gérard Férey. A Rationale for the Large Breathing of the Porous Aluminum Terephthalate (MIL-53) Upon Hydration. *Chem. Eur. J.* 2004, 10, 1373-1382
- ²³ Hiroyasu Furukawa *et al.*, 2013, The Chemistry and Applications of Metal-Organic Frameworks. *Science* 341.
- ²⁴ A. Corma, H. Garcia, and F. X. Llabrés i Xamena, 2010, Engineering Metal Organic Frameworks for Heterogeneous Catalysis. *Chem. Rev.* 110, 4606–4655.
- ²⁵ Youn-Sang Bae, Omar K. Farha, Joseph T. Hupp, Randall Q. Snurr, 2009, Enhancement of CO₂/N₂ selectivity in a metal-organic framework by cavity modification. *J. Mater. Chem.*, 19, 2131–2134.
- ²⁶ Marco Ranocchiari, Jeroen Anton van Bokhoven, 2011, Catalysis by metal–organic frameworks: fundamentals and opportunities. *Phys. Chem. Chem. Phys.*, 13, 6388–6396.

-
- ²⁷ Min Hui Yap, Kam Loon Fow, George Zheng Chen, 2017, Synthesis and applications of MOF-derived porous nanostructures. *Green Energy & Environment* 2, 218–245.
- ²⁸ Shilun Qiu, Guangshan Zhu, 2009, Molecular engineering for synthesizing novel structures of metal–organic frameworks with multifunctional properties. *Coordination Chemistry Reviews*, 253, 2891–2911
- ²⁹ Stuart L. James, 2003, Metal-organic frameworks. *Chem. Soc. Rev.*, 32, 276–288.
- ³⁰ Joonho Park, Heejin Kim, Sang Soo Han, Yousung Jung, 2012, Tuning Metal–Organic Frameworks with Open-Metal Sites and Its Origin for Enhancing CO₂ Affinity by Metal Substitution. *J. Phys. Chem. Lett.*, 3 (7), 826–829.
- ³¹ Yuki Harada, Yuh Hijikata, Shinpei Kusaka, Akihiro Hori, Yunsheng Ma, Ryotaro Matsuda, 2019, Creation of MOFs with open metal sites by partial replacement of metal ions with different coordination numbers. *Dalton Trans.*, 48, 2545–2548.
- ³² Bae, Y. S., Farha, O. K., Spokoyny, A. M., Mirkin, C. A., Hupp, J. T., Snurr, R. Q., 2008, Carborane-based metal–organic frameworks as highly selective sorbents for CO₂ over methane. *Chem. Commun.*, 35, 4135–4137.
- ³³ V. V. Butova, M. A. Soldatov, A. A. Guda, K. A. Lomachenko, C. Lamberti, 2016, Metal-organic frameworks: structure, properties, methods of synthesis and characterization. *Russian Chemical Reviews* 85 (3) 280-307.
- ³⁴ Yu-Ri Lee, Jun Kim, and Wha-Seung Ahn, 2013, Synthesis of metal-organic frameworks: A mini review. *Korean J. Chem. Eng.*, 30(9), 1667-1680.
- ³⁵ Yu-Zhen Chen, Rui Zhang, Long Jiao, Hai-Long Jiang, 2018, Metal–organic framework-derived porous materials for catalysis. *Coordination Chemistry Reviews*, 362, 1–23.
- ³⁶ Phani Rallapalli, Dinesh Patil, K. P. Prasanth, Rajesh S. Soman, R. V. Jasra, H. C. Bajaj, 2010, An alternative activation method for the enhancement of methane storage capacity of nanoporous aluminium terephthalate, MIL-53(Al). *J Porous Mater.*, 17: 523–528.
- ³⁷ Franck Millange, Richard I. Walton, 2018, MIL-53 and its Isoreticular Analogues: a Review of the Chemistry and Structure of a Prototypical Flexible Metal-Organic Framework. *Isr. J. Chem.*, 58, 1019 – 1035.
- ³⁸ Sandrine Bourrelly, Philip L. Llewellyn, Christian Serre, Franck Millange, Thierry Loiseau, Gérard Férey, 2005, Different Adsorption Behaviors of Methane and Carbon Dioxide in the Isotypic Nanoporous Metal Terephthalates MIL-53 and MIL-47. *J. Am. Chem. Soc.*, 127, 13519-13521.
- ³⁹ Armin Taheri, Ensieh Ganji Babakhani, Jafar Towfighi, 2018, Study of synthesis parameters of MIL-53(Al) using experimental design methodology for CO₂/CH₄ separation. *Adsorption Science & Technology*, 36 (1–2) 247–269
- ⁴⁰ Bawadi Abdullah a, Nur Azeanni Abd Ghani, Dai-Viet N. Vo, 2017, Recent advances in dry reforming of methane over Ni-based catalysts. *Journal of Cleaner Production* 162, 170-185.
- ⁴¹ Xiangyu Lv, J. Chen, Yisheng Tan, Yi Zhang, 2012, A highly dispersed nickel supported catalyst for dry reforming of methane. *Catalysis Communications*, 20, 6–11.
- ⁴² Won-Jun Jang, Jae-Oh Shim, Hak-Min Kim, Seong-Yeon Yoo, Hyun-Seog Roh, 2019, A review on dry reforming of methane in aspect of catalytic properties. *Catalysis Today*, 324, 15–26.
- ⁴³ Chang-jun Liu, Jingyun Ye, Jiaojun Jiang, Yunxiang Pan, 2011, Progresses in the Preparation of Coke Resistant Ni-based Catalyst for Steam and CO₂ Reforming of Methane. *ChemCatChem*, 3, 529 – 541.
- ⁴⁴ Nicolas Abdel Karim Aramounia, Jad G. Toumab, Belal Abu Tarbousha, Joseph Zeaitera, Mohammad N. Ahmada, 2018, Catalyst design for dry reforming of methane: Analysis review. *Renewable and Sustainable Energy Reviews* 82, 2570–2585.
- ⁴⁵ Kai Tao, Lei Shi, Qingxiang Ma, Ding wang, Chunyang Zeng, Chunlong Kong, Mingbo Wu, Liang Chen, Shenghu Zhou, Yibo Hu, Noritatsu Tsubaki, 2013, Methane reforming with carbon dioxide over mesoporous nickel–alumina composite catalyst. *Chemical Engineering Journal* 221, 25–31.
- ⁴⁶ Rosaria Anastasio, Fabio Fulchini, 2013, Preparazione e caratterizzazione di un catalizzatore a base di Ni supportato su Allumina. *Technical report*. DOI: 10.13140/2.1.2279.6803
- ⁴⁷ F. Menegazza, M. Signoretto, F. Pinnaa, P. Cantona, N. Pernicone, 2012, Optimization of bimetallic dry reforming catalysts by temperature programmed reaction. *Applied Catalysis A: General*, 439– 440, 80– 87.
- ⁴⁸ P. A. Sheena, K. P. Priyanka, N. Aloysius Sabu, Boby Sabu, Thomas Varghese, 2014, Effect of calcination temperature on the structural and optical properties of nickel oxide nanoparticles. *Nano Systems: Physics, Chemistry, Mathematics*, 5 (3), 441–449.
- ⁴⁹ Farnaz Rahbar Shamskar, Mehran Rezaei, Fereshteh Meshkani, 2017, The influence of Ni loading on the activity and coke formation of ultrasound-assisted co-precipitated Ni-Al₂O₃ nanocatalyst in dry reforming of methane. *Intenational journal of hydrogen energy*, 42, 4155-4164.
- ⁵⁰ Willem P. R. Deleu, Ivo Stassen, Dries Jonckheere, Rob Ameloot and Dirk E. De Vos, 2016, Waste PET (bottles) as a resource or substrate for MOF synthesis. *J. Mater. Chem. A*, 4, 9519–9525.

- ⁵¹ Yu-Ting Huang, Yu-Lun Lai, Chia-Her Lin, Sue-Lein Wang, 2011, Direct use of waste PET as unfailing source of organic reagents in the synthesis of intrinsic white/yellow luminescent nanoporous zincophosphates. *Green Chem.*, 13, 2000–2003.
- ⁵² Jianwei Ren, Xoliswa Dyosiba, Nicholas M. Musyoka, Henrietta W. Langmi, Brian C. North, Mkhulu Mathe, Marice S. Onyango, 2016, Green synthesis of chromium-based metal-organic framework (Cr-MOF) from waste polyethylene terephthalate (PET) bottles for hydrogen storage applications. *International Journal of Hydrogen Energy*, 41(40), 18141-18146.
- ⁵³ Moore, D. M. and R. C. Reynolds, 1997, X-Ray diffraction and the identification and analysis of clay minerals, 2nd Ed. *Oxford University Press, New York*.
- ⁵⁴ Kadine Mohamed, 2016, Thermogravimetric Analysis (TGA) Theory and Applications, *Power point presentation*.
- ⁵⁵ P. Bertier et al., 2016, On the use and abuse of N₂ physisorption for the characterization of the pore structure of shales. *The Clay Minerals Society*, Vol. 21, Chapter 12, 151–161.
- ⁵⁶ Kenneth Sing, 2001, The use of nitrogen adsorption for the characterization of porous materials. *Colloids and Surfaces A: Physicochem. Eng. Aspects*, 187–188, 3–9.
- ⁵⁷ Z. L. Wang, 2000, Transmission Electron Microscopy of Shape-Controlled Nanocrystals and Their Assemblies. *J. Phys. Chem. B*, 104, 1153-1175.
- ⁵⁸ <https://www2.chemistry.msu.edu/faculty/reusch/VirtTxtJml/Spectrpy/nmr/nmr1.htm>
- ⁵⁹ R.A. Koeppe et al., 1994, Characterization of V₂O₅/TiO₂ Eurocat samples by temperature-programmed reduction. *Catalysis Today*, 20, 45-52.
- ⁶⁰ Antonella Gervasini, 2013, Temperature Programmed Reduction/Oxidation (TPR/TPO) Methods, *Springer Series in Materials Science*, 154, 5.
- ⁶¹ Sujata K., Hamlin M. Jennings, 1991, Advances in Scanning Electron Microscopy. *MRS Bulletin*.

8. Acknowledgements

A big thanks goes to all the people I met during the months spent at Laboratoire de Réactivité de Surface. In particular, to Julien Reboul, for having host me in its lab where I met great people and professionals, I learned a lot and I had the chance to feed my passion. Thanks to Leila for always being available to help me and to answer my questions. Thanks for all the patience you showed to me and for having taught me a lot.

Inoltre, grazie alla professoressa Specchia per avermi dato l'opportunità di far parte del progetto SOL-CARE, e per avermi aiutato a presentare nel migliore dei modi il mio lavoro. Mi sarebbe piaciuto poter lavorare più a lungo insieme a lei perché sono sicura che, se ne avessi avuto la possibilità, avrei potuto imparare tanto dal suo bagaglio culturale.

Ringrazio i miei genitori per essere stati sempre presenti, per avermi consigliato e supportato ma lasciandomi sempre la libertà di decidere e sbagliare da sola, per la totale fiducia che avete sempre riposto in me, e per le migliaia di panzerotti e caffè che avete fatto per farmi raggiungere questo traguardo. Mi reputo una ragazza davvero fortunata perché ho dei genitori che per me farebbero di tutto e non so se riuscirò mai a ringraziarvi abbastanza.

Mamma non parli molto di quello che senti e non lasci quasi mai trasparire le tue emozioni, ma anche se in tutti questi anni non ho mai visto una lacrima prima di ogni mia partenza so che in realtà stavi male e che il giorno dopo avresti sentito la nostra casa troppo silenziosa. Ti ringrazio per avermi sempre spronata a fare di più dicendomi che i miei voti non erano abbastanza alti e che avrei sempre potuto fare di più, e soprattutto ti ringrazio per non esserti mai vantata di me perché non ho bisogno che gli altri mi credano una ragazza brava e intelligente ma ho bisogno che tu sia fiera di me sempre.

Papà io e te purtroppo o fortunatamente siamo molto simili, da te ho preso la voglia di fare, di viaggiare, la testardaggine, l'amore per la vita, la generosità e il bisogno insito di aiutare le persone a cui teniamo. E tu caro papà in questi anni mi hai sempre aiutato, supportato e sopportato, spinto a fare del mio meglio e a non mollare quando le cose si complicavano.

Un grazie speciale va a mia sorella **Angela** per aver sempre creduto in me, per avermi dato tanti spunti di riflessione e per aver riempito le mie giornate con lunghe telefonate.

Nonostante la nostra diversità caratteriale e il nostro diverso modo di vivere, abbiamo un rapporto davvero forte e speciale, sentiamo il bisogno costante di raccontarci, di confrontarci e di vivere appieno ogni singolo istante. So che molto probabilmente la vita ci porterà a stare lontano ma ti prometto che, anche se non fisicamente, troverò il modo di essere sempre presente nella tua vita e in quella di Alexander.

Grazie a tutto il resto della mia famiglia, le nonne, gli zii, i cugini, i prozii e i procugini per essermi stati accanto in questi anni, per avermi fatto sentire meno la mancanza di casa e della nostra grande famiglia anche con una semplice telefonata o un messaggio. Vorrei ringraziare in particolar modo zio Mimmo e zia Giuseppina, forse non ve l'ho mai detto ma vi considero l'esempio di quello che per me vuol dire famiglia, vita e amore.

Francesco, se dovessi mettere per iscritto tutti i motivi per cui dovrei ringraziarti riempirei pagine e pagine, ma di una cosa ti sono particolarmente grata ed è la tua incommensurabile pazienza. In questi anni mi sei stato sempre vicino, hai pazientemente ascoltato tutti i miei sfoghi e i miei problemi, e con la tua calma e tranquillità mi ha sempre portato a superare ogni

difficoltà. Mi hai insegnato che nella vita non serve sbraitare, arrabbiarsi e perdere le staffe se qualcosa non va esattamente come l'avevi programmato, ma fare un lungo respiro e parlarne, perché come dici tu a tutto c'è una soluzione. Un anno fa ero seduta a leggere i tuoi ringraziamenti e in una frase hai scritto che speravi di diventare il mio grande uomo. In questo anno ci sono stati tanti cambiamenti, tu hai raggiunto la tua tanto ambita indipendenza economica e non solo, io ho fatto un'esperienza all'estero che ci ha portato a stare lontani, ma che ha rafforzato ancora di più il nostro rapporto. Quindi, ad oggi posso dirti con assoluta certezza che sei il mio grande uomo e che sono pronta a costruire il mio futuro insieme a te.

Grazie ai miei amici di sempre **Luca** e **Rosaria**, che anche se con chilometri di lontananza hanno trovato il modo di essere presenti, consigliarmi e supportarmi. Grazie Luca per avermi insegnato a prendere la vita con un po' più di leggerezza, a non preoccuparmi sempre degli altri e di quello che pensano ma di mettere al primo posto me stessa e la mia felicità. Grazie per avermi spronato, con un modo tutto tuo, a non abbattermi e a cercare di fare sempre del mio meglio. Con te riesco a parlare di qualunque cosa e tu riesci sempre a capirmi, sono fortunata ad averti come amico. Rosaria, la nostra amicizia come le relazioni importanti è fatta di alti e bassi, di incomprensioni e chiarimenti, ma ogni volta che sbagliamo ammettiamo i nostri errori (io ci metto un po' di più ad ammetterli) e tutto torna come prima, questo perché ci vogliamo bene e perché anche se siamo totalmente diverse abbiamo bisogno l'una dell'altra. Ti ringrazio per trovare sempre del tempo per me, per ascoltare le mie pippe mentali e i discorsi sul futuro anche se lontano. Ti ringrazio per essere sempre presente nella mia vita e ti chiedo scusa se io sono presente a tratti nella tua, ma cercherò di migliorare.

Grazie alle mie amiche e coinquiline **Serena** e **Federica** per aver reso gli anni universitari indimenticabili, per avermi fatto sentire sempre a casa e per essere state il mio punto di riferimento.

Un grazie particolare ad **Esther** e **Carlotta** per avermi spinto a fare l'Erasmus, per avermi aiutato ad aprire la mente, per essermi state sempre e sottolineo sempre vicine, e avermi portato a scoprire e vedere il mondo con occhi diversi. Esther sei una persona straordinaria, ti osservo e non riesco proprio a capire da dove tu riesca a prendere tanta forza, energia e voglia di vivere. Grazie per avermi trasmesso in questi anni un po' della tua forza, per aver stravolto le mie giornate e per avermi fatto vivere in un modo diverso da come l'avevo programmato.